Forschungszentrum Karlsruhe

in der Helmholtz-Gemeinschaft

Wissenschaftliche Berichte

FZKA 6880

A Thermodynamically and Microscopically Motivated Constitutive Model for Piezoceramics

Marc Kamlah, Zhenggui Wang*

Institut für Materialforschung

*Institut für Zuverlässigkeit von Bauteilen und Systemen, Universität Karlsruhe

Forschungszentrum Karlsruhe GmbH, Karlsruhe
2003

Impressum der Print-Ausgabe:

Als Manuskript gedruckt

Forschungszentrum Karlsruhe GmbH
Postfach 3640, 76021 Karlsruhe

Mitglied der Hermann von Helmholtz-Gemeinschaft
Deutscher Forschungszentren (HGF)

ISSN 0947-8620

Abstract

This progress report presents a thermodynamically and microscopically motivated constitutive model for piezoceramics within the framework of a research project supported by the Deutsche Forschungsgemeinschaft. This project is aimed at developing a finite element tool for the analysis of piezoceramic components taking into account the full range of large signal electromechanical hysteresis effects exhibited by these materials. Such a tool is necessary for the stress analysis being the basis for a reliability assessment of piezoceramic devices subject to domain switching processes.

In a first step, the hysteresis phenomena of piezoceramics and their microscopic origin were discussed, and the phenomena to be described were selected. Concerning the balance laws, the simplest form consisting of balance of momentum and Gauß' Law was derived by physically motivated assumptions step by step from nonlinear thermomechanics and Maxwell's Equations. Revision of the current literature revealed that a commonly accepted thermodynamic framework for phenomenological modeling has been established in the international scientific discussion.

Most of the work was devoted to constructing a phenomenological constitutive model for piezoceramics under multiaxial electromechanical loadings as the physical basis for the analysis tool. The unique feature of the model are microscopically motivated internal variables, which describe domain switching in the material, and which are related to the macroscopic irreversible polarization and strain. A switching condition was used to characterize the onset of the change of domain structure. The differential evolution equations of the internal variables were deduced by using the normality flow rule, such that thermodynamic restrictions are satisfied. An energy barrier function, which characterizes the saturation of the domain switching, was introduced to enforce a kinematical constraint for the evolution of the internal variables. In this way, only consistent irreversible polarization and strain states are possible. Numerical simulations of the material responses to some typical loading cases show that the model is capable of describing the nonlinear behavior of the piezoceramics.

In closing, the assumptions underlying the model are discussed in view of microscopic considerations.

Kurzfassung

Ein thermodynamisch und mikroskopisch motiviertes Konstitutivmodell für Piezokeramiken

Dieser Fortschrittsbericht beschreibt ein thermodynamisch und mikroskopisch motiviertes Konstitutivmodell für Piezokeramiken, das innerhalb eines von der Deutschen Forschungsgemeinschaft unterstützten Forschungsprojektes entstanden ist. In diesem Projekt soll für die Analyse piezokeramischer Komponenten ein Finite-Elemente-Werkzeug entwickelt werden, wobei der gesamte Großsignalbereich der elektromechanischen Hystereseeffekte, die in diesen Materialien auftreten, abgedeckt werden soll. Solch ein Werkzeug wird für Spannungsanalysen benötigt, die grundlegend sind für Zuverlässigkeitsbetrachtungen von piezokeramischen Bauteilen, in denen Domänenumklappprozesse stattfinden.

In einem ersten Schritt werden Hysteresephänomene von Piezokeramiken und deren mikroskopischer Ursprung diskutiert, und es werden die Phänomene, die im Weiteren beschrieben werden müssen, ausgewählt. Motiviert durch physikalische Annahmen wird das einfachst mögliche System von Bilanzgleichungen, bestehend aus Impulserhaltung und Gaußschem Gesetz, schrittweise aus der nichtlinearen Thermomechanik und den Maxwellgleichungen abgeleitet. Eine Durchsicht der aktuellen Literatur hat verdeutlicht, dass sich für die phänomenologische Modellierung ein allgemein anerkannter thermodynamischer Ansatz in der internationalen wissenschaftlichen Diskussion etabliert hat.

Der größte Teil der Arbeit widmet sich dann der Aufstellung eines phänomenologischen Konstitutivmodells für Piezokeramiken unter mehrachsiger elektromechanischer Belastung, das das physikalische Fundament für das Berechnungswerkzeug bildet. Besondere Merkmale des Modells sind mikroskopisch motivierte innere Variablen, die das Umklappen im Material beschreiben, und die zur makroskopischen irreversiblen Polarisation und der Dehnung in Beziehung stehen. Eine Umklappkriterium wird benutzt, um das Einsetzen des Umklappens in der Domänenstruktur zu charakterisieren. Die Differentialgleichungen der inneren Variablen werden mit Hilfe der Normalitäts Regel abgeleitet, wobei die thermodynamischen Nebenbedingungen erfüllt werden. Eine energetische Hürde wird eingeführt, welche die Sättigung des Domänenumklappens charakterisiert, um eine kinematische Beschränkung bei der Entwicklung der inneren Variablen zu erzwingen. Damit wird erreicht, dass ausschließlich konsistente irreversible Polarisations- und Dehnungszustände möglich sind. Numerische Simulationen des Materialverhaltens für einige typische Belastungsfälle zeigen, dass das Modell geeignet ist, das nichtlineare Verhalten von Piezokeramiken zu beschreiben.

Abschließend werden die dem Modell zugrunde liegenden Annahmen mit Hilfe einer mikroskopischen Betrachtungsweise diskutiert.

Contents

Chapter 1

Introduction

1.1 Motivation of the present work

The piezoelectric effect causes a coupling between electric and mechanical quantities and thus it is a primary candidate for advanced sensor and actuator applications. In engineering applications the piezoelectric effect is mostly realized by the ferroelectric phase of lead zirconate titanate (PZT) and also Barium titanate ($BaTiO_3$) ceramics. These materials, also called piezoceramics, are outstanding materials for mass applications calling for short response times, high-precision positioning and considerable actuation forces in systems of complex shape. The increasing economic importance of piezoceramics has brought about the need for an improved knowledge of them. In particular, the requirement for the reliability analysis of piezoceramic components is becoming critical.

If a piezoceramic material has been poled by an electric field above the coercive field at a temperature below the Curie point, its responses to small electro-mechanical loads may be characterized by the parameters of classical linear piezoelectricity. However, nowadays applications involve severe loading and complicated geometies so that the assumption of small signals is no longer justified in general. Rather, under large electromechanical loading the nonlinear hysteresis behavior of the material can become dominant.

In order to assess the reliability of a piezoceramic component, it is important to compute the mechanical stress state quantitatively. For this purpose, the electric and mechanical field equations have to be solved together with an appropriate constitutive assumption relating the histories of electric field, polarization, stresses, and strains to each other. The linear constitutive model for piezoelectric materials was developed many decades ago and has found widespread applications in analytical and numerical methods. However, as

discussed before, the linear model is not valid for the stress calculations in critical cases, where the material exhibits nonlinear behavior at locations in a component under large loading.

The purpose of this research project is creating a finite element tool for the stress analysis of piezoceramic components taking into account the full range of nonlinear electromechanical hysteresis phenomena exhibited by the material. Now, even in microsystem technology, the order of magnitude of typical dimensions of components still belongs to the macroscopic level of consideration, if compared to typical dimensions of the microstructure of the material. Therefore, a macroscopic theory is appropriate as basis for a tool of the type mentioned above, and such a theory consists of two types of equations. First, there are the balance laws, which are basically a combinations of thermomechanics and Maxwell's Equations. Second, a phenomenological constitutive model is needed, which, mathematically, closes the system of equations and, physically, is capable of representing the specific macroscopic properties of the material under consideration.

1.2 Plan of the report

In view of the above motivating remarks, this report and the underlying research work have been organized as follows:

The first task of our project was to collect and discuss large signal hysteresis phenomena present in typical soft-PZT actuator materials. In this way, the phenomena to be represented by our theory should be selected. Furthermore, the microscopic origin of these phenomena should be considered at least qualitatively to gain the physical insight necessary for the motivation of a sound constitutive model. Especially for the latter reason, the report about this in Chapter 2 is quite lengthy, even though conducting experiments has not been subject of the present project. However, besides some data from the relevant literature, which are still limited, most of the experiments presented have been conducted by Dayu Zhou at our institute during his dissertation project and have not been published yet.

The second preparing activity in the work plan of our research project was to collect and review the recent literature on constitutive modeling. Chapter 3 outlines and discusses the basic ideas of the relevant papers. We consider it important for a productive scientific interaction to acklowledge the ideas of others and to adopt them, if they are superior to own ideas. As the main outcome, this part of the work confirmed that a common thermodynamical framework for constitutive modeling with internal variables has been established. (For reasons of a consistent presentation, this aspect is reported in the

next chapter.) Almost all papers rely on remanent or irreversible polarization and strain as internal variables.

A macroscopic theory consists of balance laws and constitutive equations. In contrast to the field of constitutive modeling, the research area of balance laws can generally considered settled. In engineering electromechanics, usually the simplest form of the balance laws being a combination of the balance of momentum and Gauß' Law is used without justifying discussion. Therefore, we included in our work plan an activity devoted to the systematical derivation of this simple theory from nonlinear thermomechanics and Maxwell's Equations. In its first part, Chapter 4 lists step by step the physical assumptions leading to the simple theory thus yielding some kind of a hierarchy of physical generality. This makes it possible, to decide in each case, which level of complexity of the theory has to be adopted. One questionable assumption is, for instance, to take a piezoceramic subject to poling processes to be ideally insulating. The second part of Chapter 4 presents the thermodynamical framework mentioned in the previous paragraph.

Having finished the presentation of all preparing work, the report now turns to the main subject of our research project. A constitutive model for piezoceramics has been constructed to complete the theory within the given framework. Constitutive modeling is still a field of research in the sense that not only existing theories and ideas are reviewed and applied. In Chapter 5, a new approach to phenomenological constitutive modeling of piezoceramics is developed for uniaxial loadings, which is based on ideas given in KAMLAH AND JIANG [1999]. In building the model, care was taken for the model not to become too involved such that the effort for its numerical evaluation would not be too large. Two internal variables, also called microstructural parameters, are introduced to quantify the overall domain orientation and level of polarization. The evolution equations of the internal variables are derived and irreversible polarization and strain are calculated as functions of the internal variables. Thereby, as a specific feature, this model allows for consistent irreversible strain and polarization states only, which is enforced by a kinematical constraint for the microstructural parameters. In order to verify the underlying a priori assumptions and to examine the ability of the model in describing the material responses to electromechanical loadings, the model is used to simulate different loading histories and loading combinations in the uniaxial loading case. It can be seen that the model represents the typical hysteresis and nonlinear electromechanical coupling phenomena.

In Chapter 6, a three dimensional formulation of the model is proposed by the introduction of additional internal variables. At this stage of our work, an approximate formulation was derived by restricting ourselves to transverselly isotropic irreversible strain states instead of orthotropic ones.

In this way, the simple structure of the one dimensional model could be kept by introducing two additional vectorial internal variables. They represent the history dependence of the irreversible polarization direction and of a preferred direction for the allignment of c-axes, respectively. Again, this version of the model is compared to experimental findings.

Due to the close relation of our internal variables to the microstructure of tetragonal ceramics, it turned out that many of our assumptions can be checked by discussing them in relation to microscopic investigations. The key point is the approximate represention of the orientation distribution function of the domains in the polycrystal by a finite set of parameters. These parameters can be related to our internal variables and to the irreversible polarization and strain.

Chapter 8 contains a brief summary and an outlook on the work which will be done in the coming time.

Chapter 2

Nonlinear electromechanical properties of piezoceramics

Experimental investigations into the physical properties of piezoceramics provide us with the basic knowledge about this material, which is the starting point for all theoretical studies. Furthermore, the validity and the descriptive ability of a constitutive model can only be examined and modified with the help of experimental results. In this section only a brief description of the experimental studies of the nonlinear electromechanical properties of piezoceramics related to our project is presented. Detailed physical properties can be found elsewhere (*eg.* Cao and Evans [1993], Damjanovic [1998], Hall [2001], Kamlah [2001], Jaffe *et al.* [1971], Lynch [1996], Schäufele and Härdtl [1996], Zhou [2003]). Though a great deal of experimental research has been carried out, there are relatively few experimental investigations into macroscopic nonlinear properties. The studies reported by Cao and Evans [1994], Lynch [1996] and Schäufele and Härdtl [1996] are the pioneering works in this field and have been cited by many authors. In his recent dissertation Zhou [2003] reported a thorough experimental study of nonlinear constitutive behavior of piezoceramics. In this work the nonlinear properties of piezoceramics under uniaxial electric, mechanical and combined electromechanical loading were thoroughly investigated. The commercially available PIC151 soft PZT ceramics was used for test samples. The detailed experimental results provide a solid data base for the development of nonlinear phenomenological constitutive models. As the works by Zhou [2003] have been carried out at our institute, this section relies mainly on them to demonstrate the nonlinear behavior of the piezoceramics (see the remarks in Section 1.2).

2.1 Pure electric loadings

In this section, we consider a test series where a quasi-static cyclic electric field of ± 2kV/mm in amplitude at a rate of $0.08\text{kV}/(\text{mm}\cdot\text{s})$ (corresponding a frequency of 0.01Hz) is applied on a sample in the longitudinal direction, whose dimension is $5 \times 5 \times 15$ mm^3. The polarization, longitudinal strain and lateral strain are measured.

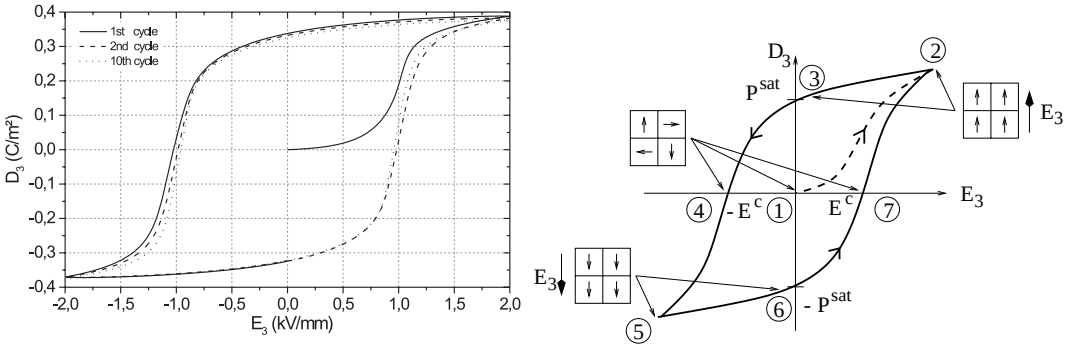

Figure 2.1: Dielectric Hysteresis: Left: Polarization *vs.* electric field with $|\dot{\text{E}}_3| = 0.08\text{kV}/(\text{mm}\cdot\text{s})$, three loading cycles. Right: Schematic sketch of the dielectric hysteresis. To the selected $\text{E}_3 - \text{D}_3$ states, the simplifying domain state symbols in the boxes are asigned. The dashed line belongs to the first polarization process of initially unpoled material.

Figure 2.1 shows the typical response of an initially unpoled sample to a cyclic electric field. In the initial state ①, as indicated by the arrows in the corresponding schematic domain structure, the domains are randomly distributed and the macroscopic polarization is zero. If the applied electric field is sufficiently small, the domain structure is unchanged and the ions of the unit cells are shifted within the neighborhood of their equilibrium positions only. The corresponding macroscopic dielectric behavior of the material is reversible and approximately linear.

As the electric field reaches the *coercive field strength* E^c, switching processes of domains are initiated. In this irreversible process the polarization increases rapidly until the microscopic polarization of all domains is gradually aligned as close in the direction of the electric field as possible, *i.e.*, the material approaches a saturation state. The state indicated by ② in Figure 2.1 is reached when the reservoir of switchable domains is exhausted. Further changes of the polarization can only result from the shifting of ions near their new equilibrium positions and, thus, the increase of the polarization is slower and essentially reversible.

Upon unloading the ions remain in their new equilibrium positions and the poled domain structure is preserved. Consequently, a remanent macroscopic polarization is induced even after the complete removing of the electric field (see state ③ in Figure 2.1). In the example of Figure 2.1, it assumes the maximum value of the *saturation polarization* due to complete alignment of domains by a sufficiently high electric field.

If an electric field applied in the opposite direction reaches the coercive field, switching processes are initiated again. The fully aligned domain state is disturbed such that the remanent polarization decreases until a more or less depoled state is assumed at ④. Further loading leads to a domain state oriented in the new electric field direction (⑤ in Figure 2.1). Upon reversing the electric field again, the material responds in the same manner as before (along the path ⑥-⑦-② in Figure 2.1).

In summary, three different ranges of material response can be indentified: In the initial state the behavior is reversible for sufficiently small loadings. If the loading exceeds a critical value, irreversible processes will be initiated and hysteresis will occur. After saturation of these irreversible processes, further changes are merely of a reversible character.

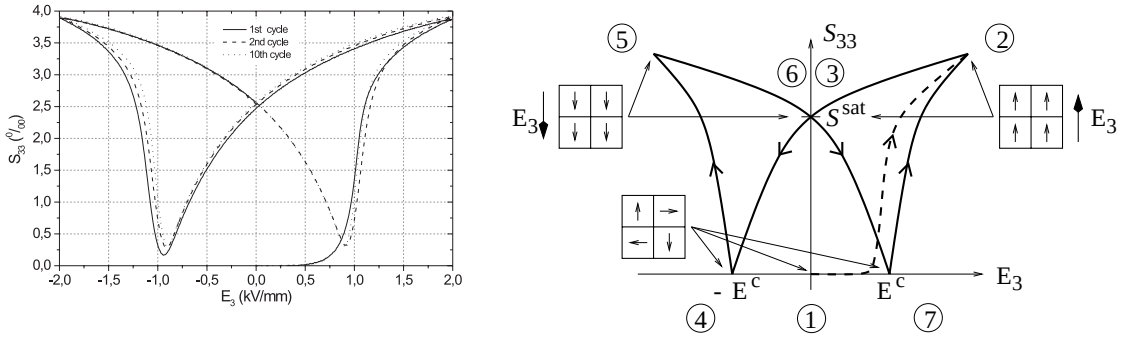

Figure 2.2: Butterfly Hysteresis. Left: Strain *vs.* electric field with $|\dot{E}_3| = 0.08\text{kV}/(\text{mm}\cdot\text{s})$, three loading cycles. Right: Schematic sketch of the butterfly hysteresis. To the selected $E_3 - S_{33}$ states belonging to the corresponding states in Figure 2.1, the simplifying domain state symbols in the boxes are asigned. Again, the dashed line belongs to the first polarization process of initially unpoled material.

During the electric field cycle the deformation of the sample occurs simultaneously with the polarization. As a counterpart of Figure 2.1, Figure 2.2 shows the relationship between electric field and strain of the sample. The numbers in both figures are in correspondence with each other. The thermally depoled and macroscopically isotropic initial state is defined as the state of

zero strain. When electric field is below the coercive value, the distribution of the polarization orientation of the domains is random. Therefore, the microscopic contributions of the domains cancel each other, and we observe no electrically induced macroscopic strain.

When the applied electric field exceeds E^c, switching processes are initiated. The *c*-axes of more and more unit cells are aligned in the direction of the electric field. We observe a rapid elongation of the specimen because of two contributions: The first one is due to the increasing number of domains oriented with their longer *c*-axes parallel to the electric field. Secondly, as we observed before, a resultant macroscopic remanent polarization is produced and this is accompanied by a macroscopic piezoelectric effect resulting in reversible strain. As soon as switching processes are completed and a fully switched domain state is reached, only the second contribution leads to further changes of the strain. This is indicated by the reduced slope of the electric field-strain curve as state ② in Figure 2.2 is approached.

Upon unloading, from state ② to ③ in Figure 2.2, the aligned new domain state remains unchanged, the change of strain is due to the piezoelectric effect of the poled specimen. At ③, the electric field is zero and the reversible strain is recovered, and only the strain induced by the alignment of the *c*-axes of the domains remains. If the alignmemt is complete, as in the case considered here, the remanent strain at zero electric field assumes the *saturation strain* S^{sat}.

Upon reversing the electric field beyond $-E^c$, back-switching processes are initiated and the degree of order of the domains is reduced. Because of this electric depolarization the macroscopic polarization decreases and the material loses its inverse piezoelectric effect. The distribution of the orientation of the *c*-axes becomes more random, such that the resultant switching strain is reduced. In the state ④, the lowest degree of order is reached and the strain goes a sharp minimum. From this minimum strain on, the alignment of the domains and thereby the switching strain as well as the piezoelectric strain starts to increase again. Finally, at ⑤, a domain state oriented fully in the new direction of the electric field is reached. The material will behave in the same manner as in the previous poled state, but oriented oppositely.

The most significant feature of the butterfly hystersis is its symmetry with respect to the strain axis at $E = 0$. For the remanent strain, only the alignment level of the *c*-axes counts but not the orientation of the spontaneous polarization vectors. In particular, two opposite remanent polarization states will lead to the same remanet strain state. During poling by both a positive and a negative electric field, the induced piezoelectric strain is positive, since it is caused by a corresponding positive or negative remanent polarization, respectively. The piezoelectric constants in the poled states ② and ⑤ have

the same absolute value, but opposite signs.

2.2 Pure mechanical loadings

In this section we discuss the piezoceramic material response to mechanical loading. We focus on uniaxial compressive states since they can be realized comparably more easily for a brittle material with a low tensile strength. Under small stress the material responses are reversible and nearly linear. If the stress exceeds a critical value, the stress-strain behavior exhibits significant non-linearity and remanent strain is induced. As before, the experimental results by Zhou [2003] are used in the discussion.

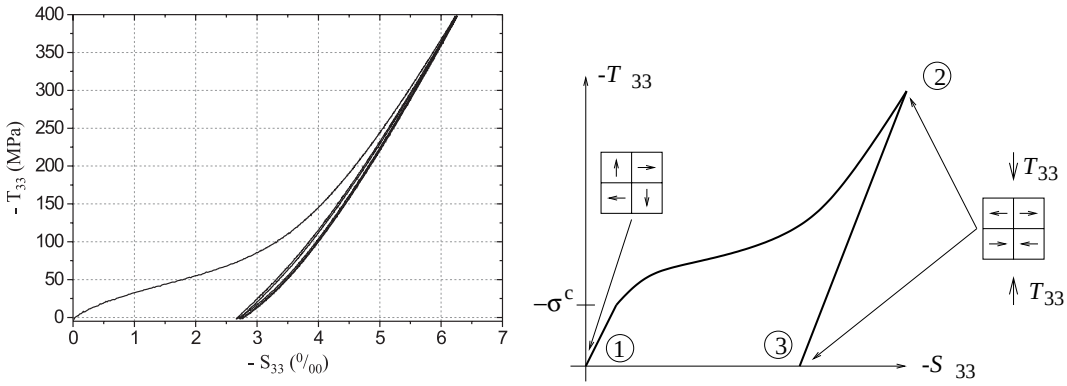

Figure 2.3: Ferroelastic Hysteresis. Left: Ferroelastic Hysteresis behavior under mechanical loading: Compressive stress -T_{33} *vs.* compressive strain -S_{33} starting from an unpoled state with a loading rate of $|\dot{T}_{33}| = 5$MPa/s. Right: Schematic sketch of the ferroelastic behavior for compressive loading of an initially unpoled material. To selected $T_{33} - S_{33}$ states, the simplifying domain state symbols in the boxes are asigned.

To the left, Figure 2.3 shows the results of a compressive experiment performed on initially unpoled PIC151 soft PZT ceramic specimen, which was subjected to three subsequent ramp-shaped loading-unloading cycles by a compressive stress with an amplitude of -400 MPa and a loading rate of 5 MPa/s. We discuss it with the help of the symbolic sketch on the right panel. We will recognize a certain analogy with the dielectric behavior, since the microscopic switching mechanisms are active in this case as well. For small loadings near ① the ions will be displaced only slightly from their equilibrium positions and the material shows a linearly elastic behavior. After passing the critical load $|T_{33}| = \sigma^{\mathrm{c}}$, which is called *coercive stress* and is analogous to the dielectric case, switching processes are initiated. Certain ions assume

new equlibrium positions such that the longer c-axes of the domains are oriented as closely as possible to a direction which is perpendicular to the compressive loading. This gives rise to a rapid increase of the remanent strain. At higher stress levels when the switching process is nearly completed, a fully switched domain structure is achieved and the remanent strain takes the maximum value $S^{\text{sat}}_{\text{comp}}$ at ②. Under further loading, the material reacts more and more stiffly and approximately elastically. After unloading, at ③, the switched domain structure is preserved which leads to significant remanent strains. For further loading and unloading cycles, the stress-strain loops become quite narrow and only a slight hysteresis can be observed. This is because of the nearly complete exhaustion of the switchable domains after the first loading-unloading cycle. It should be pointed out that in this mechanical loading cycle the resultant macroscopic polarization remains zero. A mechanical stress cannot trigger a unique switching direction of the spontaneous polarization of a unit cell with the following consequence: While all the c-axes will prefer to a position close to a plane perpendicular to the compressive stress, the distribution of these c-axes within this plane remains random. Thus, the domain state results from uniaxial compresive stress is transversely isotropic, but possesses no macroscopic polarization.

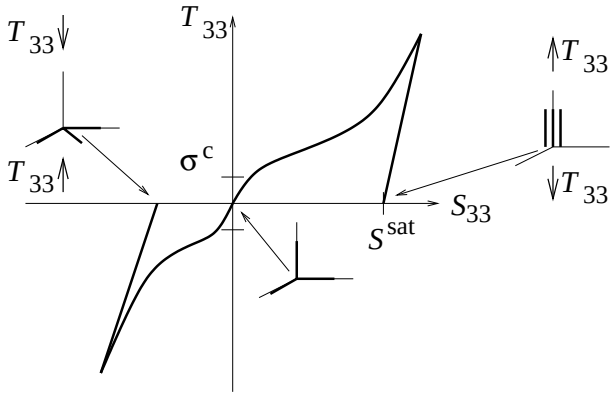

Figure 2.4: Shown in the same plot, mechanical stress T_{33} and strain S_{33} of two fictitious compression and tension experiments, respectively, with both starting from a thermally depoled initial state. The distribution of the c-axes for the initial and unloaded states is symbolized in simplifying manner by three thick lines each representing a possible position of c-axes within a unit cell.

Experimental results by Fett *et al.* [1998a, 1998b] demonstrate that the deformation of piezoceramics under tensile and compressive stress is

asymmetric. However, in real tensile tests, the maximum remanent strain will never be reached, because the stress needed is much larger than the tensile strength of the material. Therefore, theoretical considerations are needed.

In order to give a microscopic explanation of this asymmetry, we start with a simplifying picture. We consider a single crystal with the mechanical loading parallel to one of its lattice axes and assume a thermally depoled initial state. As we have seen, the arrangement of the c-axes is responsible for the amount of remanent strain. The orientation distribution of the c-axes in the space is represented in Figure 2.4 roughly by three thick lines assigned to the states before loading and after unloading. From this consideration we would expect that the reservoir of switchable unit cells under tension can be up to twice as large as the reservoir of switchable unit cells under compression. Thus, starting from an unpoled state, the maximum tensile switching strain would be twice the maximum compressive switching strain. In this context it is noted, that the maximum remanent strain in tension, where all c-axes are more or less parallel to the loading direction, is equal to the maximum remanent strain due to poling, *i.e.*, S^{sat}.

In experiments, we encounter the reponse of a polycrystal with a random distribution of the orientation of its grains. In an investigation of the effective properties of polycrytalline $BaTiO_3$, the maximum tensile and compressive remanent strains were studied by Fröhlich [2001]. 10000 unit cells with random distribution of the initial orientation were taken into account to simulate the macroscopic and global behavior of the unit cells. The maximum tensile remanent strain $S^{\mathrm{sat}}_{\mathrm{tens}}$ is reached at a domain state at which all c-axes have switched into a cone of 45° around the axis of loading. The maximum compressive remanent strain is reached if all c-axes are situated as closely as possible to a plane perpendicular to the loading direction. It is found that

$$S^{\mathrm{sat}}_{\mathrm{tens}} = 0.5520 S^{\mathrm{spon}} \quad \text{and} \quad S^{\mathrm{sat}}_{\mathrm{comp}} = -0.4035 S^{\mathrm{spon}}, \tag{2.1}$$

where S^{spon} is the spontaneous strain of the unit cell with respect to the undistorted paraelectric state. According to this result, the ratio between maximum tensile and compressive remanent strains is $1.37 : 1$, much smaller than the expected $2 : 1$ from the aforementioned single crystal consideration.

2.3 Combined electromechanical loadings

For a better understanding of the behavior of piezoceramics under complex loading conditions, it is necessary to experimentally examine the material responses to the combined electromechanical loadings (Lynch [1996],

Schäufele and Härdtl [1996]). Again, here we use the experimental results of Zhou [2003] for the discussion. Zhou has conducted a series of experiments such as mechanical depolarization, electric field cycling with prescribed compressive stress and compressive stress cycling with prescribed bias field on piezoceramic specimens. Below we give a brief discussion of these tests. The detailed descriptions and discussions are found in Zhou [2003].

In order to study the mechanical depolarization behavior of the material, an initially unpoled PIC151 soft PZT specimen was first subjected to a total of five cycles of ramp-shaped electric field loading under mechanical load free state, with an amplitude of ± 2 kV/mm and a loading rate of 0.08 kV/(mm $\cdot$ s). Changes of strain and polarization were monitored simultaneously. Right after removal of the electric field, a uniaxial compressive stress parallel to the prepoling direction was applied to the specimen. By this procedure, the polarization and deformation history of the material is fully known.

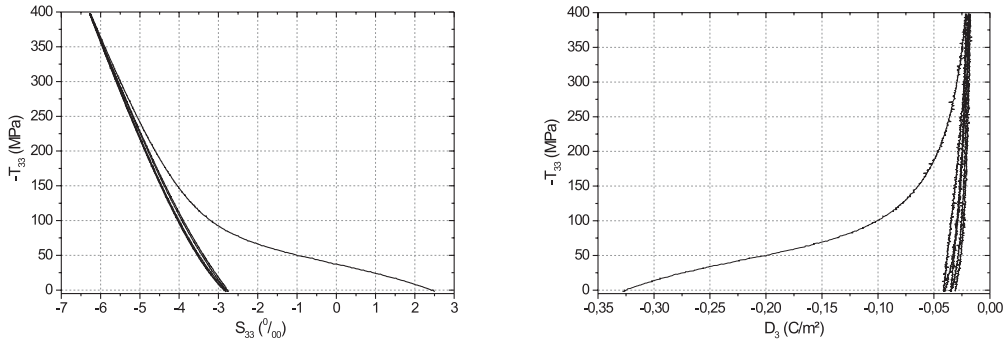

Figure 2.5: Mechanical depolarization of poled specimen under compressive stress with a loading rate of $|\dot{T}_{33}| = 5$ MPa/s. Left: Stress *vs.* strain. Right: Stress *vs.* polarization.

The left panel of Figure 2.5 shows the variation of longitudinal strain and polarization of the prepoled specimen with the application of a compressive stress. The electric field induced remanent longitudinal strain is 0.251%. With application of an increasing compressive stress, the microscopic spontaneous polarization vectors of unit cells will be gradually redistributed randomly within or close to a plane perpendicular to the compressive load. In the course of this non-180° domain switching process, the original order of the domains in the previous poling direction is lost, therefore the electric field induced remanent strain vanishes gradually and the compressive stress

induced irreversible strain is observed. The ferroelastic domain switching process will be nearly completed at a higher stress level. The stress-strain responses during further increased stress loading and the initial unloading period become approximately linear elastic. When unloading the compressive load below about -150 MPa, similar to the unpoled material, the plots display a slight non-linearity. The remanent longitudinal strain after the first compression loading cycle is -0.276%. Only very slightly can more remanent strains be further induced during subsequent cyclic stress loading.

Besides the non-linear stress-strain behavior, as shown in the right panel of Figure 2.5, ferroelastic domain switching induced by a compressive stress will simultaneously give rise to the gradual removal of the remanent polarization of a prepoled material. This phenomenon is called *mechanical depolarization*. The shape of the depolarization curve resembles the corresponding stress-strain behavior, suggesting that the origin of non-linear deformation is also responsible for the polarization changes (Cao and Evans [1993]). The initial remanent polarization induced by the electric field is about -0.328 C/m^2 . With the increasing of the compressive stress, the remanent polarization non-linearly decreases. After achieving a much higher stress level (*eg.*, -300 MPa), the change of the polarization becomes quite slow for further increasing load time. The remanent polarization remaining at -400 MPa is about -0.022 C/m^2. Therefore, the material can not be completely depolarized by a compressive stress loading with the maximum magnitude of -400 MPa in this experiment. Upon unloading from -400 MPa, the stress-depolarization curve initially traces a nearly vertical line. This phenomenon indicates that the specimen behaves electromechanically decoupled due to mechanical depolarization. After about -200 MPa, the unloading curve exhibits a slight non-linearity, which indicates that a small part of the polarization can be gradually recovered. The remanent polarization after the first loading cycle is about -0.041C/m^2 , which is apparently larger than the minimum value induced at -400 MPa. A little bit more remanent polarization can be removed by further stress loading cycles. Directly after a total of three loading-unloading cycles, the remanent polarization is about -0.031 C/m. When the stress magnitude is lower than a certain value during the unloading period, both strain and polarization curves are observed to deviate from their initially linear behavior and exhibit slight nonlinearities.

The material responses to full electric field cycling with different prescribed uni-axial compressive stress are studied by Zhou [2003]. The experiment was performed on initially unpoled PIC151 soft PZT ceramics and full cycles of a ramp-shaped electric field were applied to the specimen under different constant compressive stresses. The electric field and the bias stress were coaxial. The electric field range was selected between -2 kV/mm and +2

kV/mm, with a loading rate of 0.08 kV/(mm · s). The superimposed stress levels were increased from 0 to -400 MPa, with a loading rate of 5 MPa/s. Polarization, longitudinal and transverse strains *vs.* electric field hysteresis loops were monitored simultaneously.

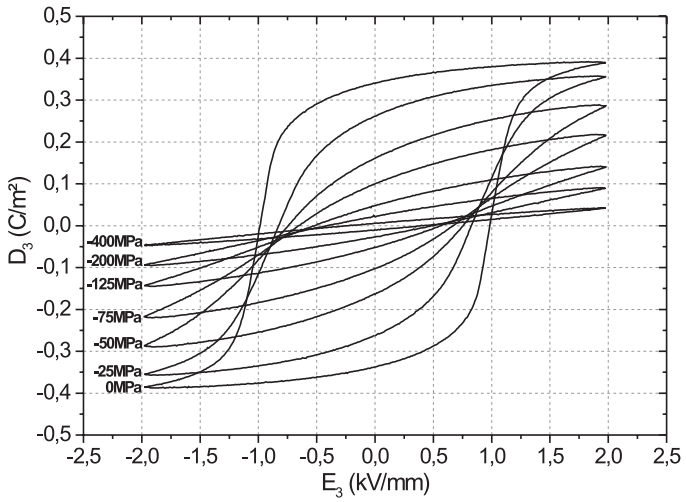

Figure 2.6: Polarization *vs.* electric field hysteresis loops under different constant preloaded compressive stresses.

Figure 2.6 shows polarization *vs.* electric field hysteresis loops to different constant preload stresses. It can be seen that the hysteresis become narrow and loops area decreases with increasing preloaded stress. Under a compressive stress of 400 MPa the hysteresis nearly become a straight line. Figure 2.7 is the counterpart of Figure 2.6 and it shows the butterfly curves during electric field cycling. One of the most notable features of the butterfly curves is that both the maximum (at ±2 kV/mm) and remanent (at 0 kV/mm) strains decrease with increasing compressive stress levels. Similar to the polarization *vs.* electric field hysteresis, the butterfly hysteresis becomes narrower with increasing preloaded stress. Under high compression, it nearly becomes a straight line.

The applied compressive stress hinders domain switching into the electric field direction, thus a higher electric field is needed to induce domain switching. At the stress free state, when the electric field is unloading from +2 kV/mm to 0 kV/mm, most of the domains are preserved with orientation parallel to the positive electric field loading direction (only a few unstable domains are switching back to their initial unpoled states). From 0 kV/mm, the first non-180° domain switching process starts in the material with a

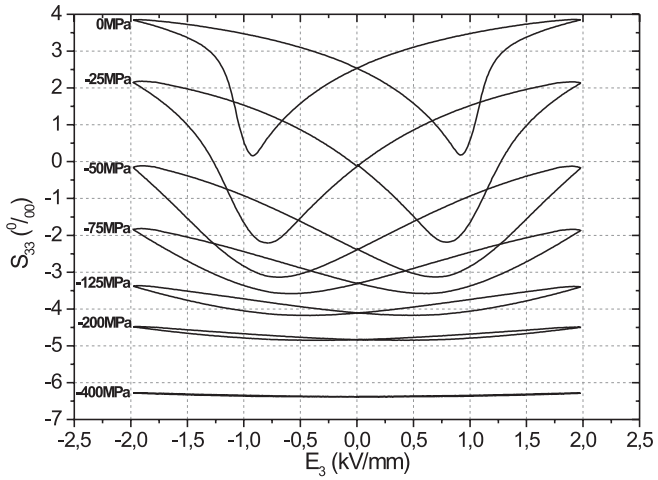

Figure 2.7: Strain *vs.* electric field hysteresis loops under different constant preloaded compressive stresses.

negative electric field application. When the negative coercive field $-E^c$ is reached, the first non-180° switching process will be completed. The strain is found to achieve its minimum absolute value and the polarization is zero. After $-E^c$ the second non-180° domain switching process begins, both polarization and strain are observed to experience an increasing jump, and finally they become saturated at higher electric field levels. (To simplify the discussion, here it is assumed that the polarization and strain achieve their minimum value simultaneously).

When a relatively small compressive stress is superimposed on the specimen (*eg.*, -25 or -50 MPa), the shapes of polarization-electric field and strain-electric field curves are different from the stress free state. Due to the compressive load induced depolarization, the resultant polarization and strain at maximum electric field ($\pm$2 kV/mm) are apparently smaller than those at the stress free state. As discussed earlier, this is because some of the domains have been constrained by the superimposed stress and cannot be reoriented by the electric field with a maximum amplitude of $\pm$2 kV/mm in this experiment. Unloading from 2 kV/mm to 0 kV/mm, the preload stress will induce part of the first non-180° domain switching even before 0 kV/mm. As a result, we can see both of the polarization and strain decrease more drastically than at stress free state. After 0 kV/mm, the negative electric field acts together with the prestress to complete the residual first non-180°

switching. Until the negative coercive field ($-E^c$) is reached, the polarization and strain achieve their minimum values. The magnitude of electric field needed to start domain switching in the specimens with compressive stress preload is larger than that at the stress free state. This is due to three reasons: (1) fewer domains take part in the polarization reversal; (2) the preload stress destabilizes the poled state and leads to a part of the first non-180° domain switching in the period of electric field unloading from ±2 kV/mm to 0 kV/mm; (3) the first non-180° switching process is completed by the combined action of electric field and prestress. After E^c, the steadily increasing electric field load will act against the prestress to induce the second non-180° domain switching. Consequently, the polarization and strain experience a more gradual development rather than a jump as in the case of $T_{33} = 0$. With further preload stress increments, less and less domains take part in the polarization reversal, and the resultant polarization-electric field and strain-electric field curves become flat. For example, at -400 MPa, the former is an approximately straight line and nearly no hysteresis can be observed in the strain curve.

Zhou [2003] studied the effect of constant preload electric field on the nonlinear stress-strain and stress-polarization responses of PIC151 soft PZT ceramics. At first an initially unpoled PIC151 soft PZT specimen was subjected to four cycles of an electric field of ±2 kV/mm in amplitude at a rate of 0.08 kV/(mm · s). After poling, the material possessed remanent polarization and remanent strain. Due to technical reasons this polarization is defined as negative in this experiment. A bias electric field is applied to the specimen before the application of mechanical loading. Therefore, a negative bias electric field acts in the same direction of the initial poling state, whereas a positive field is opposite to the poling direction. The maximum magnitude of the positive bias electric field was chosen as +0.50 kV/mm. This is about half of the material's coercive field ($E^c \approx 1$ kV/mm), such that domain switching processes induced by bias electric field alone (electric depolarization) do not occur.

Figure 2.8 shows a series of plots of compressive stress *vs.* polarization curves obtained under different bias electric field conditions. It can be seen from Figure 2.8 that, when the bias field is zero, the initial remanent polarization before stress loading is -0.330 C/m^2. As stress loading increases, we observe a nonlinear depolarization curve, which is due to the compressive stress induced non-180° domain switching orthogonal to the original poling direction. The final remanent polarization at -400 MPa is -0.019 C/m^2, *i.e.*, nearly 94% of the polarization is removed. From the tendency of the curves in Figure 2.8, we can find that the development of depolarization induced by a compressive stress becomes gradually more and more difficult with the

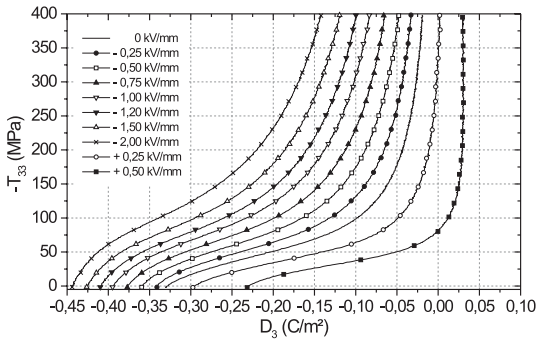

Figure 2.8: Compressive stress induced depolarization of a specimen under different bias electric fileld.

negative bias electric field increasing. At -2 kV/mm, as the stress increases up to -400 MPa, the remanent polarization is still as high as -0.142 C/m^2, only about 68% polarization is removed by the stress. These results comfirm the fact that an electric field acting in the direction of previous poling has the trend to support the existing domain state and, thus, higher stresses are needed to initiate and forward mechanically induced domain switching processes. An electric field acting oppositely to the initial poling direction (here positive bias electric field) will work together with the compressive stress to destabilize the domain state. Consequently, compressive stress induced switching processes become easier than at zero-bias electric field.

As a counterpart of Figure 2.8, Figure 2.9 shows the change of strains with the increase of the compressive stress at different bias fields. From Figure 2.8 and Figure 2.9 we can see clearly the combined effects of stress and electric field on the domain switching processes.

2.4 Time effects in piezoceramics

So far we have discussed the behavior of piezoceramics under electric, mechanical and combined electro-mechanical loadings and attributed typical hysteresis phenomena to the switching processes of unit cells. Switching of the central ions of the unit cells is of an instantaneous nature in the sense that it occurs in the very momemt a critical value of applied loads or invested energy is reached. Such a threshold gives rise to the irreversibility of the hysteresis phenomena as the changed state is preserved during unloading

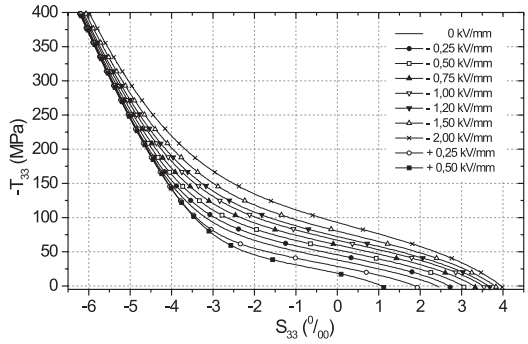

Figure 2.9: Strain responses during compressive stress induced depolarization of a specimen under different bias electric fileld.

and will stay as long as the threshold value is not passed again. Now, if the hysteresis behavior could be caused by purely instantaneous switching processes in the above sense, no time effects would occur in the constitutive response. However, significant time effects have been observed. Zhou [2003] has made detailed observations on the time effects of the behavior of piezoceramics under electric and mechanical loading. Below we give a brief description of the time effects observed by Zhou.

2.4.1 Loading rate effects in piezoceramics

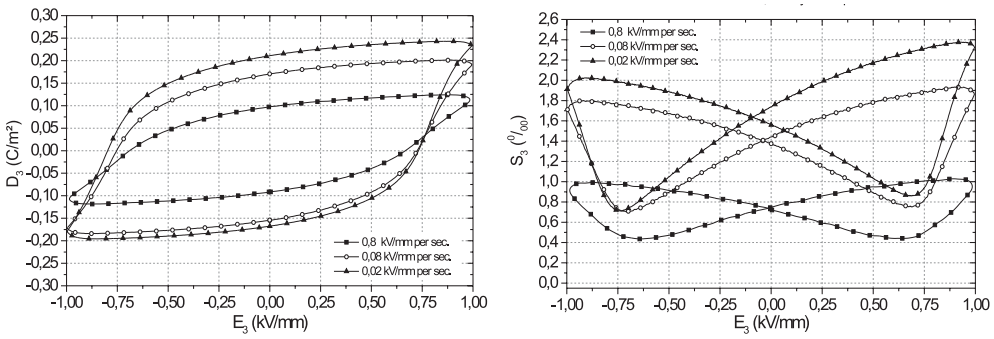

Figure 2.10: Material response to electric loading with different rates. Left: Polarization *vs.* electric field. Right: Strain *vs.* electric field.

Polarization and deformation of piezoceramics are loading rate-dependent.

In order to study this property Zhou [2003] performed experiments with different loading rates (frequencies). Figure 2.10 shows polarizaion and strain hysteresis for the loading rates of 0.02, 0.08 and 0.8 kV/(mm · s) in pure electric loading tests respectively. From the curves in Figure 2.10 it can be clearly seen that the loading rate has a remarkable influence on the polarization and deformation of the material. The lower the loading rate is, the more polarization and deformation will be induced by the same electric field strength. For instance, after ten loading cycles of 1 kV/mm in amplitude, the remanent polarization and strain in the case of a loading rate 0.02 kV/(mm · s) are about the twice of the corresponding values at the loading rate of 0.8 kV/(mm · s). For a larger electric field amplitude, the remanent polarization and strain desrease with increasing loading rate, but the differences are not so pronounced as at a smaller amplitude. For example, when the amplitude is 2 kV/mm, after six loading cycles the remanent polarization in the case of a loading rate of 0.02 kV/(mm · s) is about 7% larger than the corresponding value at a loading rate of 0.8 kV/(mm · s). These experimental results show that the loading rate effect is significant when the applied electric field is not much larger than E^c, whereas, in the case that the electric field is much larger than E^c, the rate-dependent phenomenon is not very pronounced.

Loading rate effects are also observed in tests with pure mechanical loading. Initially unpoled PIC151 soft PZT ceramic specimens were subjected to ramp-shaped uni-axial compressive stress loading, with the amplitude of -400 MPa. Three different loading rates of 0.4, 4 and 40 MPa/s were used in the experiments, respectively. The material exhibits a similar nonlinear stress-strain behavior at different loading rates. One of the notable features observed is that to achieve the same strain value a slightly higher stress is needed in the case of a higher loading rate.

2.4.2 Creep-like behavior of piezoceramics

To investigate the time-dependence of the material behavior under constant electric field, initially unpoled PIC151 soft PZT ceramic specimens were subjected to four full cycles of a ramp-like electric field, with the loading rate of 0.08 kV/(mm · s) (corresponding to a frequency of 0.01 Hz). During both the loading and unloading periods, the electric field was interrupted repeatedly by keeping it at a constant level for 300 seconds. The constant electric field holding levels were selected as ±0.50, ±1.00, ±1.50 and ±2.00 kV/mm, respectively. A total of four cycles of polarization and longitudinal strain *vs.* electric field hysteresis curves are shown in Figure 2.11 . Changes of the polarization and strain during the duration of constant electric field can clearly be observed. For the initial 1/4 period of the first loading cycle, the

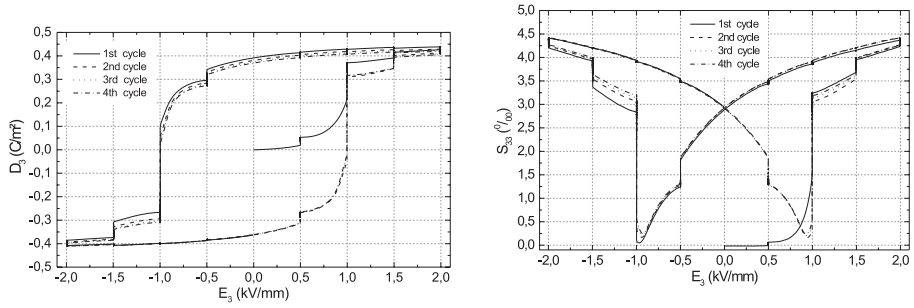

Figure 2.11: Material responses during four loading cyeles. During both loading and unloading processes the electric field was hold constant at constant levels of ± 0.5, ± 1.0, ± 1.5 and ± 2.0 kV/mm for 300 seconds respectively. Left: Dielectric hysteresis. Right: Butterfly hysteresis.

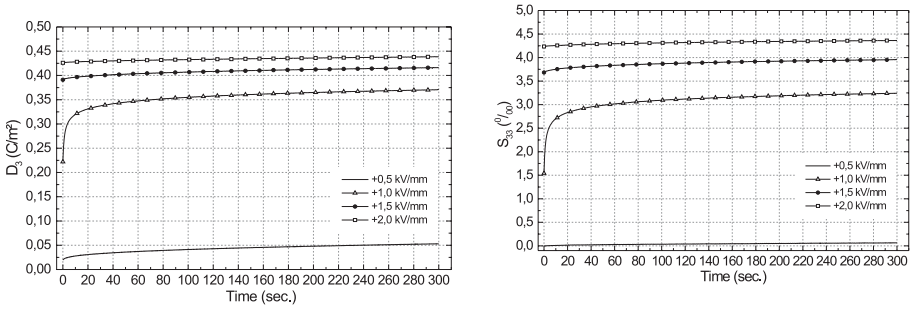

Figure 2.12: Change of polarization and strain during the hold time.

electric field increases from zero to +2 kV/mm and changes in polarization and strain at a constant electric field of 0.50, 1.00, 1.50 and 2.00 kV/mm are plotted *vs.* hold time in Figure 2.12. We can see that both polarization and strain exhibit a creep-like increase under constant electric field. As hold time increases, the changes gradually slow down and tend to saturate eventually. The creep-like development is most pronounced at 1.00 kV/mm, which is close to the coercive field of PIC151 soft PZT. For example, the initial polarization and strain at the beginning of this hold time are 0.222 C/m^2 and 0.1544%, respectively, and they increase up to 0.371 $C/m^2$and 0.3243%, respectively, after five minutes of electric field holding.

The time-dependent effect of this material is found to depend on the magnitude of the external electric field load. As seen in Figure 2.13, only slightly more polarization and strain are further induced during the hold time

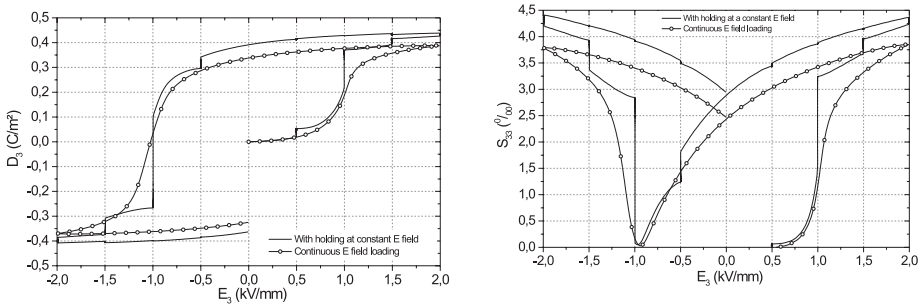

Figure 2.13: Comprison of polarization (left) and strain (right) responses to electric loading with and without hold time.

at +0.50 kV/mm. This is because, under such a low external electric field loading, most of the regions in the material possess a local electric field lower than the coercive field. With the passage of time, only a little amount of domain switching is further induced in some regions where the local electric field is approaching the coercive field. With further external electric field increase from 0.50 to 1.00 kV/mm, the coercive field will be reached in more regions in the material. A large amount of domain switching results in a significant polarization and strain increment. For the continuous loading test, the induced polarization and strain at +1.00 kV/mm are about 0.189 C/m^2 and 0.1174%, respectively. While, for the hold time experiment, the polarization and strain values at the beginning of holding at +1.00 kV/mm are 0.222 C/m^2 and 0.1544%, respectively. The larger polarization and strain values are apparently due to the contribution of time-dependent effects at +0.50 kV/mm.

The most pronounced time-dependent effect is observed at +1.00 kV/mm, which corresponds to the macroscopic coercive field of this material. During the hold time of 300 seconds, both polarization and strain increase significantly. At the end of the hold time, the new values are 0.371 C/m^2 and 0.3243% for polarization and strain, respectively. To achieve the same values in the continuous loading test, the applied electric field has to be increased up to about +1.70 kV/mm for polarization and +1.45 kV/mm for strain, respectively.

Since most of the domains have been switched during the long hold time at +1.00 kV/mm, from the end of holding at +1.00 kV/mm to the beginning of holding at +1.50 kV/mm, linear dielectric behavior and inverse piezoeffect should be the essential contributions to polarization and strain responses in

this loading period. For the subsequent electric field holding at +1.50 and +2.00 kV/mm, the time-dependent effect can still be observed but becomes relatively weaker.

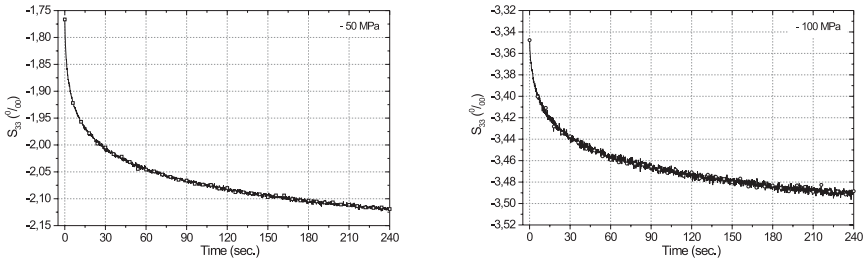

Figure 2.14: Change of strain with time under constant stress levels of -50 and -100 MPa of an unpoled specimen subjected to compressive stress.

Similar to the time-dependent effects under pure electric field loading conditions, strains induced at each constant stress level during the increase loading period exhibit creep-like behavior. Changes of strain with time under constant stress levels of -50 and -100 MPa are given in Figure 2.14, respectively.

In summary, polarization and strain exhibit creep-like behavior with the passing of time. In the case of a pure electric load, the time-dependence is most pronounced when holding the electric field close to the coercive field. While under pure mechanical loading, the most distinct time-dependent effect occurs at the stress level corresponding to the inflection point of the nonlinear stress-strain curve. It was considered that the macroscopic time-dependent polarization and strain responses were caused by further microscopic domain switching process, which was gradually induced during the hold time of the external load.

Besides the test results outlined above, Zhou [2003] also observed the material response to constant electric and mechanical loading during a holding time in the unloading phase. Detailed exprimental results and discussions are found in his dissertation.

Up to now, the mechanisms responsible for the time-dependent effects in piezoceramics have not been credibly explained. The commercial piezoceramics such as PIC151 soft PZT used in the experiments by Zhou [2003] are very sophisticatedly doped systems, whose microstructures are very complex. It is not single crystal, and various phases may coexist in the material simultaneously. Impurities and defects also exist. Under macroscopic uniform

electromechanical loading, local concentrations of electric field or stress may occur in the material, phase transition can be induced, and defect diffusion can also occur. More experimental and theoretical studies are needed for the understanding of the mechanisms, but this is subject of a seperat study.

2.5 Multiaxial experiments

There are very few experimental investigations into the behavior of piezoceramics under multiaxial electromechanical loads. Here we outline the experiments by Huber and Fleck [2001], Lynch *et al.* [2000] and Chen and Lynch [2001].

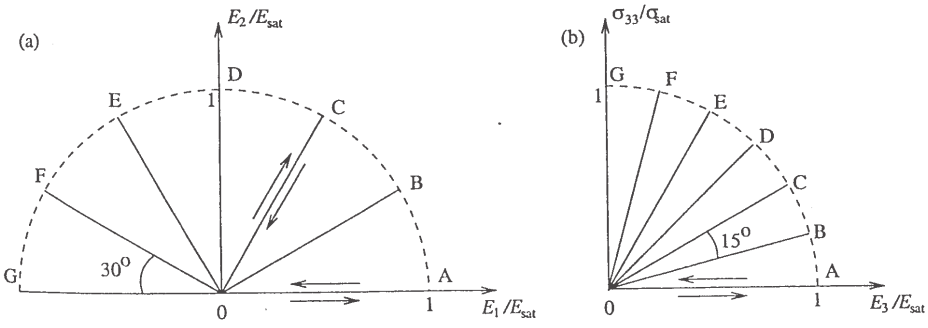

Figure 2.15: Loading paths for multiaxial electric loading and proportional electromechanical loading. Left: Intially unpoled material was poled along one of the paths OA-OG and then unloaded. After angled specimens were cut from the material, each specimen was loaded along path OA and unloaded. Right: Proportional loading with uniaxial stress σ_{33} (T_{33}) and electric field E_3. Initially unpoled specimens were loaded along one of the paths OA-Og and unloaded (Huber *et al.* [2002])

Huber and Fleck [2001] experimentally studied the multiaxial responses of hard and soft ferroelectrics under stress and electric field. Two loading paths were adopted in their experiments: (i) Poling with electric field, followed by repoling with electric field at an angle to the original poling direction, (ii) Propotional loading with electric field and coaxial compressive stress, see Figure 2.15. The materials tested in their study are soft PZT-5H, PZT-4D and Barium Titanate.

In case (i) specimens of these three materials were at first poled by application of an electric field. After poling, electric fields were applied at angles

of 0°, 30°, 60°, 90°, 120° and 180° to the remanent polarization direction, which cause the polarization to change in direction and magnitude. The change of the polarization in each direction was measured.

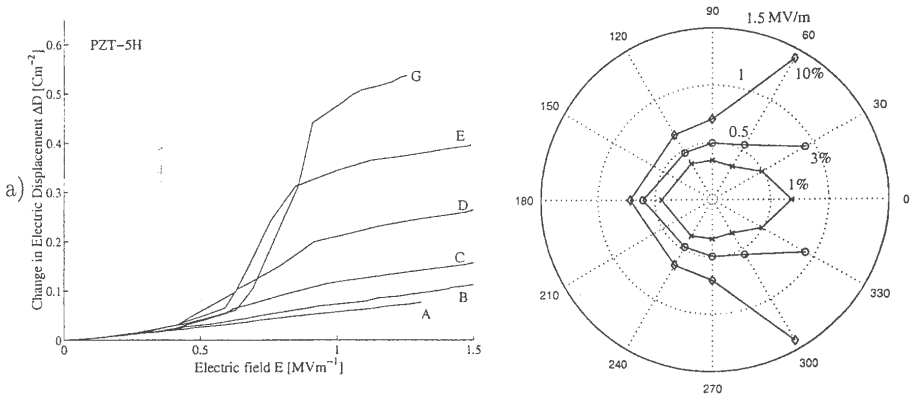

Figure 2.16: Measured response to a polarization rotation test for PZT-5H. Left: The change in electric displacement *vs.* electric field responses of specimens poled along paths A-G shown in Figure 2.15, angled at various angles to the loading direction. Right: Corresponding offset switching surfaces.

Figure 2.16 shows their test results. The letters A-G marked on the curves correspond to the loading paths shown in Figure 2.15. The right-hand side figure shows corresponding offset switching surfaces, with the radial axis showing the electric field and the polar axis showing the angle of the applied electric field direction to the initial poling direction. For each material, switching surfaces are shown for three levels of offset corresponding to 1%, 3% and 10% of the remanent polarization after the first poling.

In case (ii) coaxial electric fields and compressive stresses of different fixed proportions are applied on the specimens simutaneously, as seen on the right side of Figure 2.15. Figure 2.17 shows the measured polarization versus electric field (left panel) and polarization versus stress (right panel) relations for PZT-5H. Similar to case (i), switching curves corresponding to offsets of 1%, 3% and 10% of the initial remanent polarization are drawn on the electric field-stress plane in Figure 2.18. These experimental results are very helpful for a deeper understanding of the material behavior and for the formulation of a switching criterion in the general electromechanical loading case.

The material used in the experiments by Lynch *et al.* [2000] and Chen and Lynch [2001] was unpoled PLZT 8/65/35. The poled and unpoled

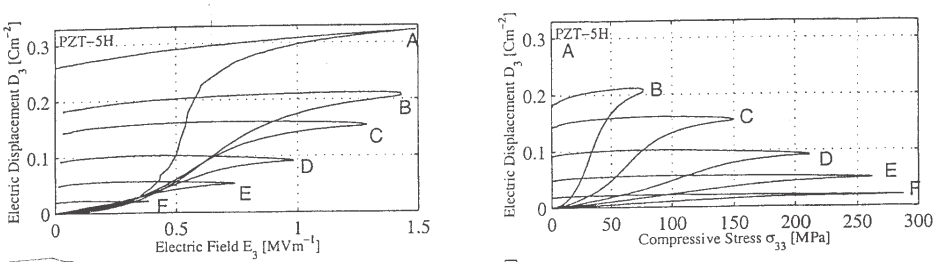

Figure 2.17: Measured response to a propoetional loading test for PZT-5H. The stress and electric field loads follow the paths A-G in the right panel of Figure 2.15.

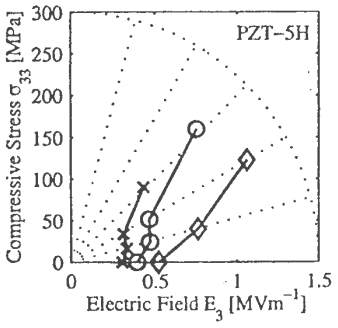

Figure 2.18: Offset switching surfaces under proportional loading for PZT-5H, corresponding to the responses shown in Figure 2.17.

specimens were 25 mm long tubes with inner and outer diameters of 10.2 mm and 12.7 mm respectively. At first they applied an axial force of 200 N to the specimen. After preloading, the displacement was held constant. After the load had stablized, the inner pressure and/or outer pressure was increased to the desired level. The axial force was then increased to some maximum value at a constant rate, and then decreased to the preload level. Stress-strain loops for each loading cycle were monitored. From the test results they found that the yield (switching) of the material can be described by a Tresca yield rule. We will discuss this further in the Chapter 3.

Chapter 3

Phenomenological constitutive models

Besides the experimental investigations into the electromechnical behavior of piezoceramic materials, a great deal of research activities have been carried out in the field of continuum theoretical modeling of constitutive properties of piezoceramics. This comparably new field is motivated by the need to calculate the stress states in piezoceramic devices as precisely as possible as a basis for reliability analyses.

In this section we only make a brief dicussion of several recently published phenomenological models, which have a high reference value to our present research. For a detailed discussion of the literature, the reader is referred to the review article by Kamlah [2001].

Lynch [1998] published a model based on a set of internal variables characterizing the domain state in terms of degree of relative polarization and the degree of alignment of c-axes. The model is restricted to proportonal loading, where the principal directions of stress and strain are fixed and coincide. The dependence of the internal variables on the principal stresses takes into account different states of loading and unloading, thus realizing the representation of hysteresis effects. The model is capable of representing the electric, butterfly and ferroelastic hysteresis and due to the choice of the internal variables it posesses a sound, microscopically motivated basis. In Lynch and Chen [2000] and Chen and Lynch [2001] the only published multiaxial experiments for mechanical loading of a thin walled piezoceramic tube to date have been reported. Based on experimental results the electromechanical domain switching criterion

$$1 = \max\left(\left|\frac{\sigma_1-\sigma_2}{\sigma^{\mathrm{c}}}+\left|\frac{\mathrm{E}_1}{\mathrm{E}^{\mathrm{c}}}\right|\right|,\left|\frac{\sigma_2-\sigma_3}{\sigma^{\mathrm{c}}}+\left|\frac{\mathrm{E}_2}{\mathrm{E}^{\mathrm{c}}}\right|\right|,\left|\frac{\sigma_3-\sigma_1}{\sigma^{\mathrm{c}}}+\left|\frac{\mathrm{E}_3}{\mathrm{E}^{\mathrm{c}}}\right|\right|\right)$$

was proposed. This criterion is an extention of the Tresca yield condition in plasticity by taking the electric field into account, in which σ_1, σ_2 and σ_3 are principal stresses, and E^{c} and σ^{c} are *coercive field* and *coercive stress* respectively. For example, for an electromechanical loading with $\mathrm{E}_1 = \mathrm{E}_2 = \mathrm{E}_3 = \frac{\sqrt{3}}{3}\mathrm{E}^{\mathrm{c}}$, $\sigma_1 = 0.1\sigma^{\mathrm{c}}$ and $\sigma_2 = \sigma_3 = 0$ the electric field vector reaches the coercive strength, $\sqrt{\mathrm{E}_i\mathrm{E}_i} = \mathrm{E}^{\mathrm{c}}$, and, additionally, there is superposed a tensile stress. But according to the above criterion, domain switching will not occur, because of which its validity is questionable.

In a recent paper Fett *et al.* [2003] presented their torsion tests carried out on a thin-walled tube made of a commercial soft PZT. These test results in combination with literature results from tensile and compressive tests allowed to the determination of the non-symmetric switching condition for the remanent deformation. They found that the Drucker-Prager criterion is in good agreement with the experimental results. This finding is based on pure mechanical loading tests, *i.e.*, an electric field is not taken into account.

A constitutive model for piezoceramics under pure electric loading is presented in Drescher *et al.* [1999, 2000]. This model also starts from the additive decompostion of the polarization and it takes into account the dependence of the transversely isotropic permittivity tensor on the direction of the polarization. An incremental evolution rule for the remanent polarization is derived from the formulation of the release of dielectric energy due to switching, and the tangent permittivities are computed. Kessler and Balke [2001] reformulated the model on the basis of a macroscopic average energy release density and extended it to the fully coupled electromechanical loading. Even though the model can only be applied to the description of the rotation of a prepoled state, it appears to be promising due to its sound physical basis and its consistent formulation. In Kessler *et al.* [2002], the model has been implemented in a finite element code and applied to the analysis of elliptic flaws. Based on the aforementioned domain switching condition, the stability of switching is analysed in Kessler *et al.* [2000]. In this context, the macroscopic fields are derived by means of an approximate representation of an orientation distribution function for the domains.

In Cocks and McMeeking [1999] a constitutive model for piezoceramics is developed in the tradition of incremental plasticity for uniaxial electromechanical loading. The model is based on the additive decomposition of polarization and strain. A convex quadratic yield surface in the space of uniaxial electric field and mechanical stress is introduced to indicate the onset of remanent polarization and remanent strain. The evolution equations for remanent polarization and strain are derived from this yield function by the normality rule and consistency condition. Similar to the kinematic hardening rule in incremental plasticity, a back electric field and a back stress

are included in the model, whose evolution equations are derived from the irreversible part of the free energy. The irreversible part of the free energy is given such that the dielectric and butterfly hystereses can be represented reasonably well.

Landis and McMeeking [1999] introduced a phenomenological constitutive law for ferroelastic switching in unpoled piezoceramics under pure mechanical loading based on the additive decomposition of strain. The elastic properties are related to the remanent strain. A switching condition of the von Mises type is used to characterize the onset of remanent deformation. The normality rule is adopted for the calculation of remanent strain increments. As an additional property, the saturation of the remananet strains due the fully switched domain structure is considered by means of so-called lock-up criteria.

Landis [2001, 2002] united the approaches by Cocks and McMeeking [1999] and Landis and McMeeking [1999] to yield a very promising phenomenological model for the fully coupled electromechanical constitutive behavior of piezoceramics. As it seems, a wide range of ferroelectric and ferroelastic hysteresis phenomena is covered by this thermodynamically consistent model by means of a sophisticated switching surface depending on appropriately chosen invariants (relying with respect to electromechanical coupling on a term lend from Huber and Fleck [2001]). However, there seem to be difficulties to represent correctly the fact that not all irreversible polarization and strain states can exist simultaneously. It is tried to handle this constraint by complicated constitutive functions, which are not easy to interpret.

The problems just mentioned are avoided (but not solved) in the model of Landis and McMeeking [2002], which can be looked at as a special case of the former with the irreversible strain tensor being a quadratic function of the irreversible polarizaion vector. This means, only electrically induced irreversible strains are possible, and this restriction may exclude the applicability of the model for many cases of practical importance.

Landis [2003] focusses on the interesting problem of the asymmetry in the attainable levels of remanent strain in tension versus compression. Motivated by the result of Fröhlich [2001] mentioned in Section 2.2, the micromechanical model of Huber *et al.* [1999] was used to probe the full range of remantent strain saturation states in a first step. In this way, the result of Fröhlich [2001], predicting a much smaller amount of asymmetry as might be expected at first sight, was confirmed. As the second step, a phenomenological saturation criterion was formulated within the constitutive framework discussed above for the special case of pure ferroelastic behavior of piezoceramics. The criterion is based on carefully selected invariants of the

remanent strain tensor and was calibrated by means of the micromechanical results derived before. While the coupling with the ferroelectric behavior under electric loadings remains an open issue, the purely ferroelastic behavior of a tetragonal polycrystal seems to be represented in a satisfying manner by this model.

With the one-dimensional model from COCKS AND MCMEEKING [1999] as a starting point, HUBER AND FLECK [2001] developed a rate-independent phenomenological model for ferroelectrics under general electromechanical loading. Remanent strain and remanent polarization are used as internal variables. Similar to plasticity, the yield (switching) function is used to characterize the onset of remanent polarization and deformation. The yield surface is a function of stress invariants, electric field and internal variables and a special electromechanical term takes care of electromechanical loadings. The increase in remanent strain and polarization are given by the associated normality rule, and the plastic multiplier is determind by the consistency condition. A lock-up condition, which represents the saturation state of the material, constrains the evolution of the internal variables. However, this criterion does not represent general electromechaical loadings.

KAMLAH *et al.* [1997] and KAMLAH AND TSAKMAKIS [1999] introduced a constitutive model representing the large signal hysteresis behavior of piezoceramics in a simplified manner. In this model the remanent polarization and the remanent strain are used as internal variables, which are governed by ordinary differential equations. Each of these evolution equations is subjected to two loading conditions of different natures. The first one indicates the onset of the changes in the remanent quantities by domain switching, while the second one characterizes the saturation value of a remanent quantity corresponding to a fully switched domain structure. This multitude of loading conditions ensures that only physically possible states of remanent polarization and strain are allowed, however, at the same time they make it hard to follow the formulation of the model and to treat it numerically. There are open questions with respect to the asymmetry in tension and compression, thermodynamic embedding, and rate dependent formulation of the model.

The model was implemented in a finite element code by KAMLAH AND BÖHLE [2001]. Irrespective of any shortcomings, finite element calculations based on this model clearly demonstrated the necessity to include for a sound physical understanding of piezoceramic components from an engineering point of view the ferroelectric and -elastic hysteresis effects in the stress analysis of piezoceramic components.

Chapter 4

Continuum theory of thermo-electromechanics

A continuum theory is given by two classes of equations. First, there is a system of partial differential equations, which is derived from universal balance laws holding for all bodies. As must be expected from the physical point view, this system is not sufficient for determining the unknown quantities. Additional information must be provided taking into account the specific properties of the material the body consists of. This is done by the second class of equations, the so-called constitutive equations.

The emphasis of this research project is in the field of constitutive modeling. However, according to our long term experience in the field of electromechanics, the commonly used, extremely simplified version of the balance laws needs profound reconsideration. There are definitely cases, where the underlying assumptions of this version are not justified or need discussion. Therefore it is one of our objectives, to derive the balance laws from the general case by employing step by step simplifying assumptions. In this way, it becomes obvious, for which particular application the theory has to used at which level of generality.

For the mathematical representation of the theory in this report, we introduce the following conventions: All component representations of tensors are referred to a Cartesian coordinate system. Cartesian index notation will be employed with summation over doubly repeated indices. When using symbolic notation, first order tensors (*vectors*) will be denoted by upright letters with superscript arrows ($\vec{\mathrm{a}}$, $\vec{\mathrm{A}}$) and second order tensors (*tensors*) by bold slanted letters ($\boldsymbol{a}$, $\boldsymbol{A}$, $\boldsymbol{\alpha}$). A dot between tensors indicates the contraction relative to one index, for example, the inner product between vectors, *i.e.*, $\vec{\mathrm{a}} \cdot \vec{\mathrm{b}} = \mathrm{a}_i \mathrm{b}_i$, the composition of two tensors, it i.e., $\boldsymbol{A} \cdot \boldsymbol{A}^{-1} = \boldsymbol{I}$ ($\boldsymbol{A}^{-1}$: inverse of $\boldsymbol{A}$, $\boldsymbol{I}$: identity tensor, $(\boldsymbol{I})_{ij} = \delta_{ij}$, $\delta_{ij} = 1$ for $i = j$ and $\delta_{ij} = 0$ for

$i \neq j$), the inner product between tensors, *i.e.*, $\boldsymbol{A} : \boldsymbol{B} = \mathrm{tr}(\boldsymbol{A} \cdot \boldsymbol{B}^T) = A_{ij}B_{ij}$ ($\mathrm{tr}\boldsymbol{A}$: trace of $\boldsymbol{A}$. $\boldsymbol{B}^T$: transpose of $\boldsymbol{B}$), the linear mapping of a vector by a tensor, *i.e.*, $\boldsymbol{A} \cdot \vec{\mathrm{a}} = A_{ij}\mathrm{a}_j$. $\boldsymbol{A}^D = \boldsymbol{A} - \frac{1}{3}(\mathrm{tr}\boldsymbol{A})\boldsymbol{I}$ stands for the deviator of $\boldsymbol{A}$ and $\|\boldsymbol{A}\| = \sqrt{\boldsymbol{A} : \boldsymbol{A}}$ is the norm of the tensor $\boldsymbol{A}$. $\vec{\mathrm{e}}_{\mathrm{a}} = \vec{\mathrm{a}}/\|\vec{\mathrm{a}}\|$ is the unit vector in the direction of the vector $\vec{\mathrm{a}}$ ($\|\vec{\mathrm{a}}\| = \sqrt{\vec{\mathrm{a}} \cdot \vec{\mathrm{a}}}$: norm of $\vec{\mathrm{a}}$). For a third order tensor $\mathbf{dl}$ the follwing defintions are made: $(\mathbf{dl} : \boldsymbol{A})_k = (\mathbf{dl})_{kij}A_{ij}$, $(\mathbf{dl}^T \cdot \vec{\mathrm{a}})_{ij} = (\mathbf{dl})_{kij}\mathrm{a}_k$, $(\mathbf{dl}^T)_{ijk} = (\mathbf{dl})_{kij}$, and $\mathrm{d}_{ijk} = (\mathbf{dl})_{ijk}$. The symbol $\otimes$ indicates the dyadic product, e. g. $\vec{\mathrm{a}} \otimes \vec{\mathrm{b}}$ yields a second order tensor with components $\mathrm{a}_i\mathrm{b}_j$. The component representation of the cross product $\vec{\mathrm{a}} \times \vec{\mathrm{b}}$ between two vectors can be written by means of the alternating symbol: $(\vec{\mathrm{a}} \times \vec{\mathrm{b}})_i = \varepsilon_{ijk}\mathrm{a}_j\mathrm{b}_k$, where $\varepsilon_{ijk} = 1$ for a cyclic permutation of {1,2,3}, $\varepsilon_{ijk} = -1$ for an anti-cyclic permutation of {1,2,3}, and $\varepsilon_{ijk} = 0$ otherwise. An index following a comma denotes the partial deriviative with respect to the corresponding space coordinate: $()_{,i} = \partial()/\partial \mathrm{x}_i$. div is the divergence operator: $(\mathrm{div}\,\vec{\mathrm{a}}) = \mathrm{a}_{i,i}$, $(\mathrm{div}\,\boldsymbol{A})_i = A_{ij,j}$, and grad symbolizes the gradient operator: $(\mathrm{grad}\,a)_i = a_{,i}$, $(\mathrm{grad}\,\vec{\mathrm{a}})_{ij} = \mathrm{a}_{i,j}$. $\dot{()} = \mathrm{d}()/\mathrm{d}t$ denotes the material time derivative of a field $()$. The componenent of the curl of a vector field can be represented with the help of the alternating symbol: $(\mathrm{curl}\,\vec{\mathrm{a}})_i = \varepsilon_{ijk}\mathrm{a}_{k,j}$. Very often, we will not distinguish between a function and its value. $\approx$ means "approximately equal". Further mathematical definitions will be given where they are needed.

4.1 Balance laws

A set of *material points* $\mathcal{X}$ constitutes a *material body* $\mathcal{B} = \{\mathcal{X}\}$, to which an arbitrary but fixed *reference configuration* $R : \mathcal{X} \mapsto \vec{\mathrm{X}} = R(\mathcal{X})$ is assigned. This allows for the referential representation of the *motion*

$$\vec{\mathrm{x}} = \vec{\chi}_R(\vec{\mathrm{X}}, t) \quad , \tag{4.1}$$

yielding the position $\vec{\mathrm{x}}$ of $\mathcal{X}$ in the *current configuration* $\vec{\chi}_R(R(\mathcal{B}), t)$ at every instant t. The component representation of the motion is taken as

$$\mathrm{x}_i = \mathrm{x}_i(\mathrm{X}_K, t) \quad , \tag{4.2}$$

where lower case and capital indices refer to the the current and reference configurations, respectively. From the motion, the *deformation gradient*

$$\boldsymbol{F} = \frac{\partial\, \vec{\chi}_R(\vec{\mathrm{X}}, t)}{\partial \vec{\mathrm{X}}} \quad , \quad F_{iL} = \mathrm{x}_{i,L}(\mathrm{X}_K, t) \tag{4.3}$$

can be derived, which possesses the polar decomposition

$$\boldsymbol{F} = \boldsymbol{R} \cdot \boldsymbol{U} \quad , \quad F_{iL} = R_{iK} U_{KL} \tag{4.4}$$

into the orthogonal *rotation tensor* $\boldsymbol{R}$ and the symmetric, positive definite *right stretch tensor* $\boldsymbol{U}$. Furthermore, we introduce the *displacement gradient* as

$$\boldsymbol{H} = \frac{\partial \vec{\mathrm{u}}(\vec{\mathrm{X}}, t)}{\partial \vec{\mathrm{X}}} \quad , \tag{4.5}$$

where

$$\vec{\mathrm{u}} = \vec{\chi}_R(\vec{\mathrm{X}}, t) - \vec{\mathrm{X}} \tag{4.6}$$

is the *displacement vector*. Then the *Green's strain tensor* is given by

$$\boldsymbol{G} = \tfrac{1}{2}\left(\boldsymbol{F}^T \cdot \boldsymbol{F} - \boldsymbol{I}\right) = \tfrac{1}{2}\left(\boldsymbol{H} + \boldsymbol{H}^T + \boldsymbol{H}^T \cdot \boldsymbol{H}\right) \quad , \tag{4.7}$$

$$G_{KL} = \tfrac{1}{2}\left(u_{K,L} + u_{L,K} + u_{K,M} u_{M,L}\right) \tag{4.8}$$

The *velocity* is given by

$$\vec{\mathrm{v}} = \frac{\mathrm{d}\vec{\mathrm{x}}}{\mathrm{d}t} = \frac{\partial\, \vec{\chi}_R(\vec{\mathrm{X}}, t)}{\partial t} \quad , \quad \mathrm{v}_i = \frac{\partial \mathrm{x}_i(\mathrm{X}_K, t)}{\partial t} \quad , \tag{4.9}$$

with the property

$$\frac{\mathrm{d}()}{\mathrm{d}t} = \frac{\partial()}{\partial t} + ()_{,i} \mathrm{v}_i \quad . \tag{4.10}$$

The *velocity gradient* is then defined as

$$\boldsymbol{L} = \mathrm{grad}\vec{\mathrm{v}}(\vec{\mathrm{x}}, t) \quad , \quad L_{ij} = \mathrm{v}_{i,j} \quad , \tag{4.11}$$

the symmetric and antisymmetric parts of which according to

$$\boldsymbol{L} = \boldsymbol{D} + \boldsymbol{W} \tag{4.12}$$

are called *strain rate tensor* and *spin tensor*, respectively.

If not stated otherwise, we will employ in the following a *spatial representation* of the theory, *i.e.*, vector and tensor fields refer to the current configuration.

Right at the beginning of our considerations we introduce the first simplification:

Assumption 1:
Any relativistic effects are neglected.

Thus, the most general framework of balance laws for continua consists of a combination of Maxwell's equations of classical electro-magneto-dynamics and the classical balance equations of thermomechanics. The uncoupled electric and mechanical theories are represented in the classical textbooks Landau and Lifschitz [1960], Jackson [1975], Truesdell and Noll [1965], and Gurtin [1981], to mention but a view prominent examples. The coupled theory is discussed in the textbooks Hutter *et al.* [1978], Maugin [1988], and Eringen and Maugin [1989]. (A first look at these works gives an impression of the breathtaking complexity of the theory, and this is probably the reason, why most authors (including us) usually turn without discussion to the most simplyfied version of the theory.) Recently, a very fine discussion of the combined theory focussed on appilcations closely related to the topic of our project has been given in Harper [1999] and was summarized in Harper and Hagood [2000].

4.1.1 Reduced Maxwell's Equations

Before we get into equations, let us make from the beginning on a second assumption which means no loss of generality with respect to the topic of our research project:

> **Assumption 2:**
> The partial derivative of the *magnetic induction* $\vec{\mathrm{B}}$ and the magnetic induction itself can be neglected:
>
> $$\frac{\partial \vec{\mathrm{B}}}{\partial t} \approx \vec{0} \quad , \quad \vec{\mathrm{B}} \approx \vec{0} \tag{4.13}$$

Here, the first relation is the usual "electroquasistatic" assumption. Additionally, static magnetic induction is disregarded for convenience by the second relation, as it allows to eliminate magnetic terms from the coupling terms in the thermomechanical balance laws. (For a quasi-electrostatic approximation for the special case of a elastic dielectric see Maugin [1988], p. 235ff.) Assumption 2 will be justified in our case, as piezoceramic materials are very bad conductors with a specific resistance of at least $10^9\ \Omega$ cm. Thus, for weak electric currents, the magnetic fields are taken to be negligible (Harper [1999], p. 34, Harper and Hagood [2000], p. 29). On the other hand, the idealization as perfect insulator is not necessarily adequate for actuator applications with a quasistatic rate of change of the loading. In this case, there may be enough time for the migration of free charges due to external or depolarizing electric fields to modify the electromechanical state of the body under consideration.

In view of Assumption 2, the local and global forms of Maxwell's Equations are reduced (HARPER [1999], p. 34f, HARPER AND HAGOOD [2000], p. 29, cf. ERINGEN AND MAUGIN [1989], p. 51 and JACKSON [1975], p. 254f). In the following, V denotes the volume of the material body $\mathcal{B}$ in the current configuration and ∂V its surface with outward normal $\vec{\mathrm{n}}$, while C is a material line in the body.

The *electric displacement vector* is defined as

$$\vec{\mathrm{D}} = \vec{\mathrm{P}} + \epsilon_0 \vec{\mathrm{E}} \quad , \tag{4.14}$$

where $\vec{\mathrm{P}}$ is the *polarization vector*, ϵ_0 is the *dielectric constant in vacuo*, and E is the *electric field vector*.

Gauß' Law:

$$\mathrm{div}\,\vec{\mathrm{D}} = q^{\mathrm{f}} \quad , \quad \oint_{\partial V} \vec{\mathrm{D}} \cdot \vec{\mathrm{n}}\ \mathrm{d}A = \int_V q^{\mathrm{f}}\ \mathrm{d}V \tag{4.15}$$

Here, q^{f} is the *density of free charges*. From Faraday's Law, it follows that the electric field vector can be represented by the scalar *electric potential* φ.

electric potential:

$$\vec{\mathrm{E}} = -\mathrm{grad}\varphi \quad , \quad \oint_C \vec{\mathrm{E}} \cdot\ \mathrm{d}\vec{\mathrm{x}} = 0 \tag{4.16}$$

Furthermore, Ampère's Law yields the

conservation of charge:

$$\frac{\mathrm{d}q^{\mathrm{f}}}{\mathrm{d}t} + q^{\mathrm{f}}\mathrm{div}\vec{\mathrm{v}} + \mathrm{div}\vec{\mathrm{J}} = 0 \quad , \quad \frac{\mathrm{d}}{\mathrm{d}t}\int_V q^{\mathrm{f}}\ \mathrm{d}V + \oint_{\partial V} \vec{\mathrm{J}} \cdot \vec{\mathrm{n}}\ \mathrm{d}A = 0 \tag{4.17}$$

Here, $\vec{\mathrm{J}}$ is the *conduction current*. The conservation of magnetic flux becomes trivial.

4.1.2 Thermomechanical balance laws with electric coupling terms

For a theory of thermo-electromechanics, to the balance laws of thermomechanics terms are added that represent the influence of the electric fields on the thermomechanical fields. For the form of these terms see HUTTER *et al.*

[1978], Maugin [1988], p. 170-182, Eringen and Maugin [1989], p. 55-65, Harper [1999], p. 36-47, and Harper and Hagood [2000], p. 28f. Again, we give the balance laws in local and global form. The definition and motivation of these coupling terms will be given right after summarizing the balance laws.

conservation of mass:

$$\frac{\mathrm{d}\rho}{\mathrm{d}t} + \rho \,\mathrm{div}\vec{\mathrm{v}} = 0 \quad , \quad \frac{\mathrm{d}}{\mathrm{d}t}\int_V \rho \,\mathrm{d}V = 0 \tag{4.18}$$

Here, ρ is the *mass density*. The *Cauchy stress tensor* $\boldsymbol{T}$ yields the surface force density $\vec{\mathrm{t}} = \boldsymbol{T} \cdot \vec{\mathrm{n}}$ called *traction vector* (see the remark in Hutter *et al.* [1978], p. 10).

balance of linear momentum:

$$\rho \frac{\mathrm{d}\vec{\mathrm{v}}}{\mathrm{d}t} = \mathrm{div}\,\boldsymbol{T} + \rho\,\vec{\mathrm{k}} + \rho\,\vec{\mathrm{k}}^{\mathrm{e}} \quad , \tag{4.19}$$

$$\frac{\mathrm{d}}{\mathrm{d}t}\int_V \rho\,\vec{\mathrm{v}}\;\mathrm{d}V = \int_{\partial V} \vec{\mathrm{t}}\;\mathrm{d}A + \int_V (\rho\,\vec{\mathrm{k}} + \rho\,\vec{\mathrm{k}}^{\mathrm{e}})\;\mathrm{d}V \tag{4.20}$$

Here, $\vec{\mathrm{k}}$ is the *volume force* and $\vec{\mathrm{k}}^{\mathrm{e}}$ is the electric volume force or *ponderomotive force*. Different from a purely thermomechanical theory, the Cauchy stress tensor is in general not symmetric.

balance of moment of momentum:

$$\boldsymbol{T} - \boldsymbol{T}^T = \boldsymbol{M}^{\mathrm{e}} \quad , \tag{4.21}$$

$$\frac{\mathrm{d}}{\mathrm{d}t}\int_V (\vec{\mathrm{x}} - \vec{\mathrm{x}}_0)\times(\rho\vec{\mathrm{v}})\;\mathrm{d}V =$$

$$\int_{\partial V} (\vec{\mathrm{x}} - \vec{\mathrm{x}}_0)\times\vec{\mathrm{t}}\;\mathrm{d}A + \int_V \left((\vec{\mathrm{x}} - \vec{\mathrm{x}}_0)\times(\rho\vec{\mathrm{k}} + \rho\vec{\mathrm{k}}^{\mathrm{e}}) + \rho\,\vec{\mathrm{m}}^{\mathrm{e}}\right)\;\mathrm{d}V \tag{4.22}$$

Here, the electric moment stress or *ponderomotive couple* $\vec{\mathrm{m}}^{\mathrm{e}}$ is the axial vector of the antisymmetric part $\boldsymbol{M}^{\mathrm{e}}$ of the Cauchy stress tensor, and $\vec{\mathrm{x}}_0$ corresponds to an arbitrary fixed reference point.

balance of energy:

$$\rho \frac{\mathrm{d}e}{\mathrm{d}t} = \boldsymbol{T} : \boldsymbol{L} - \operatorname{div} \vec{\mathrm{q}} + \rho\, r + \rho\, r^{\mathrm{e}} \quad , \tag{4.23}$$

$$\frac{\mathrm{d}}{\mathrm{d}t} \int_V (\frac{1}{2}\, \rho\, \vec{\mathrm{v}}^2 + \rho\, e)\ \mathrm{d}V =$$

$$\int_{\partial V} (\vec{\mathrm{t}} \cdot \vec{\mathrm{v}} - \vec{\mathrm{q}} \cdot \vec{\mathrm{n}})\ \mathrm{d}A + \int_V \Big((\rho\, \vec{\mathrm{k}} + \rho\, \vec{\mathrm{k}}^{\mathrm{e}}) \cdot \vec{\mathrm{v}} + \rho\, r + \rho\, r^{\mathrm{e}} \Big)\ \mathrm{d}V \tag{4.24}$$

Here, e is the *internal energy density*, $\vec{\mathrm{q}}$ is the *heat flux vector*, r is the *volume heat supply density*, and r^{e} is the *electric power density*. The balance of entropy in form of the Clausius Duhem inequality is not modified and reads in its local form as

$$\rho \frac{\mathrm{d}\eta}{\mathrm{d}t} \geq - \operatorname{div} \Big(\frac{\vec{\mathrm{q}}}{T} \Big) + \rho\, \frac{r}{T} \quad , \tag{4.25}$$

where η is the *entropy density* and $T > 0$ is the *absolute temperature*.

We now turn to the definition and motivation of the additional electric terms. Beside its thermomechanical properties, each material point $\mathcal{X}$ in a macroscopic thermo-electromechanical continuum is equiped with additional properties. The first one is a value of the density of free charges q^{f}, so to say, a local charge. The second one is a value of the polarization vector $\vec{\mathrm{P}}$, which is the density of the total dipolmoment of the body (for this physical interpretation see, for instance, Landau and Lifschitz [1960], p. 36-37). Furthermore, there is a current density in the case of a non-perfect insulator, which allows for a stationary flow of charges.

The ponderomotive force is given by

$$\rho\, \vec{\mathrm{k}}^{\mathrm{e}} = q^{\mathrm{f}}\, \vec{\mathrm{E}} + \operatorname{grad} \vec{\mathrm{E}} \cdot \vec{\mathrm{P}} \quad . \tag{4.26}$$

The first term is motivated from the fundamental property of the electric field to represent the force on electric charges. The occurence of the second term corresponds to the fact that only in an inhomogenous electric field ($\operatorname{grad} \vec{\mathrm{E}} \neq \vec{0}$), there is a resultant force acting on an electric dipol. The ponderomotive force can be represented as the divergence of some tensor. For instance, the *electrostatic stress tensor*

$$\boldsymbol{T}^{\mathrm{e}} = \vec{\mathrm{E}} \otimes \vec{\mathrm{P}} + \epsilon_0 \Big(\vec{\mathrm{E}} \otimes \vec{\mathrm{E}} - \tfrac{1}{2} (\vec{\mathrm{E}} \cdot \vec{\mathrm{E}})\, \boldsymbol{I} \Big) \tag{4.27}$$

yields

$$\operatorname{div} \boldsymbol{T}^{\mathrm{e}} = q^{\mathrm{f}}\, \vec{\mathrm{E}} + \operatorname{grad} \vec{\mathrm{E}} \cdot \vec{\mathrm{P}} \quad . \tag{4.28}$$

In the global form of the balance of moment of momentum, the additional term $(\vec{\mathrm{x}} - \vec{\mathrm{x}}_0) \times \rho\vec{\mathrm{k}}^{\mathrm{e}} + \rho\,\vec{\mathrm{m}}^{\mathrm{e}}$ occurs with the ponderomotive couple being given by

$$\rho\,\vec{\mathrm{m}}^{\mathrm{e}} = \vec{\mathrm{P}} \times \vec{\mathrm{E}} \tag{4.29}$$

The density of the of the couple of the ponderomotive force $\rho\vec{\mathrm{k}}^{\mathrm{e}}$ is by analogy to the corresponding term for $\rho\vec{\mathrm{k}}$. The term $\rho\,\vec{\mathrm{m}}^{\mathrm{e}}$ is related to an additional local couple, caused by the electric field acting on the local dipolmoment $\vec{\mathrm{P}}$ of a material point. As a consequence of $\vec{\mathrm{m}}^{\mathrm{e}}$, the Cauchy stress tensor is not symmetric:

$$\boldsymbol{T} - \boldsymbol{T}^T = \boldsymbol{M}^{\mathrm{e}} = \vec{\mathrm{P}} \otimes \vec{\mathrm{E}} - \vec{\mathrm{E}} \otimes \vec{\mathrm{P}} \tag{4.30}$$

We recognize that the antisymmetric part of $\boldsymbol{T}$ is equal to the antisymmetric part of the electrostatic stress tensor.

In the balance of energy, the occurence of the term $\rho\vec{\mathrm{k}}^{\mathrm{e}} \cdot \vec{\mathrm{v}}$ is again by analogy to the corresponding term for $\rho\vec{\mathrm{k}}$. The additional electric power is given by

$$\rho\, r^{\mathrm{e}} = \rho\,\vec{\mathrm{E}} \cdot \frac{\mathrm{d}}{\mathrm{d}t}\left(\frac{\vec{\mathrm{P}}}{\rho}\right) + \vec{\mathrm{E}} \cdot \vec{\mathrm{J}} \quad . \tag{4.31}$$

From a thermodynamical point of view, the electric field has to be looked at as a force type quantity, as we have mentioned before. Thus, it plays in the energy balance an analogous role to the stress. The corresponding thermodynamic deformation quantity is the displacement of charges. With respect to the local dipole $\vec{\mathrm{P}}$, this results in a change of the polarization, *i.e.*, the so-called *displacement current*. Second, in a non-perfect insulator, a conduction current $\vec{\mathrm{J}}$ might occur, which can be stationary in contrast to the displacement current due to a change of the polarization.

4.1.3 Small deformations

In this research project, we consider piezoceramic materials where the maximum electrically and mechanically induced strains usually do not exceed the order of magnitude of one percent. Like for any other ceramic material, the right stretch tensor in the polar decomposition of the deformation gradient will therefore always be approximately equal to the unity tensor, $\boldsymbol{U} \approx \boldsymbol{I}$, implying that the deformation gradient nearly coincides with the rotation tensor $\boldsymbol{F} \approx \boldsymbol{R}$. Obviously, this finding means no loss of generality for ceramic materials, and it will result already in a simplification of the equations.

However, at this state of the project, the resulting theory has not yet been considered. Rather, we employ from now on the classical small deformation assumption, which leads to a geometrically linear theory.

Assumption 3:
The deformation Gradient $\boldsymbol{F}$ is approximately equal to the unity tensor:

$$\boldsymbol{R} \approx \boldsymbol{I} \quad , \quad \boldsymbol{U} \approx \boldsymbol{I} \tag{4.32}$$

It must be noted that the exclusion of finite rotations from the theory may be in conflict to applications to bending devices, where finite rotations may occur even though stretches are small. However, the simplification of the theory brought about by the small deformation assumption is very significant. In particular, the reference and current configurations coincide in first approximation, implying a constant mass density, $\dot{\rho} \approx 0$, and $\mathrm{div}\vec{\mathrm{v}} << 1$. Thus, material and partial time derivative can no longer be distinguished. Furthermore, there is no longer a need to distinguish between indices in the reference and current configurations. The most characteristic simplification however comes about from the fact that the norm of the displacement gradient is now small,

$$\|\boldsymbol{H}\| << 1 \quad , \tag{4.33}$$

and as a consequence the Green's strain tensor can be replaced by the *linear strain tensor*

$$\boldsymbol{S} = \tfrac{1}{2}\left(\boldsymbol{H} + \boldsymbol{H}^T\right) \quad , \quad S_{ij} = \tfrac{1}{2}\left(u_{i,j} + u_{j,i}\right) \quad , \tag{4.34}$$

i.e., the nonlinear terms are dropped to yield a linear geometrical setting. For the velocity gradient, it follows

$$\mathrm{v}_{i,j} \approx \dot{u}_{i,j} \quad , \quad \boldsymbol{L} \approx \dot{\boldsymbol{S}} + \boldsymbol{W} \quad , \tag{4.35}$$

where the spin tensor $\boldsymbol{W}$ is now approximately equal to the antisymmetric part of $\dot{u}_{i,j}$. For more details on geometric linearization see Haupt [2000], p. 53-57.

The relevant equations in local form for the geometrically linear case are summarized in the following box without derivation, which is quite straight forward.

electric potential:

$$\vec{\mathrm{E}} = -\mathrm{grad}\varphi \tag{4.36}$$

linear strain tensor:

$$\boldsymbol{S} = \tfrac{1}{2}\left(\mathrm{grad}\vec{\mathrm{u}} + (\mathrm{grad}\vec{\mathrm{u}})^T\right) \tag{4.37}$$

electric displacement:

$$\vec{\mathrm{D}} = \vec{\mathrm{P}} + \epsilon_0\vec{\mathrm{E}} \tag{4.38}$$

electrostatic stress tensor:

$$\boldsymbol{T}^{\mathrm{e}} = \vec{\mathrm{E}} \otimes \vec{\mathrm{P}} + \epsilon_0\left(\vec{\mathrm{E}} \otimes \vec{\mathrm{E}} - \tfrac{1}{2}(\vec{\mathrm{E}} \cdot \vec{\mathrm{E}})\,\boldsymbol{I}\right) \tag{4.39}$$

Gauß' Law:

$$\mathrm{div}\,\vec{\mathrm{D}} = q^{\mathrm{f}} \tag{4.40}$$

conservation of charge:

$$\dot{q^{\mathrm{f}}} + \mathrm{div}\vec{\mathrm{J}} = 0 \tag{4.41}$$

balance of linear momentum:

$$\rho\,\ddot{\vec{\mathrm{u}}} = \mathrm{div}\,(\boldsymbol{T} + \boldsymbol{T}^{\mathrm{e}}) + \rho\,\vec{\mathrm{k}} \tag{4.42}$$

balance of moment of momentum:

$$\boldsymbol{T} - \boldsymbol{T}^T = \boldsymbol{T}^{\mathrm{e}} - \boldsymbol{T}^{\mathrm{e}T} \tag{4.43}$$

balance of energy:

$$\rho\,\dot{e} = \boldsymbol{T} : \dot{\boldsymbol{S}} + \boldsymbol{T}^{\mathrm{e}} : \boldsymbol{W} + \vec{\mathrm{E}} \cdot \dot{\vec{\mathrm{P}}} + \vec{\mathrm{E}} \cdot \vec{\mathrm{J}} - \mathrm{div}\,\vec{\mathrm{q}} + \rho\,r \tag{4.44}$$

4.1.4 Towards the simplest form of the theory of a deformable dielectric

In the last three equations of the above theory, there is a significant deviation from classical thermomechanics in that the stress tensor $\boldsymbol{T}$ is not symmetric.

As pointed out before, the antisymmetric part of the stress tensor is equal to the antisymmetric part of the electrostatic stress tensor. MAUGIN [1988], p. 222f, points out that the electrostatic stress tensor vanishes asymptotically for a theory linearized about the neighborhood of a so-called natural configuration that is free of fields, strains and stresses. This will be fulfilled for classical linear piezoelectricity or for electrostrictive behavior. However, piezoceramic materials may exhibit after unloading a remanent polarization and a remanent strain, which in general can not be neglected compared to total polarization and strain. Therefore, omitting the terms related to $\boldsymbol{T}^{\mathrm{e}}$ is subject to an independent assumption, the justification of which needs careful consideration for the application at hand.

Assumption 4:
The absolute magnitude of the electrostatic stress tensor, and, thus of the ponderomotive forces and couples is neglected:

$$\|\boldsymbol{T}^{\mathrm{e}}\| << 1 \tag{4.45}$$

As just mentioned, for ferroelectric ceramics, the condition of asymtotically vanishing polarization generally is not met even in the unloaded state. Instead, there may be a finite non-zero remanent polarization state after poling by a high electric field and subsequent removal of the loading. Now, in order to obtain an impression of the influence of $\boldsymbol{T}^{\mathrm{e}}$, we may estimate its order of magnitude with the help of some characteristic material parameters. Under regular conditions, the strength of the electric field $\left\|\vec{\mathrm{E}}\right\|$ will hardly exceed twice the coercive field E^{c}, and the magnitude of the polarization will not be much larger than the saturation polarization $\mathrm{P}^{\mathrm{sat}}$. For a conservative estimate, we may take $\mathrm{E}^{\mathrm{c}} \approx 1.0\,\mathrm{kV/mm}$ and $\mathrm{P}^{\mathrm{sat}} \approx 0.5\,\mathrm{C/m^2}$ which is not too far above typical values of PZT ceramics. Thus, we can expect

$$\|\boldsymbol{T}^{\mathrm{e}}\| \approx \mathrm{P}^{\mathrm{sat}}\ 2\,\mathrm{E}^{\mathrm{c}} \approx 1.0\ \mathrm{MPa} \tag{4.46}$$

for regular conditions. However, this value is small compared to the magnitudes of the stress tensor $\boldsymbol{T}$ relevant to reliability issues of technical applications. These considerations demonstrate, to which extent it might be justified to follow common practice by neglecting the electrically induced contributions to the mechanical field equations.

Commonly, materials with a specific resistance of at least $10^9\ \Omega$cm may be considered perfect insulators. (For instance, the company PI Ceramic in Lederhose (Thüringen), Germany, gives values of 10^{10} ... $10^{12}\ \Omega\,\mathrm{cm}$ for their PZT materials.)

Assumption 5:
The conduction current is assumed to vanish.

$$\vec{\mathrm{J}} = \vec{0} \tag{4.47}$$

As the main simplifacation, this assumption makes the conservation of charge trivial: $\dot{q}^f = 0$. However, as pointed out in the context with assumption 2, the idealization of materials with a high but finite resistence as perfect insulator might be questionable for cases with slow changes of the fields.

As a result of the above consideration we end up with the generally used, simplest theory of a deformable dielectric:

electric potential:

$$\vec{\mathrm{E}} = -\mathrm{grad}\varphi \quad , \quad \mathrm{E}_i = -\varphi_{,i} \tag{4.48}$$

linear strain tensor:

$$\boldsymbol{S} = \tfrac{1}{2}\left(\mathrm{grad}\vec{\mathrm{u}} + (\mathrm{grad}\vec{\mathrm{u}})^T\right) \quad , \quad S_{ij} = \tfrac{1}{2}\left(u_{i,j} + u_{j,i}\right) \tag{4.49}$$

electric displacement:

$$\vec{\mathrm{D}} = \vec{\mathrm{P}} + \epsilon_0 \vec{\mathrm{E}} \quad , \quad \mathrm{D}_i = \mathrm{P}_i + \epsilon_0 \mathrm{E}_i \tag{4.50}$$

Gauß' Law:

$$\mathrm{div}\,\vec{\mathrm{D}} = q^{\mathrm{f}} \quad , \quad \mathrm{D}_{i,i} = q^{\mathrm{f}} \tag{4.51}$$

balance of linear momentum:

$$\rho\,\ddot{\vec{\mathrm{u}}} = \mathrm{div}\,\boldsymbol{T} + \rho\,\vec{\mathrm{k}} \quad , \quad \rho\,\ddot{\mathrm{u}}_i = T_{ij,j} + \rho\,\mathrm{k}_i \tag{4.52}$$

balance of energy:

$$\rho\,\dot{e} = \boldsymbol{T} : \dot{\boldsymbol{S}} + \vec{\mathrm{E}} \cdot \dot{\vec{\mathrm{P}}} - \mathrm{div}\,\vec{\mathrm{q}} + \rho\, r \quad , \quad \rho\,\dot{e} = T_{ij}\dot{S}_{ij} + \mathrm{E}_i\dot{\mathrm{P}}_i - \mathrm{q}_{i,i} + \rho r \tag{4.53}$$

Clausius-Duhem inequality:

$$\rho\,\dot{\eta} \geq -\,\mathrm{div}\left(\frac{\vec{\mathrm{q}}}{T}\right) + \rho\,\frac{r}{T} \quad , \quad \rho\,\dot{\eta} \geq -\left(\frac{\mathrm{q}_i}{T}\right)_{,i} + \rho\,\frac{r}{T} \quad , \tag{4.54}$$

If we focus on the pure electromechanical behavior, this theory is basically the combination of classical small deformation mechanics with Gauß' Law, *i.e.*, classical electrostatics. For the remainder of this report, we shall adopt this simplified framework. Furthermore, for convenience we will switch from this point on to the admittedly less instructive but mathematically easier to handle index notation.

4.2 Thermodynamical framework for constitutive modeling

As mentioned at the beginning of this chapter, the system of balance laws has to be completed by a constitutive law representing the specific response properties of the material under consideration. It is a generally accepted understanding that constitutive models have to be formulated such that the resulting theory excludes any processes that might contradict the Second Law of thermodynamics. Coleman and Noll [1963] have develped a methodology to meet this demand by exploiting the the Clausius-Duhem inequality, which has been extended to theories with internal variables by Coleman and Gurtin [1967]. At this point, we will not go into the long lasting and controversal discussion about the physical justification of this approach. Rather, we sketch in this section a framework for constitutive modeling based on this approach, which has been established in the international scientific discussion on phenomenological constitutive modeling for piezoceramic materials (Kamlah and Jiang [1999], Cocks and McMeeking [1999], Landis [2002], Landis and McMeeking [2002], see also Lynch [1998], Huber and Fleck [2001]). In order to focus on the relevant aspects and in absense of related experimental information, we take the constitutive functions and parameters to be independent of the temperature.

4.2.1 Basic model structure

The *grain* of a ferroelectric polycrystal consists of *domains*, in which all unit cells have the same orientation. It is the defining property of a *ferroelectric material* that a By definition, a *ferroelectric* material undergoes polarization switching at high electric fields (Jaffe *et al.* [1971], p. 37, Lines and Glass [1977], p. 9). As a result, the well known ferroelectric hysteresis occurs for loadings by a cyclic electric field. Switching processes can also be initiated by mechanical loadings leading to ferroelastic behavior (Cao and Evans [1993], Schäufele and Härdtl [1996]). On the macroscopic level, these hysteresis phenomena represent irreversible changes in the

material and they can be observed for arbitrary slow loadings (CHEN AND TUCKER [1981]).

Motivated by the findings mentioned above, *polarization* and *strain* are decomposed additively into reversible and irreversible parts (cf. also BASSIOUNY *et al.* [1988]):

$$\mathrm{P}_i = \mathrm{P}_i^{\mathrm{r}} + \mathrm{P}_i^{\mathrm{i}} \quad , \tag{4.55}$$

$$S_{ij} = S_{ij}^{\mathrm{r}} + S_{ij}^{\mathrm{i}} \tag{4.56}$$

Here, the superscripts "r" and "i" indicate the *reversible* and *irreversible* parts of the corresponding quantities.

The irreversible quantities $\mathrm{P}_i^{\mathrm{i}}$ and S_{ij}^{i} represent macroscopic averages of the microscopic spontaneous polarization and strain of the ferroelectric crystal structure, respectively. Irreversible polarization and strain depend on the loading history, which is represented by a set of internal variables $q^1, \ldots, q^n$:

$$\mathrm{P}_i^{\mathrm{i}} = \mathrm{P}_i^{\mathrm{i}}(q^1, \ldots, q^n) \quad , \tag{4.57}$$

$$S_{ij}^{\mathrm{i}} = S_{ij}^{\mathrm{i}}(q^1, \ldots, q^n) \tag{4.58}$$

These internal variables are associated with the microstructure in such a way that they reflect on the macroscopic level the microscopic state of the material. In our case, they refer to the domain structure and their evolution describes domain switching during electromechanical loading. Note that formally a purely phenomenological theory is included here, if we identify the set of internal variables $(q^1, \ldots, q^9)$ with the components $(\mathrm{P}_1^{\mathrm{i}}, \ldots, S_{33}^{\mathrm{i}})$ of the irreversible quantities. (In this contex, a purely phenomenological theory would be one, where the irreversible quantities themselves are taken as internal variables having the conceptual physical meaning of macroscopic averages of the corresponding spontaneous quantities.)

Reversible polarization and strain are assumed to be related to the *electric field* and the *stress* by equations possessing the structure of linear piezoelectricity, *i.e.*,

$$\mathrm{P}_i^{\mathrm{r}} = \kappa_{ij}\mathrm{E}_j + \mathrm{d}_{ikl}T_{kl} \quad , \tag{4.59}$$

$$S_{ij}^{\mathrm{r}} = \mathrm{d}_{kij}\mathrm{E}_k + C_{ijkl}^{-1}T_{kl} \quad . \tag{4.60}$$

Here, κ_{ij} are the components of the second order tensor of *susceptibilities*, d_{kij} are the components of the third order tensor of *piezoelasticity* and C_{ijkl} are the components of the forth order tensor of *elastic stiffnes* measured at constant electric field. For fixed internal state $(q^1, \ldots, q^n)$, these equations approximate the response behavior linearily. However, the reversible properties depend on the domain state and, thus, on the loading history. We

take this into account by allowing the material tensors to be functions of the internal variables:

$$\kappa_{ij} = \kappa_{ij}(q^1, \ldots, q^n) \quad , \tag{4.61}$$
$$\mathrm{d}_{ikl} = \mathrm{d}_{ikl}(q^1, \ldots, q^n) \quad , \tag{4.62}$$
$$C_{ijkl} = C_{ijkl}(q^1, \ldots, q^n) \tag{4.63}$$

4.2.2 Thermodynamical model restrictions for reversible processes

In the next step, restrictions to the further formulation of the constitutive model within the reasonable model structure motivated above are established, such that the Second Law is obeyed in the sense of the methodology of Coleman and Noll [1963] and Coleman and Gurtin [1967]: For every *admissible* thermodynamic process, the Clausius-Duhem inequality has to be satisfied. According to our assumptions, we find for a deformable dielectric body in an isothermal process with uniform temperature

$$\mathrm{E}_i \dot{\mathrm{P}}_i + T_{ij} \dot{S}_{ij} \geq \rho \dot{\psi} \quad . \tag{4.64}$$

Here, $\psi = u - Ts$ is the *Helmholtz free energy density*, which is chosen as function of strain, polarization and the internal variables. With the consideration of equations (4.55), (4.56), (4.57), and (4.58), ψ can be expressed as

$$\psi = \psi(\mathrm{P}^{\mathrm{r}}_i, S^{\mathrm{r}}_{ij}, q^1, ..., q^n) \quad . \tag{4.65}$$

Then, the potential relations

$$\mathrm{E}_i = \rho \frac{\partial \psi}{\partial \mathrm{P}^{\mathrm{r}}_i}(\mathrm{P}^{\mathrm{r}}_k, S^{\mathrm{r}}_{kl}, q^1, ..., q^n) \tag{4.66}$$
$$T_{ij} = \rho \frac{\partial \psi}{\partial S^{\mathrm{r}}_{ij}}(\mathrm{P}^{\mathrm{r}}_k, S^{\mathrm{r}}_{kl}, q^1, \ldots, q^n) \tag{4.67}$$

are necessary and sufficient conditions for the Clasius-Duhem inequality to be satisfied for reversible processes in the sense $\dot{q}^\alpha = 0$ $(\alpha = 1, ..., n)$.

Assuming the latter relations to be solvable for $\mathrm{P}^{\mathrm{r}}_i$, S^{r}_{ij}, we may introduce the *Gibbs engergy density* by the Legendre transform

$$\rho g = -\rho\psi + \mathrm{E}_i \mathrm{P}^{\mathrm{r}}_i + T_{ij} S^{\mathrm{r}}_{ij} \quad , \tag{4.68}$$

which has the property

$$\mathrm{P}_i^{\mathrm{r}} = \rho \frac{\partial g}{\partial \mathrm{E}_i}(\mathrm{E}_k, T_{kl}, q^1, ..., q^n) \quad , \tag{4.69}$$

$$S_{ij}^{\mathrm{r}} = \rho \frac{\partial g}{\partial T_{ij}}(\mathrm{E}_k, T_{kl}, q^1, ..., q^n) \quad . \tag{4.70}$$

For fixed $q^1, ..., q^n$, these equations represent the reversible piezoelectric behavior, which was assumed to be linear with respect to electric field and stress by equations (4.59) and (4.60). Therefore, upon splitting the Gibbs engergy according to

$$g = g^{\mathrm{r}}(\mathrm{E}_i, T_{ij}, q^1, ..., q^n) + g^{\mathrm{i}}(q^1, ..., q^n) \quad , \tag{4.71}$$

the "reversible" part has to depend quadratically on E_i and T_{ij} in the form

$$\rho g^{\mathrm{r}} = \frac{1}{2}\kappa_{kl}\mathrm{E}_k\mathrm{E}_l + \mathrm{d}_{kij}\mathrm{E}_k T_{ij} + \frac{1}{2}C^{-1}_{ijkl}T_{ij}T_{kl} \tag{4.72}$$

for the potential relations (4.69) and (4.70) to be consistent with the required linear relations (4.59) and (4.60).

4.2.3 Thermodynamical model restrictions for irreversible processes

Next, we consider irreversible processes, *i.e.*, $\dot{q}_\alpha \neq 0$ $(\alpha = 1, ..., n)$. In particular, we want to exploit the Clausius-Duhem inequality in view of restrictions for the evolution equations of the internal variables. With the help of the potential relations (4.69), (4.70) we find from the Legendre transform (4.68)

$$\rho\dot{\psi} = \mathrm{E}_i\dot{\mathrm{P}}_i^{\mathrm{r}} + T_{ij}\dot{S}_{ij}^{\mathrm{r}} + \rho\sum_{\alpha=1}^{n}\frac{\partial g}{\partial q^\alpha}\dot{q}^\alpha \quad . \tag{4.73}$$

Substitution of the right hand side of this equation into inequality (4.64) yields with consideration of the additive decompositions (4.55), (4.56)

$$\sum_{\alpha=1}^{n}\left(\mathrm{E}_i\frac{\partial \mathrm{P}_i^{\mathrm{i}}}{\partial q^\alpha} + T_{ij}\frac{\partial S_{ij}^{\mathrm{i}}}{\partial q^\alpha} + \rho\frac{\partial g}{\partial q^\alpha}\right)\dot{q}^\alpha \geq 0 \quad . \tag{4.74}$$

Motivated by this inequality, we call each of the the quantities

$$\phi^\alpha = \mathrm{E}_i\frac{\partial \mathrm{P}_i^{\mathrm{i}}}{\partial q^\alpha} + T_{ij}\frac{\partial S_{ij}^{\mathrm{i}}}{\partial q^\alpha} + \rho\frac{\partial g}{\partial q^\alpha} \quad , \quad \alpha = 1, \ldots, n \tag{4.75}$$

the *driving force* of the corresponding internal variable q^α. The quantity

$$\varsigma = \sum_{\alpha=1}^{n} \phi^\alpha \dot{q}^\alpha \tag{4.76}$$

is called *internal dissipation* (Coleman and Gurtin [1967]). In the original work Kamlah and Jiang [1999], the requirement of a non-negative internal dissipation was satisfied in a sufficient manner by assuming

$$\dot{q}^\alpha = \Lambda^\alpha \phi^\alpha \quad , \quad \Lambda^\alpha \geq 0 \quad , \quad \alpha = 1, \ldots, n \quad \text{(no sum on } \alpha) \quad . \tag{4.77}$$

However, following Cocks and McMeeking [1999], Huber and Fleck [2001], and Landis [2002], a theory closer to the established structure of incremental plasticity can be obtained by means of a convex *switching function*

$$f = f(\phi^1, \ldots, \phi^n) \tag{4.78}$$

containing the origin and the associated flow rule

$$\dot{q}^\alpha = \Lambda \frac{\partial f}{\partial \phi^\alpha} \quad , \quad \alpha = 1, \ldots, n \tag{4.79}$$

for the evolution equations of the internal variables. For a rate independent theory, the *irreversible multiplier* Λ is determined by the consistency condition:

$$\Lambda \begin{cases} \text{solves } \dot{f} = \displaystyle\sum_{\alpha=1}^{n} \frac{\partial f}{\partial \phi^\alpha} \dot{\phi}^\alpha = 0 & \text{in case of } f(\phi^1, \ldots, \phi^n) = 0 \\ & \text{and } \dot{f}\Big|_{\dot{q}^1, \ldots, \dot{q}^n = 0} > 0 \\ = 0 & \text{else} \end{cases} \tag{4.80}$$

A rate dependent theory can be obtained by taking, for instance,

$$\Lambda = \Lambda^0 \langle f \rangle \quad , \tag{4.81}$$

where Λ^0 is a non-negative material constant associated with the materials viscosity and $\langle f \rangle = 0$ if $f \leq 0$ and $\langle f \rangle = f$ if $f > 0$ holds for the MacAuley bracket.

As we have seen that piezoceramics exhibit rate effects and, furthermore, the rate independent theory is approximated for slow processes or small values of Λ^0 (cf. Haupt *et al.* [1992]), we adopt the conceptually less complicated formulation (4.81). In both cases, a threshold indicates that only

external loads of sufficient magnitude can lead to an evolution of the microstructural parameters, *i.e.*, to irreversible processes. Note that in case of a rate independent theory, potential relations of the kind (4.69), (4.70) are only sufficient conditions for a non-negative internal dissipation during irreversible processes (LUBLINER [1973]). For the rate dependent formulation, the potential relations are necessary and sufficient conditions for a non-negative internal dissipation, as infinite slowing down of the process will lead to infinitely small contributions of the internal variables (COLEMAN AND GURTIN [1967]).

One closing remark will be made with respect to the relation to models in the literature: If we choose in the spirit of a phenomenological theory $(q_1, \ldots, q_9)$ as $(\mathrm{P}^{\mathrm{i}}_1, \ldots, S^{\mathrm{i}}_{33})$, we can identify the structure of the theories presented in COCKS AND MCMEEKING [1999] and LANDIS [2002] with the "back" quantities $\mathrm{E}^{\mathrm{B}}_i = -\rho\, \partial g^{\mathrm{i}} / \partial \mathrm{P}^{\mathrm{i}}_i$ and $T^{\mathrm{B}}_{ij} = -\rho\, \partial g^{\mathrm{i}} / \partial S^{\mathrm{i}}_{ij}$, for instance.

Chapter 5

Microscopically motivated constitutive model

Kamlah and Jiang [1999] developed a phenomenological constitutive model for piezoceramics under uniaxial electromechanical loading. In this model two internal variables are used to indicate the degree of alignment of the domains and the degree of the orientation of their microdipoles. These two variables are related to the macroscopic irreversible polarization and strain. Their evolution equations are developed from thermomechnical considerations. A switching function is used to indicate the onset of domain switching (and from there, the onset of internal variables evolution). An indicator function is used to constrain the internal variables evolution to physically possible values and if a limit state is reached. The model presented below is a significant improvement of Kamlah and Jiang's model and an extention that enables it to be used for more general loading cases.

The general constitutive framework established in the previous section is specialized to uniaxial electromechanical loadings on piezoelectric ceramics. The properties of the ferroelectric phase of the polycrystal are assumed to be dominated by the tetragonality of the microstructure. A consideration of the tetragonal microstructure provides probably the most obvious insight into the relation between microstructure and macroscopic response.

A tetragonal unit cell is characterized by the fact that one of its lattice axes, the so-called c-axis, is about 1% longer than the other two axes, the a-axes. The c-axis of unit cells can be oriented in any one of the three lattice directions of a grain. A region within a *grain* of ferroelectric polycrystal is named a *domain* if all microdipoles of the unit cells have the same orientation. A characteristic property of ferroelectric materials is the reorientation of c-axes and microdipoles, if the electromechanical loadings on the material reach critical values. At a critical state the original c-axes may move to their

inverse direction (180° switching), or change into a-axis with an original a-axes changing into a c-axis (90° switching).

In the thermally depoled *reference state* of polycrystalline ceramics the distribution of domains is random and no direction is prefered. In the case of uniaxial loading, the loading direction may eventually become prefered and lead the material to exhibit transverse isotropy at the macroscopic level irrespective of the details of its microscopic anisotropic properties.

5.1 Uniaxial formulation of the model

The loading is assumed to be in the x_3-direction. In this case the external loads are T_{33} and E_3, and the independent strain and polarization are S_{33} and P_3, respectively. For convenience these quantities are denoted by σ, E, S and P respectively. The additive decomposition of polarization and strain in equations (4.55) and (4.56) become

$$\mathrm{P} = \mathrm{P}^{\mathrm{r}} + \mathrm{P}^{\mathrm{i}} \quad , \tag{5.1}$$

$$S = S^{\mathrm{r}} + S^{\mathrm{i}} \quad . \tag{5.2}$$

Again, a superscript "i" denotes the remanent or *irreversible* part and a superscript "r" indicates the *reversible* part of the repective quantity. The piezoelectricity equations (4.59) and (4.60) read as

$$\mathrm{P}^{\mathrm{r}} = \kappa \mathrm{E} + \mathrm{d}\sigma \quad , \tag{5.3}$$

$$S^{\mathrm{r}} = \mathrm{d}\mathrm{E} + \frac{1}{Y}\sigma \quad , \tag{5.4}$$

where κ, d and Y are the *susceptibility coefficient*, the *piezoelectric coefficient*, and *Young's modulus*, respectively. They are functions of the internal variables (see equations (4.61) through (4.63)). The reversible part (4.72) of the Gibbs energy function then is

$$g^{\mathrm{r}} = \frac{1}{2}\kappa \mathrm{E}^2 + \mathrm{d}\mathrm{E}\sigma + \frac{1}{2}\frac{1}{Y}\sigma^2 \quad . \tag{5.5}$$

5.2 Domain switching and internal variables

5.2.1 Internal variables motivated by microscopic consideration

Internal variables q^α ($\alpha = 1, 2, \ldots, n$) are chosen with some simplifying considerations on the domain structure of the material. They represent the

microscopic state of the ceramic in the sense of macroscopic averages. To begin with, a ferroelectric sample in its unpoled reference state is considered. Such a sample exhibits irreversible deformation under compressive stresses of sufficient magnitude without any changes to the macroscopic polarization state. This phenomenon is due to 90° switching processes of the c-axes of the tetragonal unit cells. While the distribution of the c-axes is initially uniform over the unit sphere, the fraction of c-axes aligned with the x_3-axis, the axis of loading, is reduced due to 90° switching processes. The length of the sample in the direction of loading is decreased irreversibly and it gives way to the compressive stress. We now introduce cones of 45° angle with the

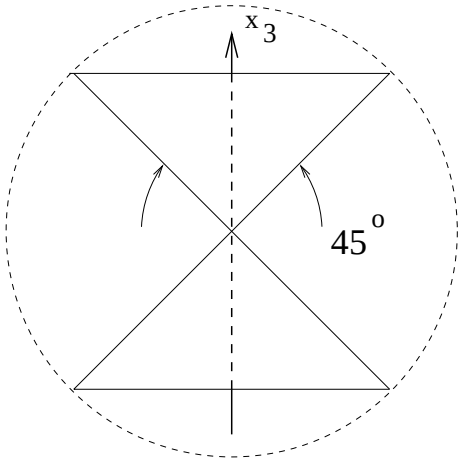

Figure 5.1: Two cones of 45° about x_3-axis, being the axis of loading.

x_3-axis being the cone axis (see Figure 5.1). The fraction of domains with their c-axis situated within these cones has been reduced in the previously discussed example of mechanical compressive loading. On the other hand, the domains with their c-axis outside the cones have no more favorable positions under compression in the direction of the cone axis and hence will remain unchanged. Thus, the microscopic state of the distribution of the c-axes may be described with the help of these cones: The first internal variable, denoted by $\beta = q^1$, represents the *fraction of domains* with their c-axes situated within the 45°-cones.

As mentioned above, each unit cell of a ferroelectric material forms a microdipole with its axis parallel to the c-axis of the tetragonal unit cell. Within a grain there are six possible orientations for the microdipole of a unit cell. In particular, there are two orientations for each lattice direction. As a result different states of macroscopic polarization can result from the microdipoles belonging to the same degree of alignment of the c-axes with

respect to the x_3-axis, *i.e.*, for the same value of β. Therefore we need additional information to determine the macroscopic state of polarization associated with the microscopic domain state given by the local distribution of the spontaneous polarization. In this sense the second internal variable, $\gamma = q^2$, represents the state of *relative irreversible macroscopic polarization* in x_3-direction resulting from the distribution of the spontaneous polarization:

$$\gamma = \frac{P^i}{P^{sat}} \tag{5.6}$$

In this equation, the *saturation polarization* P^{sat} is the maximum irreversible macroscopic polarization.

According to the definition just introduced, γ indicates the degree of orientation of the microdipoles with respect to the x_3-axis. Since β represents the fraction of cells whose c-axes are located within the 45°-cones about the x_3-axis, γ may not assume values completely independent of β. In particular, $\gamma = \pm 1$ is possible only, if the c-axes of all domains are situated within the 45°-cones about the x_3-axis, *i.e.*, $\beta = 1$. On the other hand, if no c-axes are left within the 45°-cones, *i.e.*, $\beta = 0$, only a reduced amount of relative irreversible polarization is possible: $|\gamma| \leq \gamma^{limit,min}$. For values of β between 0 and 1, the maximum possible relative irreversible polarization will be some function of β: $|\gamma| \leq \gamma^{limit}(\beta)$. Furthermore, the maximum possible relative irreversible polarization will not decrease with increasing degree of alignment of the c-axes, meaning that $\gamma^{limit}(\beta)$ is a monotonous function. In summary, the *limit function* describing the maximum possible relative irreversible polarization has the following general properties:

$$\gamma^{limit}(0) = \gamma^{limit,min} \geq 0 \tag{5.7}$$

$$\frac{d\gamma^{limit}(\beta)}{d\beta} \geq 0 \quad \text{for } 0 \leq \beta \leq 1 \tag{5.8}$$

$$\gamma^{limit}(1) = 1 \tag{5.9}$$

Admissible internal states β and γ may take values from the set

$$G = \left\{ (\beta, \gamma) \;\middle|\; |\gamma| \leq \gamma^{limit}(\beta) \;,\; 0 \leq \beta \leq 1 \right\} \tag{5.10}$$

represented with the help of $\gamma^{limit}(\beta)$ possessing the properties (5.7) through (5.9). Further details will be introduced below in section 5.2.4.

5.2.2 Relations between internal variables and macroscopic quantities

From the above discussion it can be seen that the irreversible deformation S^{i} should be chosen as a function of β, while the state of relative polarization of these domains will have no influence on the remanent distortion of the lattice. Thus,

$$S^{\mathrm{i}} = S^{\mathrm{i}}(\beta) \tag{5.11}$$

is assumed to link the macroscopic irreversible strain to the microstructural state variables. For convenience the unpoled state is defined as the reference state with a vanishing value of the irreversible strain, *i.e.*, $S^{\mathrm{i}}(\beta^{\mathrm{ref}}) = 0$. If all c-axes are switched into the 45°-cones about the x_3-axis, *i.e.*, $\beta = 1$, the irreversible strain reaches a saturation value: $S^{\mathrm{i}}(1) = S^{\mathrm{sat}}$. Here, the *saturation strain* S^{sat} is the maximum value of the macroscopic irreversible strain of the ceramic which is assumed for a domain state of highest order with respect to a certain axis.

For the sake of simplicity the linear relation

$$S^{\mathrm{i}}(\beta) = \frac{\beta - \beta^{\mathrm{ref}}}{1 - \beta^{\mathrm{ref}}} S^{\mathrm{sat}} \tag{5.12}$$

may be considered. Since β^{ref} represents the thermally depoled reference state, its value is given by the intersection of our 45°-cones with the spherical surface, or in other words by the cutoff of the spherical surface by these cones. This value is slightly below one third, because of which

$$\beta^{\mathrm{ref}} = \frac{1}{3} \tag{5.13}$$

may be taken for simplicity. From (5.13) we get $S^{\mathrm{i}}(0) = -\frac{1}{2} S^{\mathrm{sat}}$ for the state $\beta = 0$, where all c-axes are oriented out of the 45°-cones, as will result from strong compressive stresses acting in x_3-direction. In a ferroelectric material with a tetragonal microstructure one may expect some difference in the maximum magnitudes of the irreversible strain for compressive and tensile loadings. Therefore, the linear relation (5.12), which reflects the situation of an ideally oriented single crystal, can be used as a first approximation.

As discussed in section 2.2, the ratio between maximum tensile and compressive irreversible strains is 1.37 : 1, much smaller than the 2 : 1 expected from the single crystal consideration. In order to take this deformation asymmetry into account, a quadratic relation between the alignment of c-axes and the resultatnt irreversible strain of the kind

$$S^{\mathrm{i}}(\beta) = a(\beta - \beta^{\mathrm{ref}})^2 + b(\beta - \beta^{\mathrm{ref}}) \tag{5.14}$$

can be used, in which

$$\begin{aligned} a &= \frac{1}{\beta^{\mathrm{ref}}\left(1-\beta^{\mathrm{ref}}\right)} S_{\mathrm{tens}}^{\mathrm{sat}} - \frac{1}{\beta^{\mathrm{ref}}}(S_{\mathrm{tens}}^{\mathrm{sat}} - S_{\mathrm{comp}}^{\mathrm{sat}}), \\ b &= \frac{1-\beta^{\mathrm{ref}}}{\beta^{\mathrm{ref}}}(S_{\mathrm{tens}}^{\mathrm{sat}} - S_{\mathrm{comp}}^{\mathrm{sat}}) - \frac{1-2\beta^{\mathrm{ref}}}{\beta^{\mathrm{ref}}\left(1-\beta^{\mathrm{ref}}\right)} S_{\mathrm{tens}}^{\mathrm{sat}} \quad . \end{aligned}$$

In this formulation the maximum strain in tension ($S_{\mathrm{tens}}^{\mathrm{sat}}$) and in compression ($S_{\mathrm{comp}}^{\mathrm{sat}}$) are two independent parameters, thus the strain asymmetry can be described. Independent of the value of β^{ref}, from (5.14) we get $S^{\mathrm{i}}(0) = S_{\mathrm{comp}}^{\mathrm{sat}}$ and $S^{\mathrm{i}}(1) = S_{\mathrm{tens}}^{\mathrm{sat}}$. If we take $S_{\mathrm{tens}}^{\mathrm{sat}} = S^{\mathrm{sat}}$, $S_{\mathrm{comp}}^{\mathrm{sat}} = -S^{\mathrm{sat}}/2$ and $\beta^{\mathrm{ref}} = 1/3$, this quadratic formulation becomes the linear relation (5.12). Another, admittedly somewhat remote motivation for a quadratic $S^{\mathrm{i}}(\beta)$-formulation may be taken from the quadratic dependence of electrostrictive strains on polarization. This thought is questionable in the first place with repect to the relation between polarization and β.

A simplified alternative to (5.14) is the piece-wise linear relation

$$S^{\mathrm{i}}(\beta) = \begin{cases} (1 - \frac{\beta}{\beta^{\mathrm{ref}}}) S_{\mathrm{comp}}^{\mathrm{sat}} & , \quad 0 \le \beta \le \beta^{\mathrm{ref}} \\ \\ \frac{\beta-\beta^{\mathrm{ref}}}{1-\beta^{\mathrm{ref}}} S_{\mathrm{tens}}^{\mathrm{sat}} & , \quad \beta^{\mathrm{ref}} < \beta \le 1 \end{cases} \quad . \tag{5.15}$$

From the defintion of the second internal variable γ as relative irreversible polarization in equation (5.6) we get

$$\mathrm{P}^{\mathrm{i}} = \gamma\, \mathrm{P}^{\mathrm{sat}} \quad . \tag{5.16}$$

As discussed at the end of section 5.2.1, the two internal variables β and γ are not totally independent of each other. The second internal variable γ represents the state of relative polarization and it is limited by the degree of aligment of c-axes given by β. The relationship between them and their admissible values will be discussed in section 5.2.4 in detail.

It remains to specify the dependence of the coefficients in the piezoelectricity relations (5.3) and (5.4) on the microstructural parameters β and γ. In order to keep the model as simple as possible, the susceptibility coefficient κ and Young's modulus Y are assumed to be independent of the microstructural parameters and therefore constant. In the unpoled state the phenomenon of piezoelectricity is totally absent: $\mathrm{d} = 0$ if $\mathrm{P}^{\mathrm{i}} = 0$. In the fully poled state ($\mathrm{P}^{\mathrm{i}} = \pm\mathrm{P}^{\mathrm{sat}}$), the piezoelectric coefficient reaches its maximum value: $\mathrm{d} = \pm\mathrm{d}^{\mathrm{sat}}$. For simplicity, we fit by the linear function

$$\mathrm{d}(\gamma) = \gamma \mathrm{d}^{\mathrm{sat}} \quad . \tag{5.17}$$

5.2.3 Evolution equations for internal variables

The starting point for the construction of the evolution equations (4.79) for the microstructural parameters is the Gibbs energy (4.71) from which the driving forces ϕ^α ($\alpha = 1, 2, \ldots, n$) are derived. For simplicity, we assume a quadratic dependence of the "irreversible" part of the Gibbs energy function on the internal variables of the kind

$$\rho g^{\mathrm{i}} = -\frac{1}{2} c^\beta (\beta - \beta^{\mathrm{ref}})^2 - \frac{1}{2} c^\gamma \gamma^2 - F^G(\beta, \gamma) \quad . \tag{5.18}$$

$F^G(\beta, \gamma)$ is an energy barrier function which has to ensure that β and γ take values within the region G introduced by equation (5.10). The mathematical formulation of F^G will be discussed below in section 5.2.4.

From the definition (4.75) the driving forces corresponding to the internal variables β and γ are

$$\phi^\beta = \frac{\mathrm{d}S^{\mathrm{i}}}{\mathrm{d}\beta}\sigma - c^\beta(\beta - \beta^{\mathrm{ref}}) - \frac{\partial F^G}{\partial \beta} \quad , \tag{5.19}$$

$$\phi^\gamma = \mathrm{P}^{\mathrm{sat}}\mathrm{E} + \mathrm{d}^{\mathrm{sat}}\sigma\mathrm{E} - c^\gamma \gamma - \frac{\partial F^G}{\partial \gamma} \quad . \tag{5.20}$$

If the linear $S^{\mathrm{i}}(\beta)$-relation (5.12) is used, we find

$$\phi^\beta = \frac{S^{\mathrm{sat}}}{1 - \beta^{\mathrm{ref}}}\sigma - c^\beta(\beta - \beta^{\mathrm{ref}}) - \frac{\partial F^G}{\partial \beta} \quad . \tag{5.21}$$

The primary contribution to the driving forces stems from the mechanical stress and from the electric field. If c^β und c^γ are assumed to be non-negative constants, it can be seen that the corresponding terms reduce the magnitude of the driving forces as the values of the microstructural parameters increase. In this way the fact is reflected that the unpoled state is most preferred and departing from the unpoled state experiences an increasing resistance caused by constraint from neighbouring domains and grains. In this context it can be seen that the quadratic terms in g^{i} lead to simple linear hardening properties.

According to the thermodynamic considerations in section 4.2.2, a convex switching function containing the origin in the space of driving forces needs to be introduced. The most simple way to satisfying these requirements is a quadratic dependence on the driving forces of the kind

$$f = \sqrt{\left(\frac{\phi^\beta}{\phi^{\beta,0}}\right)^2 + \left(\frac{\phi^\gamma}{\phi^{\gamma,0}}\right)^2} - 1 \quad , \tag{5.22}$$

where additionally the square root is taken for reasons of normalization in the tradition of incremental plasticity. Here, the parameters

$$\phi^{\beta,0} = \frac{\mathrm{d}S^{\mathrm{i}}}{\mathrm{d}\beta}\sigma^{\mathrm{c}} \tag{5.23}$$

$$\phi^{\gamma,0} = \mathrm{P}^{\mathrm{sat}}\mathrm{E}^{\mathrm{c}} \tag{5.24}$$

characterize the critical state of the driving forces for the onset of irreversible changes. σ^{c} and E^{c} are the *coercive stress* and the *coercive field*, respectively, characterizing the onset of mechanically and electrically induced domain switching. Note that in general, $\phi^{\beta,0}$ will be a function of β. However, in the case of the linear $S^{\mathrm{i}}(\beta)$-relation (5.12), we find

$$\phi^{\beta,0} = \frac{S^{\mathrm{sat}}\sigma^{\mathrm{c}}}{1-\beta^{\mathrm{ref}}} \tag{5.25}$$

If $f \geq 0$, domain switching occurs in the sense that internal variables will change according to their evolution equations. Otherwise, the internal variables remain constant and the model responds linearly to the loading. By the normality rule (4.79), the increment pair of the internal veriables is in the direction of the normal to the convex switching surface:

$$\dot{\beta} = \Lambda^0\langle f\rangle\frac{\partial f}{\partial \phi^\beta} = \frac{\Lambda^0\langle f\rangle}{1+f}\left(\frac{1}{\phi^{\beta,0}}\right)^2\phi^\beta \tag{5.26}$$

$$\dot{\gamma} = \Lambda^0\langle f\rangle\frac{\partial f}{\partial \phi^\gamma} = \frac{\Lambda^0\langle f\rangle}{1+f}\left(\frac{1}{\phi^{\gamma,0}}\right)^2\phi^\gamma \tag{5.27}$$

5.2.4 Admissible values for the internal variables and energy barrier function

At the end of section 5.2.1 it was discussed that the microstructural parameters γ and β are not completely independent of each other. Rather, there exists a set G of admissible internal states defined by (5.10). As the simplest choice satisfying the requirements (5.7) through (5.9), we may take

$$\gamma^{\mathrm{limit}}(\beta) = \beta \quad , \tag{5.28}$$

in which case $\gamma^{\mathrm{limit,min}} = 0$, *i.e.*,

$$0 \leq |\gamma| \leq \beta \leq 1 \quad , \tag{5.29}$$

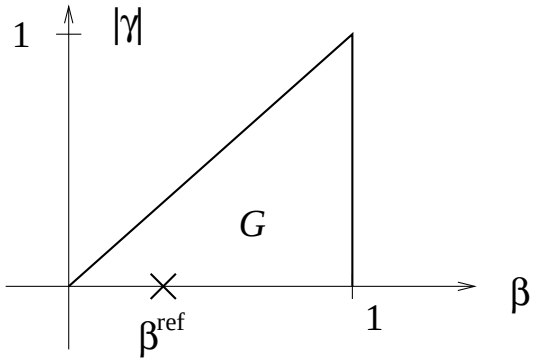

Figure 5.2: The set G of admissible (β, γ) states according to (5.30). The value β^{ref} corresponds to the unpoled reference state, see section 5.2.2.

and, thus,

$$G = \left\{ (\beta, \gamma) \;\middle|\; 0 \leq |\gamma| \leq \beta \leq 1 \right\} \quad . \tag{5.30}$$

As shown in the β-γ-plane in Figure 5.2, G is a triangle with its corners at (0,0), (1,0), and (1,1).

This shape of G can be interpreted as follows: Values of (β, γ) out of the region G are not permited. By its definition β may take values between 0 and 1. Furthermore, γ may assume values between -β and β, *i.e.*, γ indicates the degree of orientation of the microdipoles of the cells whose c-axes are located within the 45°-cones. In the case $\gamma = \beta$, all domains within the 45°-cones about the x_3-axis are polarized in the positive x_3-direction, while $\gamma = -\beta$ means the opposite. If $\gamma = 0$, the fractions of domains in the 45°-cones oriented in positive and negative x_3-direction are equal, leading to a cancelation of the resultant macroscopic irreversible polarization. In particular, in the unpoled reference state $\gamma = 0$. All together, the above microscopic interpretation of the simple triangular shape of the set of possible values for the internal variables is not completely reasonable.

We now discuss the possible energy barrier functions $F^G(\beta, \gamma)$ corresponding to the region G. Following Frémond [1989], the indicator function of set G may be chosen as $F^G(\beta, \gamma)$ in order to enforce that the pair of internal variables (β, γ) assumes only admissible values from this set. The indicator function is defined by

$$F^G(\beta, \gamma) = I^G(\beta, \gamma) = \begin{cases} 0, & (\beta, \gamma) \in G \backslash \partial G \\ \\ \infty, & \text{else} \end{cases} \quad , \tag{5.31}$$

where ∂G is the boundary of set G. As a rough physical interpretation, we may state that the indicator function surrounds the set of the admissible values of (β, γ) by an infinitely steep and infinitely high energy barrier. As long as (β, γ) takes values in the interior of G, there is no contribution from the indicator function to the driving forces. However, as soon as (β, γ) is situated on ∂G, the contribution from the indicator function to the driving forces will be such that no values outside of G can be reached. We consider this step-like behavior to be induced by using the indicator function as an idealized way to enforce the constraints for physically admissible values of the internal variables.

Here, we adopt the representation of the indicator function found in Savi *et al.* [1998]. Introducing the functions

$$h^{(1)}(\beta,\gamma) = \gamma - \beta \quad , \tag{5.32}$$

$$h^{(2)}(\beta,\gamma) = -\gamma - \beta \quad , \tag{5.33}$$

$$h^{(3)}(\beta,\gamma) = \beta - 1 \quad , \tag{5.34}$$

the set G may be represented equivalently by

$$G = \left\{ (\beta,\gamma) \;\middle|\; h^{(I)}(\beta,\gamma) \leq 0, \quad I = 1,2,3 \right\} \quad . \tag{5.35}$$

The indicator function may then be written as

$$I^G(\beta,\gamma) = -\lambda^{(1)} h^{(1)}(\beta,\gamma) - \lambda^{(2)} h^{(2)}(\beta,\gamma) - \lambda^{(3)} h^{(3)}(\beta,\gamma) \quad . \tag{5.36}$$

If we use the approximate $\beta^{\mathrm{ref}} = 1/3$ and the linear $S^{\mathrm{i}}(\beta)$-function (5.12), then the evolution equations are

$$\dot{\beta} = \frac{\Lambda^0 \langle f \rangle}{1+f} \left(\frac{1}{\phi^{\beta,0}} \right)^2 \left(\frac{3}{2} S^{\mathrm{sat}} \sigma - c^\beta (\beta - \frac{1}{3}) - \lambda^{(1)} - \lambda^{(2)} + \lambda^{(3)} \right) \quad , \tag{5.37}$$

$$\dot{\gamma} = \frac{\Lambda^0 \langle f \rangle}{1+f} \left(\frac{1}{\phi^{\gamma,0}} \right)^2 \left(\mathrm{P}^{\mathrm{sat}} \mathrm{E} + \mathrm{d}^{\mathrm{sat}} \sigma \mathrm{E} - c^\gamma \gamma + \lambda^{(1)} - \lambda^{(2)} \right) \quad . \tag{5.38}$$

Here, the multipliers $\lambda^{(I)}$ $(I = 1,2,3)$ satisfy the Kuhn-Tucker conditions

$$h^{(I)} \leq 0, \quad \lambda^{(I)} \geq 0, \quad \lambda^{(I)} h^{(I)} \leq 0, \quad I = 1,2,3 \;\; \text{(no sum on } I) \quad . \tag{5.39}$$

Now we study the role of the $\lambda^{(I)}$ terms in the driving forces. For values of the internal variables from the interior of G, $h^{(I)} < 0, (I = 1,2,3)$. According to the Kuhn-Tucker conditions (5.39), the driving forces are then given by the "regular"parts

$$\phi^\beta = \phi^{\beta,\mathrm{reg}} = \frac{3}{2} S^{\mathrm{sat}} \sigma - c^\beta (\beta - \frac{1}{3}) \tag{5.40}$$

$$\phi^{\gamma} = \phi^{\gamma,\mathrm{reg}} = \mathrm{P}^{\mathrm{sat}}\mathrm{E} + \mathrm{d}^{\mathrm{sat}}\sigma\mathrm{E} - c^{\gamma}\gamma \tag{5.41}$$

If (β, γ) is on the ∂G, for example on $h^{(1)} = 0$, $\lambda^{(1)}$ has to be chosen such that (β, γ) is not be able to get out of G. From the consistancy condition

$$\frac{\mathrm{d}h^{(1)}(\beta,\gamma)}{\mathrm{d}t}\Big|_{(\phi^{\beta} = \phi^{\beta,\mathrm{reg}} - \lambda^{(1)},\ \phi^{\gamma} = \phi^{\gamma,\mathrm{reg}} + \lambda^{(1)})} = 0 \tag{5.42}$$

we find

$$\lambda^{(1)} = \frac{\left(\phi^{\beta,0}\phi^{\gamma,0}\right)^2}{(\phi^{\beta,0})^2 + (\phi^{\gamma,0})^2}\left(\frac{\phi^{\beta,\mathrm{reg}}}{(\phi^{\beta,0})^2} - \frac{\phi^{\gamma,\mathrm{reg}}}{(\phi^{\gamma,0})^2}\right) \tag{5.43}$$

Consequently, the evolution equations are given by

$$\dot{\beta} = \frac{\Lambda^0\langle f\rangle}{1+f}\left(\frac{1}{\phi^{\beta,0}}\right)^2(\phi^{\beta,\mathrm{reg}} - \lambda^{(1)}) \tag{5.44}$$

$$\dot{\gamma} = \frac{\Lambda^0\langle f\rangle}{1+f}\left(\frac{1}{\phi^{\gamma,0}}\right)^2(\phi^{\gamma,\mathrm{reg}} + \lambda^{(1)}) \tag{5.45}$$

in this case. Substitution of (5.43) into (5.44) and (5.45) yields

$$\dot{\beta} = \dot{\gamma} = \frac{\Lambda^0\langle f\rangle}{1+f}\frac{\phi^{\beta,\mathrm{reg}} + \phi^{\gamma,\mathrm{reg}}}{(\phi^{\beta,0})^2 + (\phi^{\gamma,0})^2} \quad . \tag{5.46}$$

$\dot{\beta}/\dot{\gamma} = 1$ means that the term $\lambda^{(1)}$ corrects the driving forces such that (β, γ) moves along the boundary $h^{(1)} = 0$ of G but cannot get outside. Similarly, we will find

$$\lambda^{(2)} = \frac{\left(\phi^{\beta,0}\phi^{\gamma,0}\right)^2}{(\phi^{\beta,0})^2 + (\phi^{\gamma,0})^2}\left(\frac{\phi^{\beta,\mathrm{reg}}}{(\phi^{\beta,0})^2} + \frac{\phi^{\gamma,\mathrm{reg}}}{(\phi^{\gamma,0})^2}\right) \quad , \tag{5.47}$$

if (β, γ) is on $h^{(2)} = 0$ and

$$\lambda^{(3)} = -\phi^{\beta,\mathrm{reg}} \tag{5.48}$$

if (β, γ) is on $h^{(3)} = 0$.

Before, we used the indicator function to constrain the evolution of the internal variables such that (β, γ) takes admissible values. However, experimental results show that saturation of the irreversible polarization, *i.e.*, $\mathrm{P}^{\mathrm{sat}}$, can not be achieved even if the applied electric field is very high. Likewise, even under a compressive stress of -400 MPa, domain switching is not fully completed. These facts suggest that (β, γ) may approach ∂G, but infinitely

large loading is needed for (β, γ) to reach the boundary of G. Therefore, $F^G(\beta, \gamma)$ should be formulated in such a way that it takes a finite value in the interior of G and approachs infinity, if (β, γ) approaches the boundary of G. For this purpose, the simple formula

$$F^G = A\left(\beta^{-N} + (1-\beta)^{-N} + (\beta - |\gamma|)^{-N}\right) \tag{5.49}$$

can be used, where A and N are two positive parameters. With this formulation and the linear $S^{\mathrm{i}}(\beta)$-relation (5.12), we get the driving forces for β and γ (for $\gamma > 0$)

$$\begin{aligned} \phi^\beta &= \frac{3}{2} S^{\mathrm{sat}} \sigma - c^\beta (\beta - \frac{1}{3}) \\ &\quad + AN\left(\beta^{-N-1} - (1-\beta)^{-N-1} + (\beta - |\gamma|)^{-N-1}\right) \end{aligned} \tag{5.50}$$

$$\phi^\gamma = \mathrm{P}^{\mathrm{sat}}\mathrm{E} + \mathrm{d}^{\mathrm{sat}}\sigma\mathrm{E} - c^\gamma \gamma + AN\left(-(\beta - |\gamma|)^{-N-1}\right) \tag{5.51}$$

For the (β, γ)-states in the interior of G and far away from the boundary, the value of $F^G(\beta, \gamma)$ is finite. If A is chosen very small and N very large, the F^G value is very small and induces small influence on the evolution of β and γ (through the $\partial F^G/\partial\beta$ and $\partial F^G/\partial\gamma$ terms in the driving forces). If (β, γ) approaches the boundary, F^G, $\partial F^G/\partial\beta$ and $\partial F^G/\partial\gamma$ increase rapidly and approach infinity. This means that the energy barrier resists the approaching of (β, γ) to the boundary. In other words, infinitely large external loading is needed to overcome the resistance from the energy barrier so that (β, γ) can reach the boundary. Thus, qualitatively the behavior is similar to what is induced by the indicator function. As a matter of fact, if N is very large, F^G in (5.49) behaves like an indicator function.

Note, besides the additive formulation of F^G in (5.49), functions with similar properties can also be used. For example, the multiplicative formulation

$$F^G = A\left(\beta(1-\beta)(\beta - |\gamma|)\right)^{-N} \tag{5.52}$$

has also been used in this study.

Above we discussed the model formulation based on the triangular set (5.30) for admissible values of the internal variables. On the boundaries $h^{(1)} = 0$ and $h^{(2)} = 0$, the relation between β and γ is linear, and, as a result the relation between S^{i} and P^{i} is linear as well, if the linear $S^{\mathrm{i}}(\beta)$-function (5.12) is employed.

Piezoelectric behavior can be understood as a result of *electrostriction*, where the electrically induced deformation behavior is a quadratic function of the kind

$$S = \mathrm{q}\mathrm{P}^2 \quad . \tag{5.53}$$

Here q is the *electrostrictive constant*. For a piezoelectric material, a linearization of the quadratic dependence in the neighborhood of the spontaneous polarization will yield the linear relation of piezoelectricity (FELDTKELLER [1973], vol. II, pp. 30, 53-54). This effect may be represented by a parabolic β-γ-relation for the boundary. Thereby, we have

$$0 \leq \gamma^2 \leq \beta \leq 1 \tag{5.54}$$

and

$$G = \left\{ (\beta, \gamma) \;\middle|\; 0 \leq \gamma^2 \leq \beta \leq 1 \right\} \tag{5.55}$$

for the set for admissible values of (β, γ). Formally, this corresponds to the choice

$$\gamma^{\text{limit}}(\beta) = \sqrt{\beta} \quad . \tag{5.56}$$

G is shown in Figure 5.3. If a quadratic boundary for G really can be motivated with reference to electrostriction is certainly questionable and depends on the physical relation between the two internal variables. For the quadratically bounded set of admissible (β, γ)-values the additive energy barrier function can be formulated as

$$F^G = A \left(\beta^{-N} + (1-\beta)^{-N} + (\beta - \gamma^2)^{-N} \right) \quad . \tag{5.57}$$

The corresponding driving forces can be found by the substitution of (5.57) into equations (5.19) and (5.20).

The experimental results of ZHOU [2003] show that poled material cannot be completely depoled by a compressive stress of up to -400 MPa. This material property suggests two possible microscopic reasons: (1) The domains in the 45°-cones are not completely switched out of the cones, and (2) the orientations of the microdipoles of the domains outside of the 45°-cones is not random. The first mechanism can be modelled by a continuous energy barrier function, as we have done. For the second mechanism we have to consider the contribution of the domains out of the 45°-cones to the polarization. According to the microscopic considerations given in Chapter 7, if no domains are left with their c-axes within the 45°-cones about the x_3-axis being the axis of loading, *i.e.*, $\beta = 0$, the maximum relative irreversible polarization is

$$\gamma^{\text{limit,min}} = \frac{\cos 45^\circ}{1 + \cos 45^\circ} \quad . \tag{5.58}$$

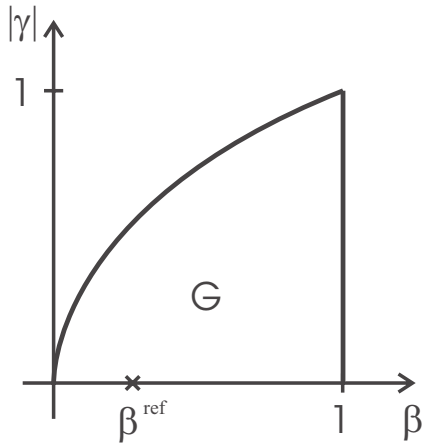

Figure 5.3: The set G of admissible (β, γ) states corresponding to (5.55).

For β-values between 0 and 1, the maximum relative irreversible polarization follows the linear relation

$$\gamma^{\text{limit}}(\beta) = \frac{\beta + \cos 45^\circ}{1 + \cos 45^\circ} \quad . \tag{5.59}$$

Thus, admissible β and γ belong to the set

$$G = \left\{ (\beta, \gamma) \;\middle|\; |\gamma| \leq \frac{\beta + \cos 45^\circ}{1 + \cos 45^\circ} \;,\; 0 \leq \beta \leq 1 \right\} \quad . \tag{5.60}$$

As shown in Figure 5.4, this set is a trapezoid in β-γ-plane. According to (5.60) and Figure 5.4, if $\beta = 0$, γ varies in the interval

$$-\frac{\cos 45^\circ}{1 + \cos 45^\circ} \leq \gamma \leq \frac{\cos 45^\circ}{1 + \cos 45^\circ} \quad . \tag{5.61}$$

The corresponding energy barrier functions can be formulated in the same way as for the other sets of admissible values of internal variables:

$$F^G = A \left(\beta^{-N} + (1 - \beta)^{-N} + \left(\gamma^{\text{limit}}(\beta) - |\gamma| \right)^{-N} \right) \tag{5.62}$$

5.3 Discussion of the hysteresis response of the model

In order to verify the ability of the model in describing the material response to electromechanical loading, some typical loading paths are simulated in this

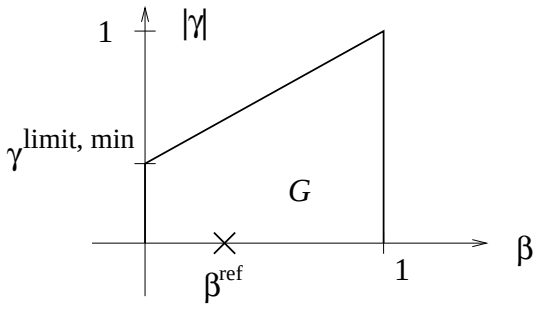

Figure 5.4: The set G of admissible (β, γ) states corresponding to (5.60).

section. In particular, the large signal hysteresis properties are discussed, which occur for stress and electric field magnitudes beyond their corresponding coercive values. The material parameters used in the numerical calculation are given in Table 5.1. They were chosen to represent approximately a typical soft material.

Table 5.1: Values of the ferroelectric material constants chosen for the numerical calculations.

κ	2.5×10^{-8}	C/V m	d_{33}	4.5×10^{-10}	m/V
d_{31}	-2.0×10^{-10}	m/V	d_{15}	5.8×10^{-10}	m/V
E^c	1.0×10^{6}	V/m	P^{sat}	0.3	C/m^2
Y	6.0×10^{10}	Pa	S^{sat}	0.2	%
c^β	1.0×10^{5}	Pa	c^γ	3.0×10^{4}	C/m^2
Λ^0	2.0×10^{12}	sec^{-1} Pa^{-2}	σ^c	3.0×10^{7}	Pa
A	5.0×10^{-2}	N/m^2	N	2.0	-
ν	0.3	-			

Both Runge-Kutta method and Euler-backward method are used to solve the evolution equations (5.26) and (5.27), if the switching condition (5.22) is satisfied. The solution of these equations gives the values of the internal variables at each time instant. From (5.16) and (5.12) we will get the related histories of remanent polarization and strain. The total polarization and strain will be obtained from the equations (5.1) through (5.4).

Below we mainly present the model responses in some typical loading

cases with linear $S^i(\beta)$-relation, the triangle G (5.30) and the additive energy barrier function (5.49) as reference formulation of the model. Model responses with other $S^i(\beta)$, G-shapes and energy barrier functions are also discussed and compared. In the simulation we used 1/3 as β^{ref}.

5.3.1 Poling and electric field cycling

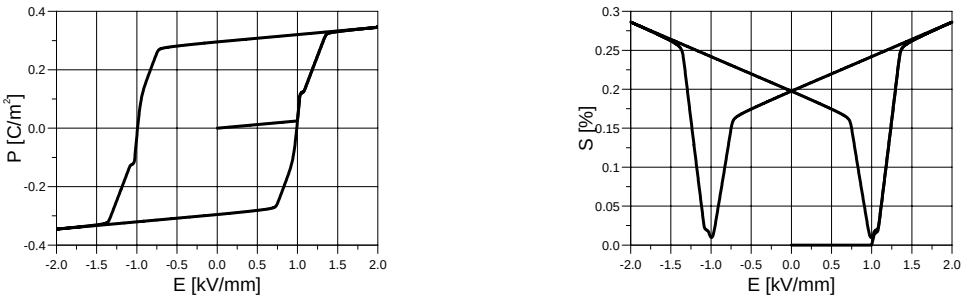

Figure 5.5: Poling and electric field cycling. Left: Dielectric hysteresis. Right: Butterfly hysteresis.

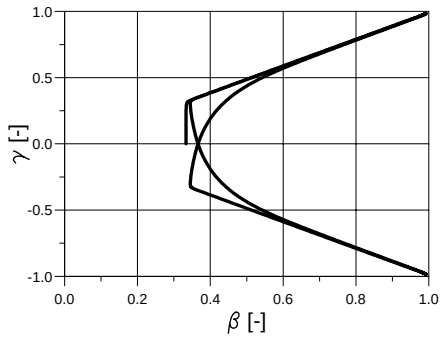

Figure 5.6: Plot of the path of the internal variables β and γ corresponding to the loading history in Figure 5.5.

The model response to electric cycling at an amplitude of twice the coercive field, *i.e.*, ± 2.0 kV/mm, is shown in Figure 5.5 (in relation to the loading rate, Λ^0 is chosen large enough so that no rate effects occur, see the

discussion of figure 5.7). The left panel shows the calculated dielectric hysteresis of initially unpoled material. For electric fields above the coercive field strength, we observe during each loading cycle of the polarization hysteresis a step which is an intermediate period of linear dielectric behavior, before the saturated state is reached by a second period of poling. This intermediate period corresponds to the point where the β-γ-path hits the boundary of the triangular region G of admissible values for $(\beta\,,\,\gamma)$. At such a point, additional evolution of the internal variables is possible only after the load has been increased further. The microscopic interpretation of this phenomenon is the change from pure 180° switching to combined 90° and 180° switching, for which a higher energy level is needed. The butterfly hysteresis during this electric field cycling is shown in the right panel of Figure 5.5, from which we recognize the inverse piezoelectric effect induced by poling. Figure 5.6 shows the evolution of the internal variables during this electric field cycling. If the electric field exceeds E^{c}, 180° switching is initiated at first, therefore the dipoles of domains located in the 45°-cones take the direction of the electric field. During this process β remains unchanged and γ increases. This is reflected by the vertical line in the β-γ-diagram. If (β, γ) approaches the boundary, the resistance induced by the energy barrier becomes very large to ensure that (β, γ) is not able to go out of the set G. If (β, γ) is very near ∂G, the terms from $\partial F^G/\partial\beta$ and $\partial F^G/\partial\gamma$ in (5.50) and (5.51) take effect. For further loading, 90° switching is also initiated and β and γ increase together nearly along the boundary towards the point $(1, 1)$. Near the point $(1, 1)$ the resistance from the boundary line $\beta = 1$ increases rapidly and prevents (β, γ) from moving across this line. Upon unloading and loading in the opposite direction, (β, γ) remains unchanged before the switching condition is fulfilled again. After this stage, because of the term $c^\beta(\beta - \beta^{\mathrm{ref}})$ in the driving force of (5.50), β reduces partially until (β, γ) approaches the boundary line $\gamma = -\beta$. In this process γ decreases continuously and takes a negative value, *i.e.*, the remanent polarization has changed its direction. Upon further loading in the oppsite direction, (β, γ) moves towards $(1, -1)$ nearly along the the boundary line $\gamma = -\beta$.

In the above calculation a very large $\Lambda^0 = 2.0 \times 10^{12}/(\mathrm{s} \cdot \mathrm{Pa}^2)$ is used, which corresponds to a rate-independent case. Figure 5.7 shows the dielectric and butterfly hystereses during the same electric field cycling, but a smaller $\Lambda^0 = 2.0 \times 10^8/(\mathrm{s} \cdot \mathrm{Pa}^2)$ is used in the calculation. It can be seen that because of the influence of viscosity the calculated dielectric and butterfly hystereses become smoother and the intermediate period disappears. Furthermore, the width of the hystereses is widened.

Figure 5.8 shows the calculated dielectric and butterfly hystereses by using the indicator function (5.36) as F^G. Because of the property of the indicator

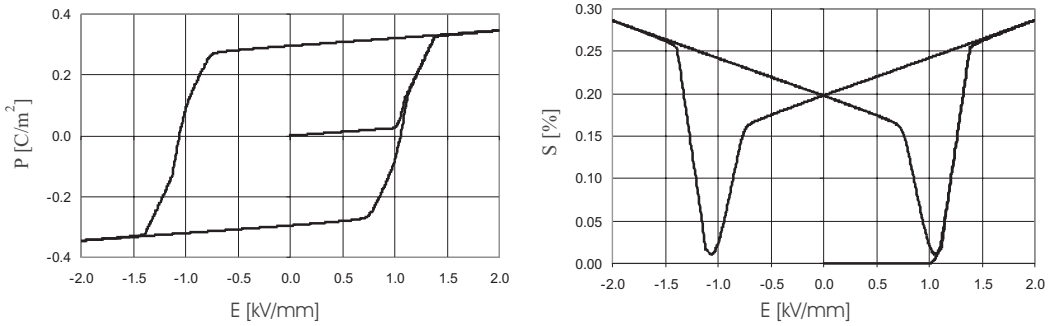

Figure 5.7: Poling and electric field cycling, $\Lambda^0 = 2 \times 10^8$. Left: Dielectric hysteresis. Right: Butterfly hysteresis.

function we see abrupt changes of polarization and strain in these hystereses. The intermediate period becomes very clear.

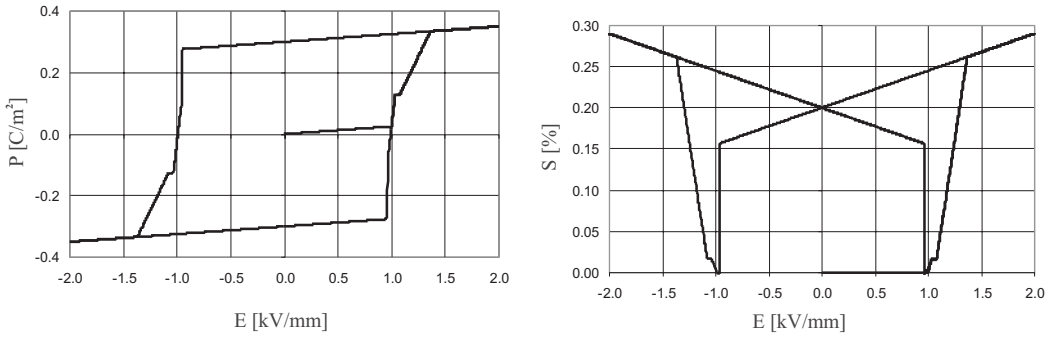

Figure 5.8: Poling and electric field cycling, where the indicator function is used as F^G. Left: Dielectric hysteresis. Right: Butterfly hysteresis.

5.3.2 Mechanical compressive-tensile stress cycling

The left panel of Figure 5.9 shows the ferroelastic hysteresis occuring in response to purely mechanical compression-tension loading. Due to the choice (5.12) of S^{i}, there is a strong asymmetry in the saturation behavior under tension and compression, just as is expected at least qualitatively from micromechanical considerations.

As we discussed before, the ratio between maximum strain in tension and in compression is near $1.37 : 1$. In order to take this property into account in the calculation, we also used the piece-wise linear $S^{\mathrm{i}}(\beta)$-relation (5.15). In this calculation, we defined $S^{\mathrm{sat}}_{\mathrm{tens}} = S^{\mathrm{sat}}$ and $S^{\mathrm{sat}}_{\mathrm{comp}} = -0.73 S^{\mathrm{sat}}$ to match

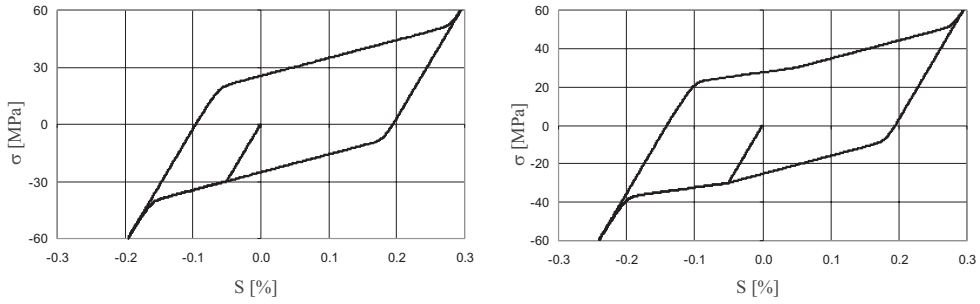

Figure 5.9: Model response to pure mechanical compression-tension loading: Ferroelastic hysteresis for two diferent types of $S^{\mathrm{i}}(\beta)$-dependence. Left: Linear, equation (5.12). Right: Piece-wise linear, equation (5.15).

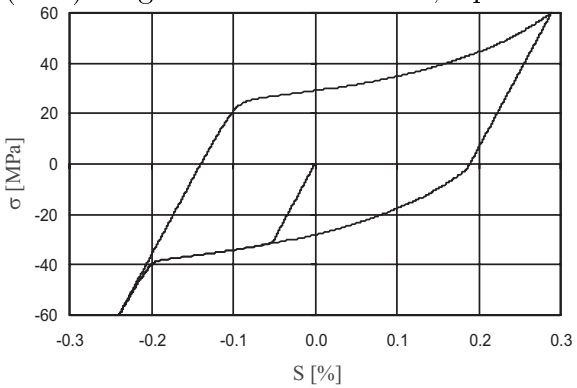

Figure 5.10: Model response to pure mechanical compression-tension loading: Ferroelastic hysteresis with quadratic $S^{\mathrm{i}}(\beta)$-relation (5.63) .

the result of FRÖHLICH [2001]. The calculated model response is shown in the right panel of Figure 5.9. It can be seen that the piece-wise linear $S^{\mathrm{i}}(\beta)$-relation reflects deformation asymmetry more realistically than the linear one. Because of the piece-wise linearity in $S^{\mathrm{i}}(\beta)$, the ferroelastic hysteresis in right panel shows a slight kink as compared to left panel of Figure 5.9.

The quadratic $S^{\mathrm{i}}(\beta)$-relation

$$S^{\mathrm{i}}(\beta) = -0.69 S^{\mathrm{sat}} (\beta - \beta^{\mathrm{ref}})^2 + 1.95 S^{\mathrm{sat}} (\beta - \beta^{\mathrm{ref}}) \tag{5.63}$$

is also used to match the deformation asymmetry. (Note that in this case the driving force is not of the simple form (5.19) and $\phi^{\beta,0}$ has to be computed from (5.23).) Figure 5.10 shows the calculated ferroelastic hysteresis. It can be seen that the $S^{\mathrm{i}}(\beta)$-relation (5.63) reflects the deformation asymmetry fairly

well. Compared with the left panel of Figure 5.9, the ferroelastic hysteresis in Figure 5.10 is smoother but shows a stronger hardening effect. These characteristics are induced by the quadratic $S^{\mathrm{i}}(\beta)$-relation (5.63).

5.3.3 Mechanical depolarization

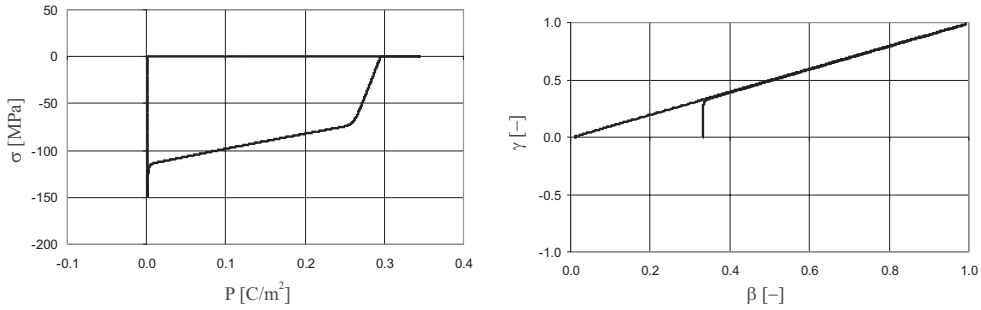

Figure 5.11: Mechanical depolarization following full polarization. Left: Polarization *vs.* stress. Right: β-γ plane.

To the left of Figure 5.11, we see mechanical depolarization by mechanical stresses of sufficient magnitude following a full poling process. In the calculation, an electric field of 2 kV/mm in amplitude is applied. After unloading the electric field, a compressive stress is applied. The right panel of Figure 5.11 shows the corresponding β-γ-path, from which we recognize that complete depolarization ($\gamma \to 0$) was enforced by driving the internal variable β to zero.

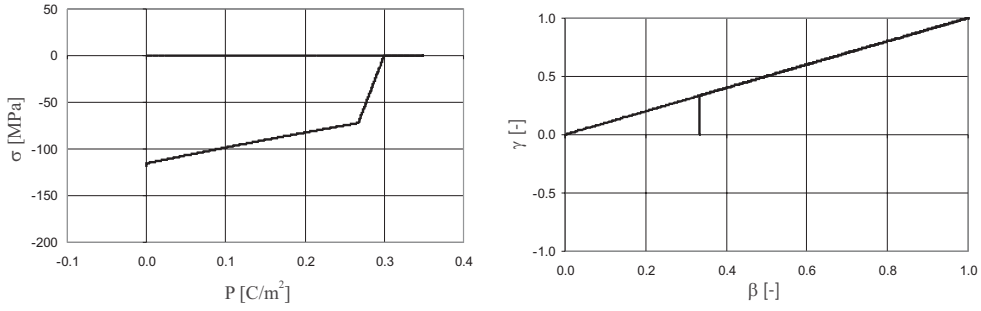

Figure 5.12: Mechanical depolarization following full polarization, indicator function is used as F^G. Left: Polarization *vs.* stress. Right: β-γ plane.

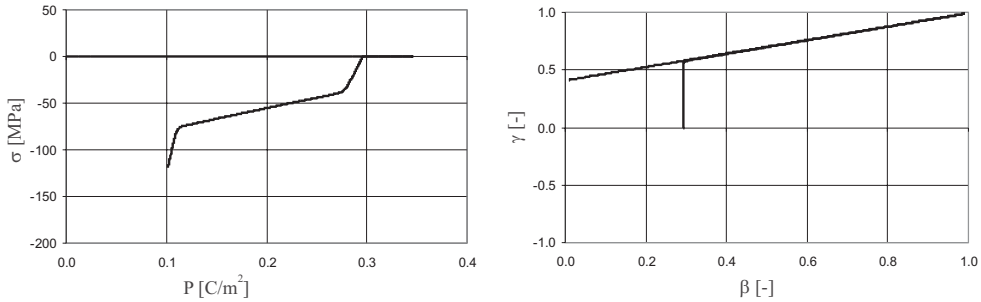

Figure 5.13: Mechanical depolarization following full polarization, the trapezoidal G (Figure 5.4) is used as the set of admissible values of $(\beta\,,\,\gamma)$. Left: Polarization *vs.* stress. Right: β-γ plane.

For the same loading history as in Figure 5.11, we used indicator function (5.36) as F^G to study the model response. Figure 5.12 shows the depoling process (left) and the evolution of the internal variables by the corresponding β-γ-path (right). Again the abrupt change of the simulated material behavior appears as the boundary of G is reached. These examples confirm that the additive F^G (5.49) gives more realistic results. For this loading history, we also used the trapezoidal G (Figure 5.4) as the set of admissible values for (β, γ) to calculate the poling and mechanical depoling process. In this calculation $\gamma^{\text{limit,min}} = 0.42$. The exact value of $\beta^{\text{ref}} = 1 - \cos 45°$ is used. Figure 5.13 shows the calculated depoling process (left) and the evolution of the internal variables by the corresponding β-γ-path (right). Because of the trapezoidal set G, a fully mechanical depolarization cannot be reached. Even under a compressive stress of up to -120 MPa, a polarization of about 0.1C/m^2 remains (left). The corresponding minimum γ is 0.42 according to $\gamma^{\text{limit,min}}$.

5.3.4 Combined electromechanical loading

We now consider the model response to combined electromechanical loading. Figure 5.14 shows the calculated dielectric and butterfly hystereses during a electric field cycling with a tensile stress preload. The applied tensile stress is $0.3\sigma^{\text{c}}$ smaller than the coercive stress so that it is not be able to induce domain switching alone. In comparison with the response to pure electric field cycling shown in Figure 5.5, the material reaches the saturation state at a lower electric field and the intermediate period vanishes. Oppositely, Figure 5.15 shows the calculated dielectric and butterfly hystereses during an

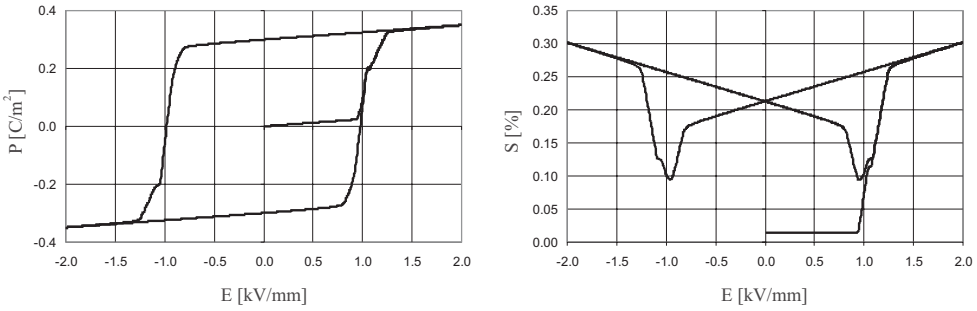

Figure 5.14: Poling and electric field cycling with a tensile stress of $0.3\sigma^{\mathrm{c}}$ applied. Left: Dielectric hysteresis. Right: Butterfly hysteresis.

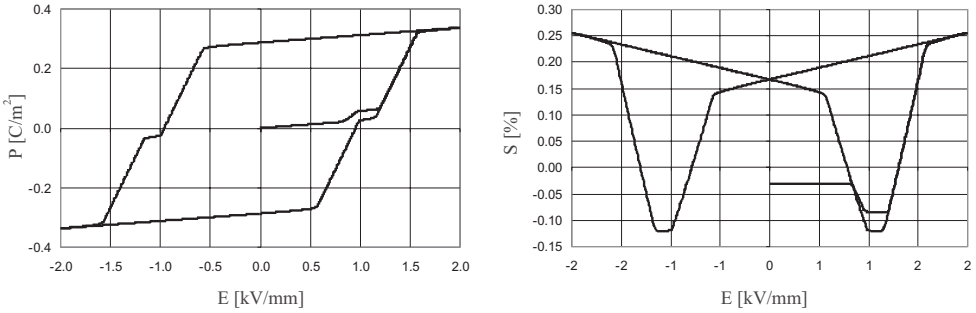

Figure 5.15: Poling and electric field cycling with a compressive stress of $-0.6\sigma^{\mathrm{c}}$ applied. Left: Dielectric hysteresis. Right: Butterfly hysteresis.

electric field cycling with a compressive stress of $-0.6\sigma^{\mathrm{c}}$ preloaded. Because the applied compressive stress hinders the domain switching in the electric field direction, we can see from the results in Figure 5.15 that the intermediate period becomes longer and that a higher electric field is needed for the material to reach the saturation state.

Now, the material response to compressive mechanical loading with a constant bias electric field applied in the poling direction is calculated. This loading path is similar to the loading history described in section 5.3.3, with the exception that a constant bias electric field is applied in the poling direction. The results of the calculations are shown in Figure 5.16. The applied constant electric filed during this mechanical depoling process are 0.2 kV/mm (left) and 0.4 kV/mm (right), respectively. Compared to the mechanical depoling process shown in the left panel of Figure 5.11 (without bias electric field), higher compressive stress is needed to initiate the domain switching if an electric field is applied in the poling direction. Under pure mechanical

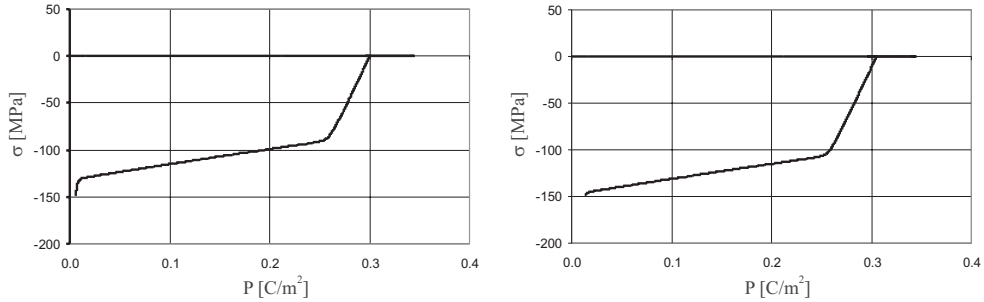

Figure 5.16: Mechanical depolarization with a constant bias electric field applied in the poling direction. Left: 0.2 kV/mm. Right: 0.4 kV/mm.

loading a fully depoled state is reached if the applied stress is about -120 MPa (left panel of Figure 5.11). If a bias electric field of 0.4 kV/mm (right panel of Figure 5.16) is applied, a fully depoled state cannot not be achieved even though the compressive stress reaches a level of -150 MPa. This model behavior is in agreement with the material properties outlined in section 2.3, that an electric field acting in the direction of previous poling tends to support the existing domain state and, thus, higher stresses are needed to initiate and continue mechanically induced domain switching processes.

Finally, proportional electromechanical loading is simulated, *i.e.*, the ratio between the electric field and the stress ramains constant. Figure 5.17 shows the dielectric and butterfly hystereses, by which $\mathrm{E}(t)/\sigma(t) = 2\mathrm{E}^{\mathrm{c}}/0.8\sigma^{\mathrm{c}}$. The loading path related to Figure 5.18 is a 180° out of phase proportional electromechanical loading, *i.e.*, $\mathrm{E}(t)/\sigma(t) = 2\mathrm{E}^{\mathrm{c}}/(-1.2\sigma^{\mathrm{c}})$.

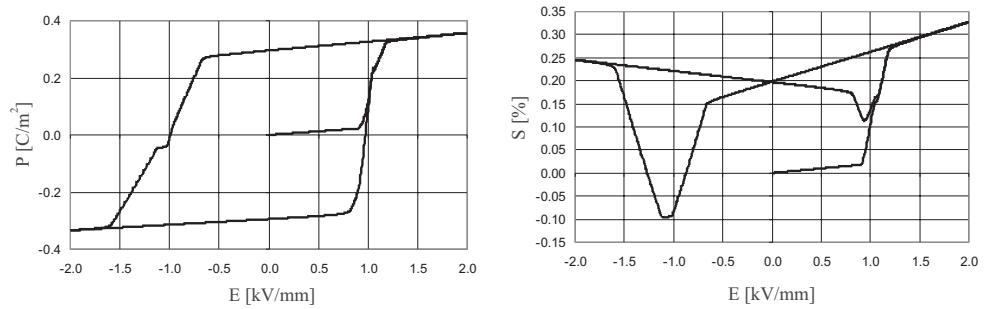

Figure 5.17: Proportional electromechanical loading, $\mathrm{E}(t)/\sigma(t) = 2\mathrm{E}^{\mathrm{c}}/0.8\sigma^{\mathrm{c}}$. Left: Dielectric hysteresis. Right: Butterfly hysteresis.

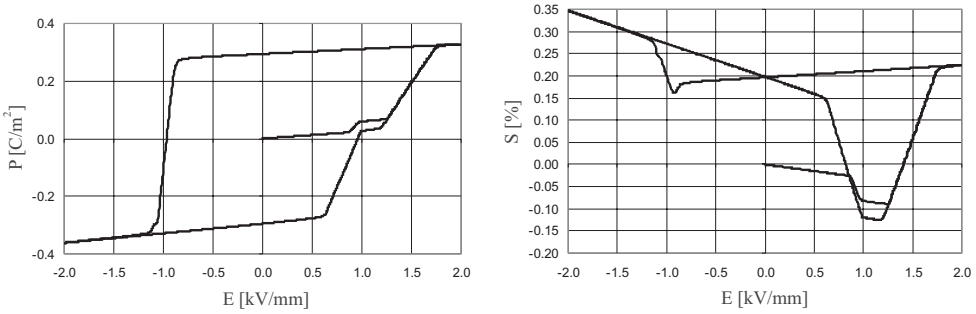

Figure 5.18: Proportional electromechanical loading, $\mathrm{E}(t)/\sigma(t) = 2\mathrm{E}^{\mathrm{c}}/(-1.2\sigma^{\mathrm{c}})$. Left: Dielectric hysteresis. Right: Butterfly hysteresis.

For the loading path related to Figure 5.17, electric field and tensile stress increase simultaneously. Therefore, the intermediate period vanishes in the positive side of electric field and the material reaches a saturation state at a lower electric field. After unloading, as the electric field increases in the opposite direction, the stress becomes compressive. Similar to the case in Figure 5.15, the intermediate period becomes longer and material reaches a saturation state at a higher electric feld. The dielectric and butterfly hystereses become asymmetric. In the case shown in Figure 5.18, electric field and compressive stress increase simultaneously in the first quarter period of the loading cycle. Because of the compressive stress a higher electric field is needed for material to reach the fully poled state. After unloading, the stress becomes tensile and a saturation state is reached at a lower electric field in the opposite direction. The dielectric and butterfly hystereses become very asymmetric.

Chapter 6

Multiaxial formulation of the model

The model formulated in the previous sections will be extended to the multiaxial case so that it is able to describe the material responses to general electromechanical loadings. In general, switching processes in a ferroelectric and ferroelastic polycrystal will lead to a state of orthotropic anisotropy on the macroscopic level. However, at the present state of our work, we simplify things by restricting ourselves to a transversally isotropic state in the sense to be explained below.

6.1 Internal variables in the multiaxial loading case

The uniaxial formulation of the model is based on two scalar valued internal variables. β represents the fraction of domains with their c-axis situated in the 45°-cones about a preferred direction, and γ is the relative irreversible macroscopic polarization. For uniaxial loadings, cones-axis and direction of polarization are both identical with the axis of loading chosen to be the x_3-axis in the previous section. For multiaxial loadings, both axes can no longer be considered to be constants. Rather, they will depend on the loading history and must not coincide. For instance, an electric field perpendicular to the poling direction will lead to polarization rotation, while the magnitude of the relative irreversible macroscopic polarization will basically stay unchanged. Similarly, it can be expected that nonproportional mechanical loading paths will induce reorientation of the axis of transverse anisotropy. Thus, two additional vectorial internal variabels are introduced. $\vec{e}^{\beta}$ is the *history dependent axis of our* 45°*-cones*, while $\vec{e}^{\gamma}$ is the *history dependent*

direction of the relative irreversible macroscopic polarization.

Thus, the model is still based on the idea that domains switch into or out of 45°-cones, if the electromechanical loading reaches a critical value. However, now the direction $\vec{\mathrm{e}}^{\beta}$ of the axis of the 45°-cones is dependent on the loading history. Furthermore, as before, the domains whose c-axes are located in the 45°-cones are assumed to contribute to the polarization, *i.e.*, the domains whose c-axes are located out of the 45°-cones are taken to be randomly distributed. But now, in the multiaxial loading case, especially under nonproportional electromechanical loadings, $\vec{\mathrm{e}}^{\gamma}$ needs not be parallel to $\vec{\mathrm{e}}^{\beta}$, in the general. Thus we have two additional internal variables given by unit vectors:

$$\vec{\mathrm{e}}^{\alpha} = \mathrm{e}_1^{\alpha}\vec{\mathrm{e}}_1 + e_2^{\alpha}\vec{\mathrm{e}}_2 + \mathrm{e}_3^{\alpha}\vec{\mathrm{e}}_3, \quad (\mathrm{e}_1^{\alpha})^2 + (\mathrm{e}_2^{\alpha})^2 + (\mathrm{e}_3^{\alpha})^2 = 1, \quad \alpha = \beta, \gamma \tag{6.1}$$

Here, $\vec{\mathrm{e}}_i$, $i = 1, 2, 3$ are the unit base-vectors of Cartesian coordinates.

As phenomenological internal variables, β and $\vec{\mathrm{e}}^{\beta}$ represent a macroscopic or average effect of domain switching. The vectorial variable $\vec{\mathrm{e}}^{\beta}$ stands for a history dependent preferred direction in which the c-axes switch to, while the scalar variable β is the fraction of domains switched in this direction. Furthermore, we assume that the c-axes outside the cones are distributed randomly in the sense that there exist no preferred directions perpendicular to the cone axis. This means a restriction with respect to the general case, in which as mentioned before, domain switching will lead to a state of orthotropic anisotropy on the macroscopic level. In the consequence of our simplified picture, we confine ourselves to a transversely isotropic irreversible strain state in the form

$$S_{ij}^{\mathrm{i}} = \frac{3}{2}\, S^{\mathrm{sat}}\, \frac{\beta - \beta^{\mathrm{ref}}}{1 - \beta^{\mathrm{ref}}} \left(\mathrm{e}_i^{\beta}\mathrm{e}_j^{\beta} - \frac{1}{3}\delta_{ij} \right) \quad , \tag{6.2}$$

where

$$\delta_{ij} = \begin{cases} 1, & i = j \\ 0, & i \neq j \end{cases} \tag{6.3}$$

is the Kronecker delta. In its macroscopic interpretation, this is a uniaxial and volume preserving strain state in the direction of $\vec{\mathrm{e}}^{\beta}$. In particular, for uniaxial loadings in x_3 direction, $\vec{\mathrm{e}}^{\beta} = \vec{\mathrm{e}}_3$, and we recover the linear relation (5.12) for the strain component S_{33}^{i}.

As mentioned before, the direction $\vec{\mathrm{e}}^{\beta}$ of the cones and the direction of the relative irreversible polarization $\vec{\mathrm{e}}^{\gamma}$ need not coincide, in general. Rather, depending on the loading history, they may deviate from each other. Therefore, we have introduced the second vectorial internal variable $\vec{\mathrm{e}}^{\gamma}$. As in

the uniaxial formulation, γ denotes the relative net polarization state of the domains. According to this definition, we have the relation

$$\vec{\mathrm{P}}^{\,\mathrm{i}} = \mathrm{P}^{\mathrm{sat}}\,\gamma\,\vec{\mathrm{e}}^{\,\gamma} \tag{6.4}$$

for the dependence of the vector of irreversible macroscopic polarization on internal variables. For the sake of convenience, we may introduce the vector

$$\vec{\gamma} = \gamma\vec{\mathrm{e}}^{\,\gamma} = \gamma_1\vec{\mathrm{e}}_1 + \gamma_2\vec{\mathrm{e}}_2 + \gamma_3\vec{\mathrm{e}}_3 \quad . \tag{6.5}$$

In a Cartesian coordinate system, the internal variables $(\gamma, \vec{\mathrm{e}}^{\,\gamma})$ can equivalently represented by the components $\gamma_i = \gamma \mathrm{e}_i^{\gamma}$ $(i = 1, 2, 3)$.

Since $\vec{\mathrm{e}}^{\,\beta}$ and $\vec{\mathrm{e}}^{\,\gamma}$ may enclose an angle, *i.e.*, $|\vec{\mathrm{e}}^{\,\beta} \cdot \vec{\mathrm{e}}^{\,\gamma}| < 1$, the set G of admissible values for the internal variables has to be reformulated. Here, we concentrate on a generalization of the triangular region (5.30). We recall that in this case, only the domains with their c-axes in the 45°-cones contribute to the net relative irreversible polarization. Therefore, it is now the projection of the relative irreversible polarization $\gamma\vec{\mathrm{e}}^{\,\gamma}$ in the direction of the cone axis given by $\vec{\mathrm{e}}^{\,\beta}$, which must not be larger than the fraction β of domains aligned with this latter direction, *i.e.*,

$$|\gamma| \leq \beta\,|\vec{\mathrm{e}}^{\,\beta} \cdot \vec{\mathrm{e}}^{\,\gamma}| \quad . \tag{6.6}$$

This is visualized on the left panel of Fig. 6.1. In the uniaxial case, $\vec{\mathrm{e}}^{\,\beta} = \vec{\mathrm{e}}^{\,\gamma}$, and we recover $|\gamma| \leq \beta$, which has been the requirement for admissible internal states in case of the triangular region (5.30). On the other hand, if $\vec{\mathrm{e}}^{\,\gamma}$ approaches a direction perpendicular to the cones axis $\vec{\mathrm{e}}^{\,\beta}$, the net relative irreversible polarization has to vanish, since we neglect any preferred directions perpendicular to $\vec{\mathrm{e}}^{\,\beta}$. Mathematically, if $\vec{\mathrm{e}}^{\,\beta} \cdot \vec{\mathrm{e}}^{\,\gamma} \to 0$, then, as a consequence of inequality (6.6), $|\gamma| \to 0$. Consequently, the set G is now given by

$$G = \left\{ (\beta, \gamma, \vec{\mathrm{e}}^{\,\beta}, \vec{\mathrm{e}}^{\,\gamma}) \;\middle|\; 0 \leq |\gamma| \leq \beta\,|\vec{\mathrm{e}}^{\,\beta} \cdot \vec{\mathrm{e}}^{\,\gamma}| \leq 1 \right\} \quad . \tag{6.7}$$

This three dimensional region is graphically presented on the right panel of Fig. 6.1 Due its geometry, full polarization ($\gamma \to \pm 1$) will cause a complete alignment of the two vectorial internal variables ($|\vec{\mathrm{e}}^{\,\beta} \cdot \vec{\mathrm{e}}^{\,\gamma}| \to 1$) and all c-axes to switch into the 45°-cones ($\beta \to 1$). On the other hand, mechanical compression in the direction of the cones-axis ($\beta \to 0$) will lead to a complete depolarization ($\gamma \to 0$) irrespective of the relative orientation of $\vec{\mathrm{e}}^{\,\beta}$ and $\vec{\mathrm{e}}^{\,\gamma}$.

From (6.7), the continuous additive energy barrier function (5.49) is generalized as

$$F^G = A\Big(\beta^{-N} + (1-\beta)^{-N} + (\beta\,|\vec{\mathrm{e}}^{\,\beta} \cdot \vec{\mathrm{e}}^{\,\gamma}| - |\gamma|)^{-N}\Big) \quad . \tag{6.8}$$

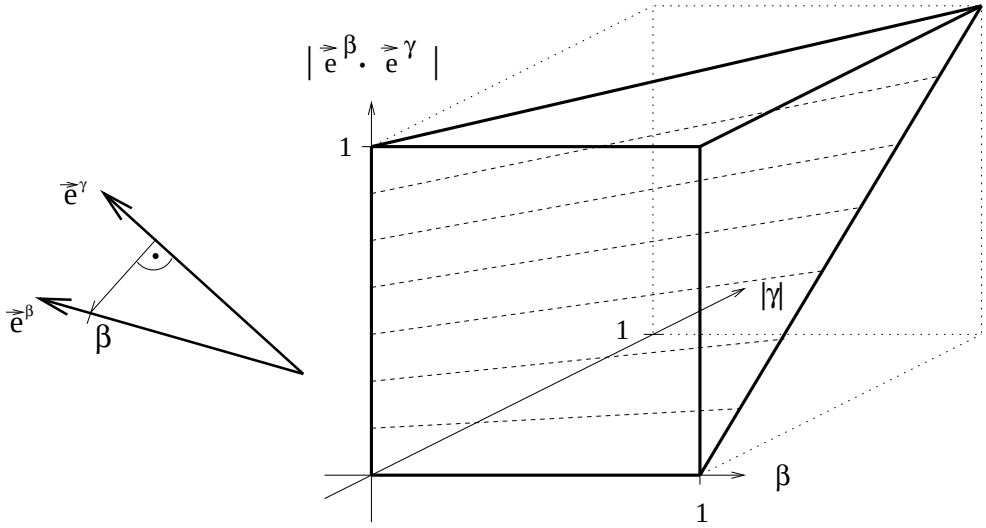

Figure 6.1: Admissible (β, γ) states. Left: Projection of β on the direction of $\vec{e}^{\gamma}$ according to relation (6.6) yields the maximum possible relative irreversible polarization. Right: The three dimensional set G according to (6.7).

6.2 Transversely isotropic material tensors

In accordance with the general thermodynamical framework for constitutive models introduced in section 4.2, our model consists of a "reversible" and an "irreversible" part. The reversible part, *i.e.*, equations (4.69) and (4.70), is determined by the reversible part (4.72) of the Gibbs free energy function (4.71). In this context, we need to state the dependence (4.61) through (4.63) of the material tensors on the internal variables, *i.e.*, the history dependent anisotropy properties of these tensors. In consistency with our assumptions in the previous section, we here restrict ourselves to transverse isotropy at the present state of our study.

The dielectric properties of a material are described by a second order tensor, *i.e.*, by a tensor of even rank. Furthermore, we expect that besides electric loadings also pure mechanical loadings may change the anisotropy properties of the dielectric behavior, which will depend on the orientation state of the c-axes of the domains in the first place. All together, the above considerations motivate us to assume that the axis of transverse isotropy of the tensor of susceptibilities is given by the axis of our 45°-cones. For simplicity, the magnitude of anisotropy is taken to be proportional to the deviation of the degree of alignment of the c-axes with the cones-axis from

the unpoled reference state.

Based on the vectorial internal variable $\vec{\mathrm{e}}^{\beta}$ representing the cones-axis, we introduce the second order structural tensor

$$m_{ij}^{\beta} = \mathrm{e}_i^{\beta}\mathrm{e}_j^{\beta} \quad , \tag{6.9}$$

for convenience. Thus, we propose the form

$$\kappa_{ij}(\beta, \vec{\mathrm{e}}^{\beta}) = \kappa\delta_{ij} + (\beta - \beta^{\mathrm{ref}}) \left(\Delta\kappa_{33} m_{ij}^{\beta} + \Delta\kappa_{11} \left(\delta_{ij} - m_{ij}^{\beta} \right) \right) \tag{6.10}$$

for the dependence of the tensor of susceptibilities. Here, κ is the susceptibility constant in the thermally depoled and isotropic reference state, and $\Delta\kappa_{33}$ and $\Delta\kappa_{11}$ describe the deviation herefrom in the direction of $\vec{\mathrm{e}}^{\beta}$ and perpendicular to it, respectively. If $\Delta\kappa_{33} = 0$ and $\Delta\kappa_{11} = 0$, we obtain a purely isotropic represenation, which does not depend an the loading history. In particular, for uniaxial loadings we recover the constant susceptibility coefficient used in equation (5.3) of the uniaxial formulation.

The situation is quite different for the piezoelectricity tensor. First of all, the history dependence of the anisotropy cannot be neglected here, since the piezoelectric properties are not just modified like it is the case with susceptibility, for instance. Instead, the phenomenon of macroscopic piezoelectricity is absent with vanishing macroscopic irreversible polarization. Furthermore, in the fully poled state, we have transversely isotropic piezoelectricity where the axis of anisotropy coincides with the direction $\vec{\mathrm{e}}^{\gamma}$ of poling. Therefore, we assume the representation

$$\begin{aligned} \mathrm{d}_{kij}(\gamma, \vec{\mathrm{e}}^{\gamma}) \;\; = \;\; \gamma \Bigg(& \mathrm{d}_{33}\, \mathrm{e}_k^{\gamma}\mathrm{e}_i^{\gamma}\mathrm{e}_j^{\gamma} \;\; + \;\; \mathrm{d}_{31}\, \mathrm{e}_k^{\gamma}(\delta_{ij} - \mathrm{e}_i^{\gamma}\mathrm{e}_j^{\gamma}) + \\ & \frac{1}{2}\,\mathrm{d}_{15} \left(\mathrm{e}_i^{\gamma}(\delta_{jk} - \mathrm{e}_j^{\gamma}\mathrm{e}_k^{\gamma}) + \mathrm{e}_j^{\gamma}(\delta_{ik} - \mathrm{e}_i^{\gamma}\mathrm{e}_k^{\gamma}) \right) \Bigg) \quad , \end{aligned} \tag{6.11}$$

which is transversally isotropic with respect to the poling direction. By this choice, magnitude and direction of the piezoelectric effect are given by magnitude γ and direction $\vec{\mathrm{e}}^{\gamma}$ of the relative irreversible polarization, respectively. d_{33}, d_{31} and d_{15} are the piezoelectric moduli of the fully poled state in Voigt's matrix notation. For uniaxial loadings in x_3-direction, we recover the uniaxial form (5.17) for the dependence of the piezoelectric coefficient, if we identify d_{33} with d.

Just as susceptibilty, elasticity is a property represented by a tensor of even rank, and the history dependent anisotropy properties may be changed

by pure mechanical loading paths (see FETT *et al.* [2002]). Therefore, we assume likewise that the axis of transverse isotropy of the elasticity tensor conicides with our cones-axis, by taking this tensor to be an even function of $\vec{\mathrm{e}}^{\beta}$ in the form of m_{ij}^{β}. With reference to BETTEN [1987], pp. 163, for a transversely isotropic material with a preferred direction $\vec{\mathrm{e}}^{\beta}$, the elastic potential energy can be expressed by the invariants of stress tensor T_{ij} and the structural tensor m_{ij}^{β} and their joint invariants. From the elastic potential energy we get the elastic compliance tensor

$$\begin{aligned} s_{ijkl}(\beta,\vec{\mathrm{e}}^{\beta}) = C_{ijkl}^{-1}(\beta,\vec{\mathrm{e}}^{\beta}) &= 2\alpha^{(6)}\delta_{ij}\delta_{kl} \\ &\quad +2\alpha^{(3)}(\delta_{ik}\delta_{jl}+\delta_{il}\delta_{jk}) \\ &\quad +\alpha^{(8)}(\delta_{ij}m_{lk}^{\beta}+\delta_{kl}m_{ij}^{\beta}) \\ &\quad +\alpha^{(5)}(\delta_{ki}m_{lj}^{\beta}+\delta_{lj}m_{ik}^{\beta}) \\ &\quad +2\alpha^{(7)}m_{ij}^{\beta}m_{kl}^{\beta} \quad , \end{aligned} \tag{6.12}$$

in which

$$\begin{aligned} \alpha^{(3)} &= \frac{1}{4}(s_{11}-s_{12}) \quad , \\ \alpha^{(5)} &= \frac{1}{4}s_{44}-\frac{1}{4}(s_{11}-s_{12}) \quad , \\ \alpha^{(6)} &= \frac{1}{2}s_{12} \quad , \\ \alpha^{(7)} &= \frac{1}{2}(s_{12}+s_{33}-\frac{1}{2}s_{44}-2s_{13}) \quad , \\ \alpha^{(8)} &= s_{13}-s_{12} \quad . \end{aligned}$$

Here, s_{11}, s_{33}, s_{44}, s_{12} and s_{13} are the elastic compliances of the transversely isotropic material in Voigt's matrix notation (FRANÇOIS *et al.* [1998], pp. 73-77, equation (2.48)). The coefficients $\alpha^{(I)}$, $I=3,5,6,7,8$ are some function of β, such that in the thermally depoled reference state ($\beta=\beta^{\mathrm{ref}}$) the isotropic representation

$$C_{ijkl}^{-1} = -\frac{\nu}{Y}\delta_{ij}\delta_{kl}+\frac{1+\nu}{2Y}(\delta_{ik}\delta_{jl}+\delta_{il}\delta_{jk}), \tag{6.13}$$

is obtained, in which ν is Poison's ratio of the material measured at constant

electric field. Of course, a linear dependence on $\beta - \beta^{\rm ref}$ of the kind

$$\begin{aligned}
\alpha^{(3)} &= \frac{1+\nu}{2Y} + (\beta - \beta^{\rm ref})\Delta\alpha^{(3)} \quad , \\
\alpha^{(5)} &= (\beta - \beta^{\rm ref})\Delta\alpha^{(5)} \quad , \\
\alpha^{(6)} &= -\frac{\nu}{Y} + (\beta - \beta^{\rm ref})\Delta\alpha^{(6)} \quad , \\
\alpha^{(7)} &= (\beta - \beta^{\rm ref})\Delta\alpha^{(7)} \quad , \\
\alpha^{(8)} &= (\beta - \beta^{\rm ref})\Delta\alpha^{(8)}
\end{aligned}$$

for the deviation from the isotropic form will be the simplest choice, as in the case of the tensor of susceptibilties. Here, $\Delta\alpha^{(I)}$, $I = 3, 5, 6, 7, 8$ are constants. The assumption of Young's modulus being a constant in equation (5.4) of the uniaxial formulation is consistent with neglecting any dependence of the elastic properties on the loading history, *i.e.*, $\Delta\alpha^{(I)} = 0$, $I = 3, 5, 6, 7, 8$. For simplicity, one may employ the assumption of independence of the internal variables for the tensors of susceptibilites and elasticity by using equation (6.13) instead of equation (6.12) and the isotropic form of equation (6.10). In closing this section we want to emphasize that while each material tensor is transversely isotropic, it is difficult to speak of a transversely isotropic material, since the respective axes of anisotropy of the tensors need not coincide.

6.3 Multiaxial formulation of evolution equations

We now turn to the "irreversible" part of our model. As multiaxial generalization of the irreversible part of the Gibbs free energy function (4.71) we take

$$\rho g^{\rm i} = -\frac{1}{2}c^{\beta}(\beta - \beta^{\rm ref})^2 - \frac{1}{2}c^{\gamma}\gamma^2 - F^G(\beta, \gamma, \vec{\rm e}^{\beta}, \vec{\rm e}^{\gamma}) \quad , \tag{6.14}$$

where c^{β} and c^{γ} are the two material parameters introduced in the context of the uniaxial formulation. The functional form of (6.14) means that no hardening properties are associated with the vectorial internal variables with the exeption via the energy barrier function F^G given in equation (6.8)

From the definition (4.75) the general form of the driving forces corresponding the internal variables β, γ, $\vec{\rm e}^{\beta}$ and $\vec{\rm e}^{\gamma}$ is expressed as

$$\phi^{\alpha} = T_{ij}\frac{\partial S^{\rm i}_{ij}}{\partial\alpha} + {\rm E}_i\frac{\partial {\rm P}^{\rm i}_i}{\partial\alpha} + \rho\frac{\partial g}{\partial\alpha} \quad , \quad \alpha = \beta, \gamma, \vec{\rm e}^{\beta}, \vec{\rm e}^{\gamma} \quad . \tag{6.15}$$

The driving forces corresponding to the vectorial internal variables $\vec{\mathrm{e}}^{\beta}$ and $\vec{\mathrm{e}}^{\gamma}$ are vectors themselves. From the above prescription, we obtain with the help of (6.2)

$$\phi^{\beta} = \frac{3}{2}\frac{S^{\mathrm{sat}}}{1-\beta^{\mathrm{ref}}}\left(\mathrm{e}_i^{\beta}\mathrm{e}_j^{\beta}-\frac{1}{3}\delta_{ij}\right)T_{ij} - c^{\beta}(\beta-\beta^{\mathrm{ref}}) - \frac{\partial F^G}{\partial \beta} \quad , \tag{6.16}$$

$$\phi^{\gamma} = \mathrm{P}^{\mathrm{sat}}\mathrm{E}_i\,\mathrm{e}_i^{\gamma} + \frac{\partial \mathrm{d}_{kij}}{\partial \gamma}\mathrm{E}_k T_{ij} - c^{\gamma}\gamma - \frac{\partial F^G}{\partial \gamma} \quad , \tag{6.17}$$

$$\vec{\phi}^{\vec{\mathrm{e}}^{\beta}} = \frac{\partial S_{ij}^{\mathrm{i}}}{\partial \vec{\mathrm{e}}^{\beta}}T_{ij} + \frac{1}{2}\frac{\partial C_{ijkl}^{-1}}{\partial \vec{\mathrm{e}}^{\beta}}T_{ij}T_{kl} + \frac{1}{2}\frac{\partial \kappa_{ij}}{\partial \vec{\mathrm{e}}^{\beta}}\mathrm{E}_i\mathrm{E}_j - \frac{\partial F^G}{\partial \vec{\mathrm{e}}^{\beta}} \quad , \tag{6.18}$$

$$\vec{\phi}^{\vec{\mathrm{e}}^{\gamma}} = \frac{\partial \mathrm{P}_i^{\mathrm{i}}}{\partial \vec{\mathrm{e}}^{\gamma}}\mathrm{E}_i + \frac{\partial \mathrm{d}_{kij}}{\partial \vec{\mathrm{e}}^{\gamma}}\mathrm{E}_k T_{ij} - \frac{\partial F^G}{\partial \vec{\mathrm{e}}^{\gamma}} \quad . \tag{6.19}$$

As straight forward extrapolation of the uniaxial switching criterion (5.22), we may use

$$f = \sqrt{\left(\frac{\phi^{\beta}}{\phi^{\beta,0}}\right)^2 + \left(\frac{\phi^{\gamma}}{\phi^{\gamma,0}}\right)^2 + \left(\frac{|\vec{\phi}^{\vec{\mathrm{e}}^{\beta}}|}{\phi^{\vec{\mathrm{e}}^{\beta},0}}\right)^2 + \left(\frac{|\vec{\phi}^{\vec{\mathrm{e}}^{\gamma}}|}{\phi^{\vec{\mathrm{e}}^{\gamma},0}}\right)^2} - 1 \quad , \tag{6.20}$$

in which $\phi^{\beta,0}$, $\phi^{\gamma,0}$, $\phi^{\vec{\mathrm{e}}^{\beta},0}$ and $\phi^{\vec{\mathrm{e}}^{\gamma},0}$ are parameters indicating critical states for the onset of switching. Equation (6.20) represents a convex surface in the driving force-space. The formulation of the multiaxial switching criterion needs further consideration, especially with repsect to a reasonable choice for the parameter $\phi^{\vec{\mathrm{e}}^{\beta},0}$. In particular, it might be worth considering to formulate the theory using the structural tensor m_{ij}^{β} instead of the unit vector $\vec{\mathrm{e}}^{\beta}$, since the latter enters the equations only via $m_{ij}^{\beta} = \mathrm{e}_i^{\beta}\mathrm{e}_j^{\beta}$. In this context, the multiaxial experimental data by Lynch *et al.* [2000], Huber and Fleck [2001] and Chen and Lynch [2001] discussed in section 2.5, as well as Fett *et al.* [2003] will be helpful.

If $f \leq 0$, the internal variables remain constant and the model responds to the loading linearly. Otherwise, domain switching occurs and the internal variables will change as determined by their evolution equations. According to the prescription (4.79), the evolution equations are derived by the normality rule with respect to the switching criterion. As in the uniaxial formulation, we employ a rate dependent theory by adopting for the factor of proportionality in the flow rule the defintion (4.81). In summary, we have

$$\dot{\alpha} = \Lambda^0\langle f\rangle\frac{\partial f}{\partial \phi^{\alpha}} = \frac{\Lambda^0\langle f\rangle}{1+f}\frac{\phi^{\alpha}}{\left(\phi^{\alpha,0}\right)^2} \quad , \quad \alpha = \beta, \gamma, \vec{\mathrm{e}}^{\beta}, \vec{\mathrm{e}}^{\gamma} \quad . \tag{6.21}$$

(The principle of the construction a corresponding rate independent theory has given in section 4.2.3.)

The solution of the evolution equations (6.21) gives the histories of the internal variables. The irreversible polarization and strain can be calculated by substituting the internal variables into equations (6.2) and (6.4). The tensor of piezoelectricity d_{kij} is determined by (6.10). (Susceptibility and elasticity are assumed to be constant, *i.e.*, isotropic, see the remark at the end of section 6.2) The reversible polarization and strain can be calculated with equations (4.59) and (4.60). Furthermore, the total polarization and strain will be obtained by using equations (4.55) and (4.56).

In section 2.5 we outlined multiaxial test results from HUBER *et al.* [2002]. To the left of Figure 6.2 the polarization rotation test results are reprinted. The constitutive model developed in this section is used to reproduce these test results. The parameters in Table 5.1 are used in the calculation. It can be seen at the right panel of Figure 6.2 that the simulation is qualitatively in good agreement with the test results.

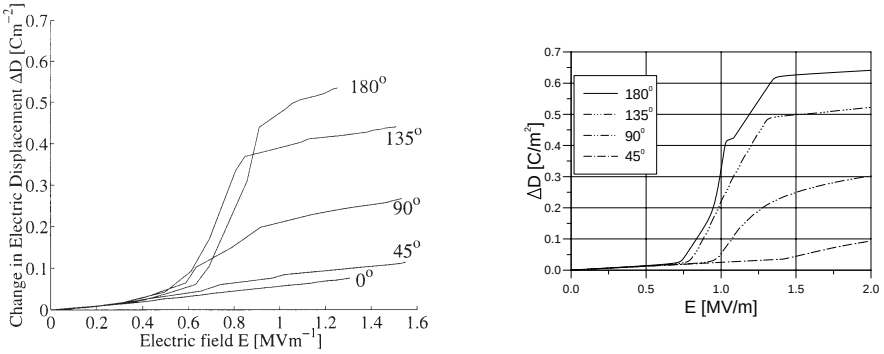

Figure 6.2: Measured and calculated dielectric response of PZT to the application of electric field at angles in the range $0 - 180°$ to the initial poling direction. Left: test results from HUBER *et al.* [2002]. Right: Calculated model response.

Chapter 7

Microscopic considerations

The microscopic motivation of the phenomenlogical constitutive model developed in the foregoing sections is based on the assumption that the domains switch into or out of 45°-cones, if the switching condition is satisfied. This assumption is most suitable for a tetragonal crystal structure, but, of course, the validity of the model is expected to apply to a broader range of materials. In this section, we want to investigate the microscopic foundation of our model by some supporting analysis based on an orientation distribution function or domain distribution density. The analysis is restricted to uniaxial loadings in x_3-direction.

7.1 Domain distribution density

Instead of the 45°-cones, we now introduce cones of arbitrary angle θ^e with the x_3-axis being the cones-axis, see Figure 7.1. Similar to the discussions in section (5.2), the fraction of domains with their c-axes situated within the two cones is chosen as the first internal variable, denoted by $\beta = q^1$. $\theta^e = q^2$ is also taken as a loading history-dependent variable. We assume that on a sphere of unit radius the domains are uniformly distributed inside and outside of the cones with the densities $\beta/(4\pi(1-\cos\theta^e))$ and $(1-\beta)/(4\pi\cos\theta^e)$, respectively. The *domain distribution density*

$$p(\theta) = \begin{cases} \dfrac{\beta}{4\pi(1-\cos\theta^e)} & \text{for} \quad 0 \le \theta \le \theta^e \\ \dfrac{1-\beta}{4\pi\cos\theta^e} & \text{for} \quad \theta^e \le \theta \le \frac{\pi}{2} \end{cases} \tag{7.1}$$

is graphically shown in Figure 7.2. It can be seen that the two internal variables have a definite physical meaning in the sense that they determine

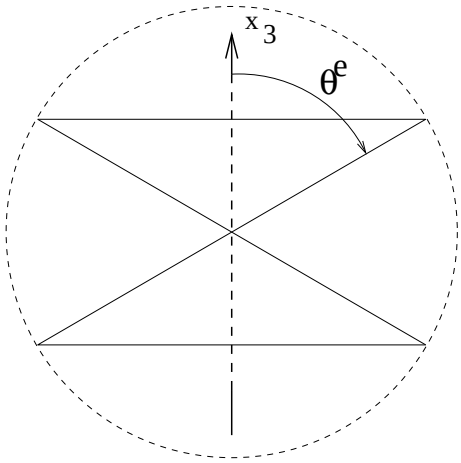

Figure 7.1: Two cones of θ^{e} about x_3-axis, being the axis of loading.

a step-function approximation to the true domain distribution density. A more sophisticated approximation would be obtained by more parameters, *i.e.*, by more steps.

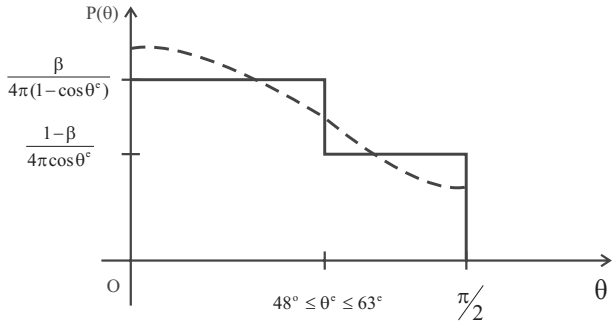

Figure 7.2: Density function $p(\theta)$ of the domain distribution. Dashed line: Real distribution. Continuous line: Approximate distribution.

7.2 Irreversible strain

If the spontaneous strain of a unit cell is S^{spon}, then we get the macroscopic irreversible strain of the material corresponding to the approximate domain distribution shown in Figure 7.2 by integration over the domain distribution

density as

$$S^{\mathrm{i}}_{33} = \frac{1}{2}(\beta + \beta\cos\theta^{\mathrm{e}} - \sin^2\theta^{\mathrm{e}})S^{\mathrm{spon}} \quad . \tag{7.2}$$

If all domains switch into the θ^{e}-cones, $\beta = 1$ and the corresponding irreversible strain is

$$S^{\mathrm{i}}_{33} = \frac{1}{2}\cos\theta^{\mathrm{e}}(1 + \cos\theta^{\mathrm{e}})S^{\mathrm{spon}} \quad . \tag{7.3}$$

In general, θ^{e} will vary between some minimum value $\theta^{\mathrm{e,min}} \geq 0$ and some maximum value $\theta^{\mathrm{e,max}} \leq \pi/2$, where $\theta^{\mathrm{e,min}}$ and $\theta^{\mathrm{e,max}}$ are treated as material constants. If $(\beta, \theta^{\mathrm{e}}) = (1, \theta^{\mathrm{e,min}})$, the irreversible strain reaches the *saturation strain*

$$S^{\mathrm{sat}} = \frac{1}{2}\cos\theta^{\mathrm{e,min}}(1 + \cos\theta^{\mathrm{e,min}})S^{\mathrm{spon}} \quad . \tag{7.4}$$

If $\theta^{\mathrm{e,min}} = 48°$, we get $S^{\mathrm{sat}} = 0.558S^{\mathrm{spon}}$ from equation (7.4). This means if the minimum cone-angle is chosen as 48°, the maximum irreversible strain, *i.e.*, the saturation strain, is $0.558S^{\mathrm{spon}}$, which is the value determined by Fröhlich [2001] and confirmed by Landis [2003]. Comparison of equations (7.2) and (7.4) yields

$$S^{\mathrm{i}}_{33}(\beta, \theta^{\mathrm{e}}) = \frac{\beta + \beta\cos\theta^{\mathrm{e}} - \sin^2\theta^{\mathrm{e}}}{\cos\theta^{\mathrm{e,min}}(1 + \cos\theta^{\mathrm{e,min}})}S^{\mathrm{sat}} \quad . \tag{7.5}$$

If a piezoceramic sample is under high compression, all domains switch out of the θ^{e}-cones. In this case $\beta = 0$, and the corresponding axial irreversible strain reads as

$$S^{\mathrm{i}}_{33} = -\frac{1}{2}\sin^2\theta^{\mathrm{e}}S^{\mathrm{spon}} \quad . \tag{7.6}$$

If now $\theta^{\mathrm{e}} = 64°$, we get $S^{\mathrm{i}}_{33} = -0.404S^{\mathrm{spon}}$, which is the value found by Fröhlich [2001] for the minimum irreversible strain under compression (cf. Landis [2003]). This finding suggests to choose $\theta^{\mathrm{e,max}} = 64°$, *i.e.*, in summary

$$\theta^{\mathrm{e,min}} = 48° \ \leq \ \theta^{\mathrm{e}} \ \leq \ \theta^{\mathrm{e,max}} = 64° \quad . \tag{7.7}$$

According to equation (7.2), the irreversible strain S^{i}_{33} is a function of β and θ^{e}. A uniform distribution of domains on the whole sphere corresponds to the thermally depoled *reference state*. For this reference state, we find by equating the two parts in equation (7.1) (see Figure 7.2)

$$\beta^{\mathrm{ref}} = 1 - \cos\theta^{\mathrm{e}} \quad . \tag{7.8}$$

From equation (7.5) we get independent of θ^{e}

$$S^{\mathrm{i}}_{33}(\beta^{\mathrm{ref}}, \theta^{\mathrm{e}}) = 0 \quad , \quad \theta^{\mathrm{e,min}} \leq \theta^{\mathrm{e}} \leq \theta^{\mathrm{e,max}} \quad . \tag{7.9}$$

7.3 Irreversible polarization

Each unit cell of a ferroelectric material forms a microdipole with its axis parallel to the c-axis of the tetragonal unit cell. Within a grain, there are six possible orientations for the microdipole of a unit cell. In particular, there are two orientations for each lattice direction. As a consequence, different states of macroscopic polarization can result from the microdipoles belonging to the same degree of alignment of the c-axes with respect to the x_3-axis, *i.e.*, for the same value of β. If for a given orientation state of the c-axes the spontaneous dipoles align in the positive x_3-axis direction, integration over the domain distribution density yields the maximum macroscopic irreversible polarization for given β and θ^{e} as

$$\mathrm{P}_3^{\mathrm{i,max}} = \frac{1}{2}\beta(1+\cos\theta^{\mathrm{e}})\mathrm{P}^{\mathrm{spon}} + \frac{1}{2}(1-\beta)\cos\theta^{\mathrm{e}}\mathrm{P}^{\mathrm{spon}} \quad . \tag{7.10}$$

The first term on the right side of this equation indicates the contribution of domains in the cones to the polarization, and the second term belongs to the contributions from the domains outside of the cones. Equation (7.10) can be written in a compact form as

$$\mathrm{P}_3^{\mathrm{i,max}} = \frac{1}{2}(\beta+\cos\theta^{\mathrm{e}})\mathrm{P}^{\mathrm{spon}} \quad . \tag{7.11}$$

If $(\beta, \theta^{\mathrm{e}}) = (1, \theta^{\mathrm{e,min}})$, $\mathrm{P}_3^{\mathrm{i,max}}$ approaches the *saturation polarization* $\mathrm{P}^{\mathrm{sat}}$, thus

$$\mathrm{P}^{\mathrm{sat}} = \frac{1}{2}(1+\cos\theta^{\mathrm{e,min}})\mathrm{P}^{\mathrm{spon}} \quad . \tag{7.12}$$

If $\theta^{\mathrm{e,min}} = 48^\circ$, $\mathrm{P}^{\mathrm{sat}} = 0.835\mathrm{P}^{\mathrm{spon}}$. This value is in agreement with Fröhlich [2001] and many other authors. With comparison of equations (7.11) and (7.12) we get:

$$\mathrm{P}_3^{\mathrm{i,max}} = \frac{\beta+\cos\theta^{\mathrm{e}}}{1+\cos\theta^{\mathrm{e,min}}}\mathrm{P}^{\mathrm{sat}} \quad . \tag{7.13}$$

In view of these considerations, we need an additional information in order to determine the macroscopic state of polarization associated with the microscopic domain state. In this sense, our third internal variable $\gamma = q^3$ represents the state of relative macroscopic polarization in the x_3-direction resulting from the distribution of the spontaneous microdipoles:

$$\gamma = \frac{\mathrm{P}_3^{\mathrm{i}}}{\mathrm{P}^{\mathrm{sat}}} \quad . \tag{7.14}$$

7.4 Range of admissible values for internal variables

From the above discussion it can be seen that for given β and θ^{e} the maximum possible value of $|\gamma|$ is

$$|\gamma| \leq \gamma^{\mathrm{limit}} = \frac{\beta + \cos\theta^{\mathrm{e}}}{1 + \cos\theta^{\mathrm{e,min}}} \quad . \tag{7.15}$$

In summary, the microstructural parameters β , γ and θ^{e} are not completely independent of each other and admissible internal states are represented by the set

$$\begin{aligned} G \;\; = \;\; \Big\{ (\beta, \gamma, \theta^{\mathrm{e}}) \;\Big|\; |\gamma| \leq \frac{\beta + \cos\theta^{\mathrm{e}}}{1 + \cos\theta^{\mathrm{e,min}}} \;, \\ 0 \leq \beta \leq 1 \;,\; \theta^{\mathrm{e,min}} \leq \theta^{\mathrm{e}} \leq \theta^{\mathrm{e,max}} \Big\} \quad . \end{aligned} \tag{7.16}$$

As shown in the β-γ-plane in Figure 7.3, for given θ^{e} G is a trapezoid with its 4 corners at

$$\begin{aligned} &\mathrm{A} \quad \Big(0, \frac{\cos\theta^{\mathrm{e}}}{1 + \cos\theta^{\mathrm{e,min}}}\Big) \quad , \\ &\mathrm{O} \quad \Big(0, 0\Big) \quad , \\ &\mathrm{B} \quad \Big(1, 0\Big) \quad , \\ &\mathrm{C} \quad \Big(1, \frac{1 + \cos\theta^{\mathrm{e}}}{1 + \cos\theta^{\mathrm{e,min}}}\Big) \quad . \end{aligned}$$

7.5 Evolution equations

We now want to derive evoltion equations for the microstuctural parameters by the very same procedure as we have used before for the uniaxial formulation of our constitutive model. Therefore, we adopt (5.5) for the reversible part of the Gibbs energy function with constant susceptibility coefficient and Young's modulus and the piezoelectric coefficient according to (5.17). Note that these properties of the coefficients are assumed and not derived. As irreversible part of the Gibbs energy function we introduce similar to (5.18)

$$\begin{aligned} \rho g^{\mathrm{i}} \;\; = \;\; & -\frac{1}{2} c^{\beta} (\beta - \beta^{\mathrm{ref}})^2 - \frac{1}{2} c^{\theta^{\mathrm{e}}} (\theta^{\mathrm{e}} - \theta^{\mathrm{e,ref}})^2 \\ & -\frac{1}{2} c^{\gamma} \gamma^2 - F^G(\beta, \theta^{\mathrm{e}}, \gamma) \quad , \end{aligned} \tag{7.17}$$

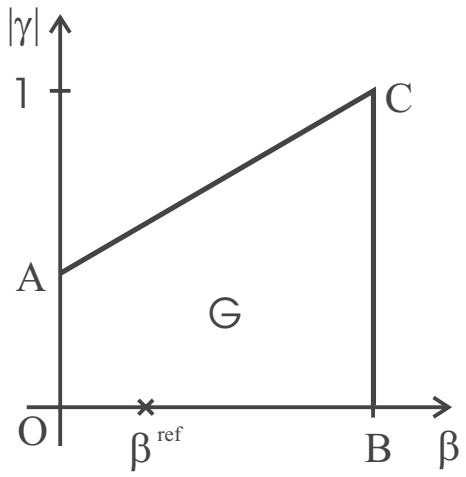

Figure 7.3: The set G of admissible (β, γ) states for given θ^{e} corresponding to (7.16).

where $\theta^{\mathrm{e,ref}}$ is some reference value for θ^{e}. A possible choice for the corresponding energy barrier function is again of the form

$$F^G = A\Bigg(\beta^{-N} + (1-\beta)^{-N} + \Big(\frac{\beta + \cos\theta^{\mathrm{e}}}{1 + \cos\theta^{\mathrm{e,min}}} - |\gamma|\Big)^{-N} + (\theta^{\mathrm{e}} - \theta^{\mathrm{e,min}})^{-N} + (\theta^{\mathrm{e,max}} - \theta^{\mathrm{e}})^{-N}\Bigg) \quad . \tag{7.18}$$

From equations (4.75), (7.5), and (7.14) we get the driving forces corresponding to the internal variables β, θ^{e}, and γ:

$$\phi^{\beta} = \frac{1 + \cos\theta^{\mathrm{e}}}{\cos\theta^{\mathrm{e,min}}(1 + \cos\theta^{\mathrm{e,min}})} S^{\mathrm{sat}}\sigma - c^{\beta}(\beta - \beta^{\mathrm{ref}}) - \frac{\partial F^G}{\partial \beta} \quad , \tag{7.19}$$

$$\phi^{\theta^{\mathrm{e}}} = -\frac{\beta \sin\theta^{\mathrm{e}} + 2\sin\theta^{\mathrm{e}}}{\cos\theta^{\mathrm{e,min}}(1 + \cos\theta^{\mathrm{e,min}})} S^{\mathrm{sat}}\sigma - c^{\theta^{\mathrm{e}}}(\theta^{\mathrm{e}} - \theta^{\mathrm{e,ref}}) - \frac{\partial F^G}{\partial \theta^{\mathrm{e}}} \ , \tag{7.20}$$

$$\phi^{\gamma} = \mathrm{P}^{\mathrm{sat}}\mathrm{E} + \mathrm{d}^{\mathrm{sat}}\mathrm{E}\sigma - c^{\gamma}\gamma - \frac{\partial F^G}{\partial \gamma} \quad . \tag{7.21}$$

The equation

$$f = \sqrt{\left(\frac{\phi^{\beta}}{\phi^{\beta,0}}\right)^2 + \left(\frac{\phi^{\theta^{\mathrm{e}}}}{\phi^{\theta^{\mathrm{e}},0}}\right)^2 + \left(\frac{\phi^{\gamma}}{\phi^{\gamma,0}}\right)^2 - \frac{\phi^{\beta}\phi^{\theta^{\mathrm{e}}}}{\phi^{\beta,0}\phi^{\theta^{\mathrm{e}},0}}} - 1 \tag{7.22}$$

may be used as a possible switching condition. f describes an ellipse and, thus, a convex surface in driving force space containing the origin. In this switching function, the critical driving forces are taken as

$$\phi^{\beta,0} = \frac{1+\cos\theta^{\mathrm{e}}}{\cos\theta^{\mathrm{e,min}}(1+\cos\theta^{\mathrm{e,min}})} S^{\mathrm{sat}}\sigma^{\mathrm{c}} \quad , \tag{7.23}$$

$$\phi^{\theta^{\mathrm{e}},0} = -\frac{\beta\sin\theta^{\mathrm{e}}+2\sin\theta^{\mathrm{e}}}{\cos\theta^{\mathrm{e,min}}(1+\cos\theta^{\mathrm{e,min}})} S^{\mathrm{sat}}\sigma^{\mathrm{c}} \quad , \tag{7.24}$$

$$\phi^{\gamma,0} = \mathrm{P}^{\mathrm{sat}}\mathrm{E}^{\mathrm{c}} \quad . \tag{7.25}$$

The mixed ϕ^{β}-$\phi^{\theta^{\mathrm{e}}}$-term in f makes sure that the critical stress magnitude in case of purely mechanical loadings is σ^{c}. The evolution equations

$$\dot{\beta} = \frac{1}{2}\frac{\Lambda^0\langle f\rangle}{1+f}\left(\frac{2\phi^{\beta}}{(\phi^{\beta,0})^2} - \frac{\phi^{\theta^{\mathrm{e}}}}{\phi^{\beta,0}\phi^{\theta^{\mathrm{e}},0}}\right) \quad , \tag{7.26}$$

$$\dot{\theta^{\mathrm{e}}} = \frac{1}{2}\frac{\Lambda^0\langle f\rangle}{1+f}\left(\frac{2\phi^{\theta^{\mathrm{e}}}}{(\phi^{\theta^{\mathrm{e}},0})^2} - \frac{\phi^{\beta}}{\phi^{\beta,0}\phi^{\theta^{\mathrm{e}},0}}\right) \quad , \tag{7.27}$$

$$\dot{\gamma} = \frac{\Lambda^0\langle f\rangle}{1+f}\frac{\phi^{\gamma}}{(\phi^{\gamma,0})^2} \quad , \tag{7.28}$$

of the internal variables β, θ^{e} and γ are derived from the switching condition (7.22) by means of the normality rule (4.79).

7.6 Consequences

The above evolution equations have been used to compute many of the typical electromechanical loading paths. The results were quite encouraging, however, in order not to enlarge this report unduely, we will not present them here. What is more important for the development of our constitutive model, the above analysis gives several hints, how the model can be improved further.

A look at equation (7.10) shows that the use of a triangular region for admissible values of the internal variables corresponds to neglecting the second term in the maximum irreversible polarization. This term represents the contribution to the maximum irreversible polarization, which stems from domains situated outside our θ^{e}-cones. If we also take into account this term, this results in a trapezodial region for admissible of the internal variables.

The relation (7.5) for the irreversible strain supports a linear dependence on β. Additionally, the introduction of θ^{e} as additional internal variable instead of taking it to be a constant equal to 45° might be helpful. By prescribing certain bounds for θ^{e}, the saturation values for minimum and maximum irreversible strain as well as maximum irrversible polarization for tetragonal polycrystals can easily be captured by the theory. As an approximation, θ^{e} might be chosen to be a constant, however the value of this constant may be different from 45°.

Chapter 8

Concluding remarks

8.1 Summary of the report

This progress report presents the work during the first phase of a research project on constitutive modeling for piezoceramics. It starts with a brief motivation of our topic and an overview over the plan of the report in Chapter 1: In short, it is our final objective to provide a finite element tool for the analysis of poling processes in piezoceramic devices. In Chapter 2, the macroscopic hysteresis phenomena to be modeled are dicussed in relation to the underlying microscopic switching mechanisms. In this way, the physical basis for the construction of a sound constitutive model is provided. Chapter 3 contains a thorough discussion of the state of the arts in the recent scientific literature. It turns out that a generally accepted thermodynamical framework for constitutive modeling of piezoceramics has been established. Furthermore, in most papers, irreversible polarization and strain are introduced as internal variables.

Macroscopic continuums theories provide very powerful tools for the mathematical description of problems in engineering science. Such a theory consists, first, of partial differential equations derived from "universal" balance laws, which are, second, supplemented by equations representing the specific material behavior. The main part of our report starts in Chapter 4 with a summary of the thermo-electromechanical balance laws. By stating step by step physical assumptions, the general, highly complex theory consisting of Maxwell's Equations and nonlinear thermomechanics is simplified to yield the most elementary form commonly used. In this way, it becomes transparent, which physical problem requires which level of complexity of the theory. The second part of Chapter 4 presents the thermodynamical framework mentioned in the previous paragraph. This framework makes use of the concept

of internal variables representing the irreversible behavior on the macroscopic level of consideration. A normality rule with respect to a convex switching criterion is employed to satisfy the Clausius-Duhem inequality in a sufficient manner.

Chapter 5 is devoted to motivating a constitutive model for piezoceramics for uniaxial loadings. The main difference to other recent models in the literature is the choice of the internal variables used in the model. Instead of irreversible polarization and strain, we introduce so-called microstructural parameters as internal variables, which represent the microscopic domain state of a ferroelelectric and ferroelastic material. One variable, denoted by β, indicates the degree of domains situated with their c-axes inside cones of 45° opening angle about the preferred axis of loading, The other variable, denoted by γ, represents the net orientation of microdipoles in this direction. Irreversible polarization and strain, as well as the material tensors are taken as functions of these parameters. Besides other features, the deformation asymmetry in tension versus compression is represented. An energy barrier function enforces the constraint that, as an intrinsic feature of this model, only consistent irreversible strain and polarization states are possible. Physical soundness on the one hand and mathematical simplicity on the other were the guidelines of our progress during which the original ideas of KAMLAH AND JIANG [1999] have been significantly developed further. Various variants of the model formulation are considered and discussed in detail by means of simulated loading paths. Even though only few material constants are involved in the present formulation of the model, the behavior of piezoceramics under electromechanical loadings can be represented well. All observations made at the macroscopic curves of the model response can be associated to microscopic interpretations of ferroelectric behavior. While the overall behavior of the model is satisfying, there remain open questions concerning the switching criterion in the context of the critical stress for mechanical depolarization.

For a three dimensional generalization of the model, the two scalar valued internal variables β and γ are supplemented by two vectorial internal variables. One indicates the history dependent cones-axis of alignment of the c-axes, while the other describes the history dependent axis of the irreversible polarization. This model formulation can represent the material behavior in a transversely isotropic approximation to the general orthotropic case. In particular, the irreversible strain is formulated as volume preserving, uniaxial strain state in the preferred direction of c-axis switching. Furthermore, for the susceptibility, piezoelectricity, and elasticity tensors transversely isotropic representations with respect to their corresponding symmetry axes are given. A tentative, simple form of the multiaxial switching criterion is given, but

this needs further consideration. Nevertheless, polarization rotation test results can be represented.

In developing the model, much emphasis has been placed on its microscopic motivation. Its sound microscopic foundation gives us a lot of confidence in model. Moreover, it turned out that microscopic basis of the model allowed to either support many of our assumptions by explicit microscopic analysis or to suggest improvements to them. If the 45° opening angle of our cones is replaced by an additional variable, denoted by θ^{e}, it is found that β and θ^{e} constitute a simple step function approximation to the domain distribution density (orientation distribution function). If we take θ^{e} as a constant of 45° and neglect contributions to the irreversible polarization from domains outside our cones, we recover the model formulation of Chapter 5.

8.2 Outlook on the work to be done in the coming time

For the further development of the model we will work on the following topics in the sequence they are listed.

1. modification and improvement of the one dimensional formulation of the switching condition (onset of mechanical depolarization)

2. improvement of the model in view of the microscopic analysis, as far as it significantly improves its description ability without sacrificing its simplicity

3. modification and improvement of the three dimensional formulation of the model, examination of the switching condition in the three dimensional case

4. study of the model response to electromechanical loading at different rates and and the creep-like behavior

5. determination of the parameters contained in the model using the experimental results from Zhou [2003]

6. full orthotropic formulation of the three dimensional model

Acknowledgement

Financial support by the Deutsche Forschungsgemeinschaft is gratefully acknowledged.

Bibliography

[1] Bassiouny, E., Ghaleb, A. F. and Maugin, G. A. [1988]. Thermomechanical formulation for coupled electromechanical hysteresis effects–I. basic equations, II. poling of ceramics. *Int. J. Engng. Sci.* **26**, pp. 1279–1306.

[2] Bassiouny, E. and Maugin, G. A. [1989]. Thermomechanical formulation for coupled electromechanical hysteresis effects–III. parameter identification, IV. combined electromechanical loading. *Int. J. Engng. Sci.* **27**, pp. 975–1000.

[3] Betten, J. [1987]. *Tensorrechnung für Ingenieure*, B. G. Teubner Stuttgart.

[4] Cao, H. and Evans, A. G. [1993]. Nonlinear Deformation of Ferroelectric Ceramics. *J. Am. Ceram. Soc.*, **76**, pp. 890 - 896.

[5] Chen, P. J. [1984]. Hysteresis Effects in Deformable Ceramics. in *The mechanical behavior of electromagnetic solid continua* (IUTAM), Maugin, G. A. ed., pp. 137–143, North Holland, Amsterdam.

[6] Chen, P. J. and Tucker, T. J. [1981]. Determination of the Polar Equilibrium Properties of the Ferroelectric Ceramic PZT 65/35. *Acta Mech.*, **38**, pp. 209 – 218.

[7] Chen, W. and Lynch, C. S. [2001]. Multiaxial constitutive behaviour of ferroelectric materials. *Journal of Engineering Materials and Technology*, **123**, pp. 169-175.

[8] Cocks, A. C. F. and McMeeking, R. M. [1999]. A phenomenological constitutive law for the behaviour of ferroelectric ceramics. *Ferroelectrics*, **228**, pp. 219–228.

[9] Coleman, B. D. and Gurtin, M. E. [1967]. Thermodynamics with Internal State Variables. *J. Chem. Phys.*, **47**, pp. 597-613.

[10] Coleman, B. D. and Noll, W. [1963]. Thermodynamics of Elastic Materials with Heat Conduction and Viscosity. *Arch. Rat. Mech. Anal.* **13**, pp. 167-178.

[11] Damjanovic, D. [1998]. Ferroelectri, dielectric and piezoelectric properties of ferroelectric thin film and ceramics. *Rep. Prog. Phys.*, **61**, pp. 1267-1324.

[12] Drescher, J., Keler, H. and Balke, H. [2000]. Numerical simulation of repolarization in ferroelectrics. GAMM 2000, Annual Scientific Conference, Göttingen (Germany), 2 - 7 April 2000.

[13] Drescher, J., Keler, H. and Balke, H. [1999]. Numerische Simulation von Repolarizationsvorgngen in Ferroelektrika. Workshop des Graduiertenkollegs "Kontinuumsmechanik inelastischer Festkrper", TU Dresden und TU Chemnitz, Oybin, 1999.

[14] Eringen, A. C. [1980] *Mechanics of Continua*, Robert E. Krieger Publishing Company, Inc.

[15] Eringen, A. C. and Maugin, G. A. [1990]. *Electrodynamics of Continua I - Foundations and Solid Media*, Springer-Verlag, New York and et al.

[16] Feldtkeller, E. [1973]. *Dielectrische und magnetische Materialeigenschaften.* Vol. I and II. Mannheim *et al.*: Bibliographisches Institut.

[17] Fett, T., Müller, S. and Munz, D. [1998a]. Nonsymmetry in the deformation behaviour of PZT. *J. Mater. Sci. Letters*, **17**, pp. 261-265.

[18] Fett, T., Munz, D. and Thun, G. [1998b]. Nonsymmetric deformation behaviour of lead zirconate titanate determined in bending tests. *J. Am. Ceram. Soc.*, **81**, pp. 269-272.

[19] Fett, T., Munz, D. and Thun, G. [2002]. Young's modulus of Soft PZT from partial unloading tests. *Ferroelectrics*, **274**, pp. 67-81.

[20] Fett, T., Munz, D. and Thun, G. [2003]. Multiaxial deformation behaviour of PZT from torsion tests. *J. Am. Ceram. Soc., to be published.*

[21] François, D., Pineau A. and Zaoui, A. [1998]. *Mechanical Behaviour of Materials, Volume I: Elasticity and Plasticity*, Kluwer Academic Publishers.

[22] Frémond, M. [1989]. Internal constraints and constitutive laws. In : Rodrigues, J. F. (ed.), *Mathematical Models for Phase Change Problems*, Vol. 88, Basel: Birkhäuser, pp. 3-18.

[23] Fröhlich, A. [2001]. Mikromechanisches Model zur Ermittlung effektiver Materialeigenschaften von piezoelektrischen Polykristallen. Dissertation, Universität Karlsruhe, IZBS, Karlsruhe.

[24] Gurtin, M. E. [1981]. *An Introduction to Continuum Mechanics*, Academic Press.

[25] Hall, D. A. [2001]. Review Nonlinearity in piezoelectric ceramics. *Journal of Materials Science*, **36**, pp. 4575-4601.

[26] Harper, J. E. [1999]. Analysis of nonlinear electroelastic continua with electric conduction. Master's thesis, Masschusettes Institute of Technology.

[27] Harper, J. E. and Hagood, N. W. [2000]. Analysis of Deformable Electroelastic Devices: Cumulative Effects of weak Electric Conduction. In: Lynch, C. S. (ed) Smart Structures and Materials 2000: Active Materials: Behavior and Mechanics, Proceedings of SPIE Vol. 3992, pp. 25-39.

[28] Haupt, P. [1993]. On the mathematical modelling of material behavior of continuum mechanics. *A*cta Mechanica, **100**, pp. 129-154.

[29] Häusler, O. [1999]. Anisotripes plastisches Fließen bei großen Deformation. Dissertation, Universität Karlsruhe, IZBS, Karlsruhe.

[30] Huber, J. E. and Fleck, N. A. [2001]. Multiaxial electrical switching of a ferroelectric: theory versus experiment. *J. Mech. Phys. Solids*, **49**, pp. 785–811.

[31] Huber, J. E., Shieh, J. and Fleck, N. A. [2002]. Multiaxial response of hard and soft ferroelectrics under stress and electric field. In: Lynch, C. S. (ed) Smart Structures and Materials 2002: Active Materials: Behavior and Mechanics, Proceedings of SPIE Vol. 3992, pp. 133-142.

[32] Hutter, K. and van de Ven A. A. F. [1978]. Field Matter Interactions in Thermoelastic Solids. Lecture Notes In Physics 88. Springer, Berlin *et al.*

[33] Jackson, J. D. [1975]. *Classical electrodynamicy*, 2nd edition. Wiley, New Yark *et al.*

[34] Jaffe, B., Cook, W. R. and Jaffe, H. [1971]. *Piezoelectric Ceramics*, Academic Press, London and New York.

[35] Kamlah, M. and Jiang, Q. [1999]. A constitutive model for ferroelectric ceramics under uniaxial loading. *Smart. Mater. Struct.* **9**, pp. 441–451.

[36] Kamlah, M., Böhle, U., Munz, D. and Tsakmakis, C. [1997]. Macroscopic description of the non-linear electro-mechanical coupling in ferroelectrics. In: Varadan, V. and Chandra, J. (ed) Smart Structures and Materials 1997: Active Materials: Mathematics and Control in Smart Structures, Proceedings of SPIE Vol. 3039, pp. 144-155.

[37] Kamlah, M. and Tsakmakis, C. [1999]. Phenomenological modeling of the non-linear electro-mechanical coupling in ferroelectrics. *Int. J. Solids Structures*, **36**, pp. 669–695.

[38] Kamlah, M. and Böhle, U. [2001]. Finite element analysis of piezoceramic components taking into account ferroelectric hysteresis behavior. *Int. J. Solids Structures*, **38**, pp. 605–633.

[39] Kamlah, M. [2001]. Ferroelectric and ferroelastic piezoceramics – modeling of electromechanical hysteresis phenomena. *Continuum Mech. Thermodyn.*, **13**, 2001, pp. 219–268.

[40] Keßler, H. and Balke, H. [2001]. On the local and average energy release in polarization switching phenomena. *J. Mech. Phys. Solids*, **49**, pp. 953–978.

[41] Keßler, H., Fuller, E. R. and Balke, H. [2002]. Modelling of Stable and Unstable Polarization Switching. In: Lynch, C. S. (ed) Smart Structures and Materials 2000: Active Materials: Behavior and Mechanics, Proceedings of SPIE Vol. 3992, 234-244.

[42] Landau, L. D. and Lifshitz, E. M. [1960]. *Electrodynamics of Continuous Media*, Pergamon Press, Oxford, *it al.*.

[43] Landis, C. M. [2001]. Symmetric constitutive laws for polycrystalline ferroelectric ceramics. In: Lynch, C. S. (ed) Smart Structures and Materials 2000: Active Materials: Behavior and Mechanics, Proceedings of SPIE Vol. 4333, 271-276.

[44] Landis, C. M. [2002]. Fully coupled, multi-axial, symmetric constitutive laws for polycrystalline ferroelectric ceramics. *J. Mech. Phys. Solids*, **50**, pp. 127–152.

[45] Landis, C. M. [2003]. On the strain saturation conditions for polycrystalline ferroelastic materials. *J. Appl. Mech., to be published.*

[46] Landis, C. M. and McMeeking, R. M. [1999]. A phenomenological constitutive law for ferroelectrc switching and a resulting asymponic crack tip solution. *J. Intelligent Material Systems Structures*, **9**, pp. 155-163.

[47] Lines, M. E. and Glass, A. M. [1977]. *P*rinciples and Applications of Ferroelectrics and Related Materials. Clarendon Press, Oxford.

[48] Lubliner, J. [1973]. On the structure of the rate equations of materials with internal variables. *Acta Mech.*, **17**, pp. 109-119.

[49] Lynch, C. S. [1996]. The effect of uniaxial stress on the electromechanical response of 8/65/35 PLZT. *Acta mater.*, **44**, pp. 4137-4148.

[50] Lynch, C. S. [1998]. On the development of multiaxial phenomenological constitutive laws for ferroelectric ceramics. *J. Intelligent Material Systems Structures*, **9**, pp. 555–563.

[51] Lynch, C. S., Chen, W. and Liu, T. [2000]. Multiaxial constitutive behaviour of ferroelectric materials. In: Lynch, C. S. (ed) Smart Structures and Materials 2000: Active Materials: Behavior and Mechanics, Proceedings of SPIE Vol. 3992, pp. 245-254.

[52] Maugin, G. A. [1988]. *Continuum Mechanics of Electromagnetic Solids.* Elsevier Science Publishers, Amsterdam *et al.*

[53] Savi, M., Braga, A., Alves, J. and Almeida, C. [1998]. Finite element model for trusses with shape memory alloy actuator. *Modelling and Control of Adaptive Mechanical Structures, Fortschritt-Berichte VDI*, Vol. 11/268, ed Gabbert, U., pp. 115-124.

[54] Schäufele, A. and Härdtl, K. H. [1996]. Ferroelastic Properties of Lead Zirconate Titanate Ceramics. *J. Am. Ceram. Soc.*, **79**, pp. 2637 - 2640.

[55] Soares, M. R., Senos, A. M. R. and Mantas, P. Q. [2000]. Phase coexistence region and dielectrc properties of PZT ceramics. *J. Eru. Ceram. Soc.*, **20**, pp. 321-334.

[56] Truesdell, C. and Noll, W. [1965]. *The Non-Linear Field Theory of Mechanics*, Handbuch der Physik III/3. Springer, Berlin *et al.*

[57] Zhou, D. [2003]. Experimental Invastigation of Non-linear constitutive behaviour of PZT ceramics. Dissertation, Universität Karlsruhe, IZBS, Karlsruhe.